# Spin Ordering

# at

# Low Temperatures

A Thesis

submitted for the degree

of

Doctor of Philosophy

at

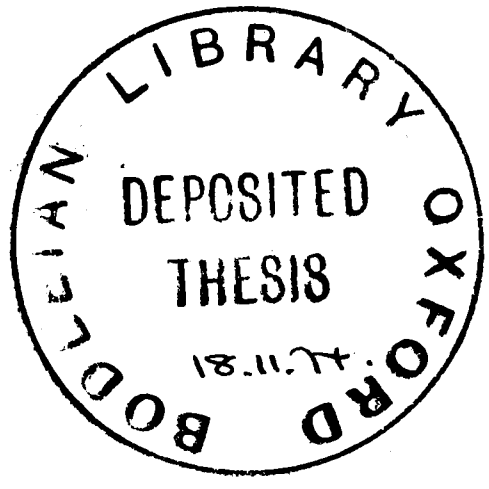
Oxford University

by

Peter Kittel

Brasenose College

September, 1974



## Abstract

This thesis investigates some aspects of the ordering of nuclear spin systems at low temperatures. The thesis is divided into two parts.

In part one some nuclear orientation experiments of $^{74}$As in Fe and $^{206}$Bi and Ni and Fe are described. These nuclei are orientated by the large hyperfine field inside Ni and Fe. The orientation is detected by the anisotropy of the emitted gamma-rays and in the case of $^{74}$As by the destruction of this anisotropy by NMR. Chapter one reviews the theory of the nuclear orientation method. To aid in the interpretation of the $^{206}$Bi results, some channelling experiments were done. A review of the method of atom location by channelling is given in chapter two. Chapter three describes the apparatus and technique used. The results of the $^{74}$As<u>Fe</u> experiments are given in chapter four. In these experiments the magnetic moment of the ground state of $^{74}$As was measured to be $\mu = 1.597(3)$, the sign of the hyperfine field was found to be positive, and the spin-lattice relaxation time was found to be 120(30) s.

The results of the $^{206}$Bi<u>Ni</u> experiments are given in chapter five. The hyperfine was found to be 390(15) kOe for both diffused polycrystalline and implanted single crystal samples. The multipolarity mixing ratios of many of the gamma-rays were found. Reorientation of the metastable state of $^{206}$Pb was observed, which had not been expected. On the basis of the channelling experiments, this reorientation has been explained by the theory

that the Bi nuclei experience a large electric field gradient because they have been displaced from substitutional sites by dislocation loops. It was found also that 23(3)% of the implanted Bi ions were on the surface of the Ni, where they had not been expected. This has been accounted for by the sputtering of the Ni surface. It was also found that the Bi migrates out of the Ni single crystals when heated to $600^{o}C$. This was contrary to expections since Bi is reported as being solubile in Ni.

The results of the $^{206}$BiFe experiments are reported in chapter six. In samples slowly cooled from melts, none of the Bi activity remained. In samples rapidly cooled from melts, 77(3)% of the Bi were in sites with a hyperfine field of 900(140) kOe. The rest were in low field sites. In the implanted samples, 91(8)% of the Bi were in 1400(30) kOe sites. The amount of reorientation was different in the two cases. In the former, the reorientation could be accounted for if the crystal structure near the Bi was similar to that in Ni. In the latter case, the channelling experiments showed that some of the Bi were in sites near single vacancies, which would account for the electric field gradient.

In part two, the developement of an apparatus for nuclear cooling experiments is described. Chapter one reviews the theory of nuclear cooling and chapter two reviews the principles of NMR thermometry. The apparatus was designed to achieve a spin temperature $< 10^{-6}$K in Cu nuclei to observe spin ordering effects caused by the internal interaction. Because of numerous difficulties the experiment has not been done. In chapters three and four, the

apparatus is described, along with an account of the many difficulties encountered in building it. A description of the methods of overcoming these difficulties is also given.

## Acknowledgements

I would like to thank the following people who have contributed to this work.

Professor B. Bleaney for extending to me the facilities of the Clarendon Laboratory.

Professor N. Kurti for his supervision.

Dr. G. Dearnaley for arranging my visits to A.E.R.E. Harwell.

Professor M. Kaplan, Dr. P. T. Callaghan, and Dr. P. D. Johnston with whom most of the nuclear orientation and channelling experiments done.

Professor R. H. March, Dr. P. Daly, Dr. P. C. Hensel, Dr. M. W. S. Parsons, Mr. K. Svec and Mr. P. Tebby for their assistance in constructing the nuclear cooling apparatus.

D. N. J. Stone, Mr. P. K. James and Mr. W. Lattimer for many useful discussions.

Mr. D. T. Smith and Mr. P. Hearst for their assistance with the electronics.

Mr. H. Jones and Mr. P. A. Hudson for their assistance with the solenoids.

The Royal Society for a research grant

Brasenose College for their part of the University's Hulme Fund.

And my wife, Mary Ellen, for her understanding and encouragement.

## Table of Contents


Abstract

Acknowledgements

Part One 1

Chapter One: Nuclear Orientation of Radioactive Nuclei 1

I. Introduction 1

II. Angular Distribution of Radiation 1

III. The Hyperfine Interaction in Ferromagnets 4

IV. Nuclear Magnetic Resonance (NMR) 6

V. Thermometry 7

Chapter Two: Channelling 9

I. Introduction 9

II. The Channelling Process 9

III. Atom Location by Channelling 10

IV. Rutherford Back-Scattering 11

V. Computer Model 12

Chapter Three: Nuclear Orientation and Channelling Apparatus and Technique 16

I. Cryogenics 16

II. Gamma-Ray Spectroscopy and NMR 17

III. Channelling 18

Chapter Four: Orientation of $^{74}As$ in Iron 20

I. Introduction 20

II Sample Preparation 21

III. Results 22

Chapter Five: Bismuth in Nickel Experiments 25

I. Introduction 25

II. $^{206}Bi$ Diffused into Nickel 28

A. Sample Preparation 27

B. The Hyperfine Field 28

C. Multipolarity Studies 30

D. Reorientation of the 2.2 MeV State of $^{206}Pb$ 33

III. $^{206}Bi$ Implanted into Nickel 37

A. Sample Preparation 37

B. Results 38

IV. Channelling in Nickel 39

A. Sample Preparation 39

B. Back-Scattering Spectrum 40

C. The Unheated "$1x10^{14}$" and "$5x10^{14}$" Samples 43

D. The Heat Treated "$5x10^{14}$" Samples 45

E. The "$1x10^{16}$" Samples 46

F. The Diffused Samples 47

V. Summary 47

Chapter Six: Bismuth in Iron 50

I. Introduction 50

II. $^{206}Bi$ Diffused into Iron 51

III. $^{206}Bi$ Implanted into Iron 52

IV. Channelling in Iron 54

V. Summary 56

References for Part One 59

Part Two 64

Chapter One: Magnetic Cooling 64

I. Intorduction 64

II. The Cooling Process 65

III. Spin Temperature 67

IV. Internal Field 68

V. Nuclear versus Electronic Magnetic Cooling 69

Chapter Two: Nuclear Magnetic Thermometry 70

I. Introduction 70

II. General Principles of Pulsed NMR 70

III. Spin-Spin Relaxation 72

IV. Spin-Lattice Relaxation 73

V. Thermometry 73

Chapter Three: An Apparatus for Nuclear Cooling Experiments 75

I. Introduction 75

II. Heat Leaks and Heat Evolution 78

III. The Helium Dewar 80

IV. The Cryostat 80

V. The Magnets 83

VI. The Dilution Refrigerator 85

VII. The NMR System 89

A. Introduction 89

B. The Crossed Coil System 89

C. The Electronics 91

VIII. The Nuclear Cooling Assembly (The Salt Pill and Nuclear Cooling Sample) 95

Chapter Four: Preliminary Experiments 100

I. Early Chrome Potassium Alum (CPA) Experiments 100

II. Early Cerium Magnesium Nitrate (CMN) Experiments 103

III. Further CMN Experiments 109

IV. Further CPA Experiments 116

References for Part Two 121

PART ONE

## Chapter One: Nuclear Orientation of Radioactive Nuclei

### I. Introduction:

The orientation of radioactive nuclei can be observed by the anisotropy of the emitted radiation. The nuclei can be oriented by large external fields. But, this 'brute force' method has only had limited use because of the difficulty of achieving sufficiently low temperatures and high fields.

A more common way is to use the large internal fields found in some materials. Gorter (1a), Rose (1b), Pound (2a) and Bleaney (2b) suggested using the hyperfine interaction in paramagnetic crystals. This method was later extended to the use of the hyperfine interaction in ferro magnets by Grace, Johnston, Kurti, Scurlock and Taylor (3). These have been not only very successful ways of orientating nuclei but also useful in studying hyperfine interactions, nuclear decay properties and nuclear structure.

In this chapter the basic principles and some of the applications of nuclear orientation of radioactive nuclei will be outlined. There have been several extensive reviews of this method by other authors (4, 5, 6).

### II. Angular Distribution of Radiation:

The angular distribution of radiation can be calculated from angular momentum considerations if the populations of the sub-states of the oriented nuclei are known. Figure (1.1) represents

a typical decay in which a nucleus of angular momentum $I_o$ decays by $\beta$ emission. The $\beta$ carries angular momentum $I_\beta$ . The daughter nucleus then under goes a cascade of $\gamma$ transitions until the nucleus has angular momentum $I_i$. This state then decays by emitting a $\gamma$-ray of multipolarity L, leaving the nucleus with angular momentum $I_f$. This transition is called the observed transition. All the preceeding ones are called unobserved transitions.

The angular distribution of the observed transition is

$$W(\theta) = \sum_{k \text{ even}}^{\min(2L,\ 2I_i)} U_k\ F_k\ B_k\ q_k\ P_k\ (\cos\ \theta) \qquad (1.1)$$

where $W(\theta)$ is the normalized count rate observed at an angle $\theta$ from the z-axis. The anisotropy is defined as $1 - W(\theta)$. In practice only the $k = 0$, 2 and occasionally $k = 4$ terms are significant. The $U_k\ F_k$ of the higher order terms are small or zero. The $k = 0$ term is unity.

The $P_k(\cos\ \theta)$ are the Legendre polynomials.

The $q_k$ are solid angle corrections. These compensate for the finite size and the geometry of the detector.

The $B_k$ are called orientation parameters. They depend on the orientation of the parent nuclei. They are

$$B_k = \sum_m (2k + 1)^{\frac{1}{2}}\ C\ (I_o\ k\ I_o;\ m_o\ 0)\ a(m) \qquad (1.2)$$

where C is a Clebsch-Gordan coefficient and the $a(m)$ are the population densities of the $2I_o + 1$ angular momentum sub-states.

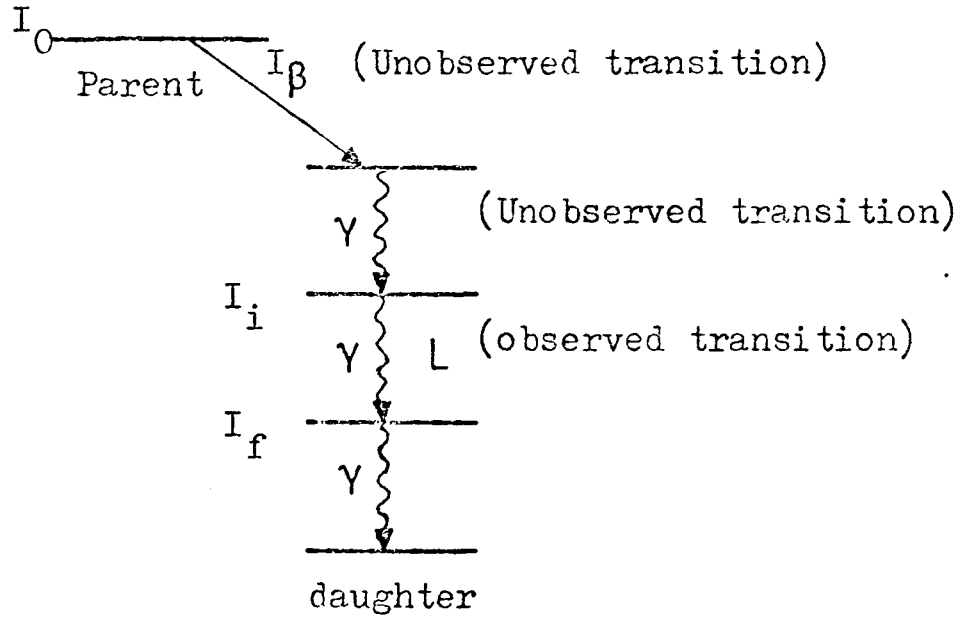

$I_0$
Parent
$I_\beta$
(Unobserved transition)
γ
(Unobserved transition)
$I_i$
γ
L
(observed transition)
$I_f$
γ
daughter

Figure (1.1)

The a(m) are functions of the orienting field and of the temperature. If $\sum_m m\, a(m) \neq 0$, the parent state is polarized. If $\sum_m m\, a(m) = 0$ and $\sum_m m^2\, a(m) \neq \frac{1}{3}I(I+1)(2I+1)$, the parent state is aligned. While the parent state is in thermal equilibrium the daughter states are in general not. This is a result of the life times of the intermediate states being very much shorter than the relaxation times. In certain cases there is some reorientation of the intermediate states. This effect has been discussed by Daniels and Misra (7). A particular example of this effect will be discussed in chapter five in relation to the $^{206}$Bi experiments.

The $F_k$ are functions of the observed transition. They depend on $I_i$, L and $I_f$. The $F_k$ coefficients have been tabulated (8, 9, 10).

The $U_k$ are functions of all the previous unobserved transitions. For each such transition $(I_{n-1} \xrightarrow{L_n} I_n)$ there is a $U'_k\ (L_n\ I_{n-1}\ I_n)$.

These combine to give

$$U_k = \prod_{n=1}^{i} U'_k\ (L_n\ I_{n-1}\ I_n) \qquad (1.3)$$

The $U'_k$ have been tabulated (10).

The multipolarity (L) of the radiation emitted in the transition is not determined uniquely by the conservation of angular momentum. The possible values of $L_n$ are

$$|I_{n-1} - I_n| \leq L_n \leq I_{n-1} + I_n$$

as long as $L_n \geq 1$. However, the multipolarity is usually the lowest possible. This is a result of the vastly different transition rates for transitions of different multipolarity and type. Magnetic transitions rates are typically an order of magnitude smaller than

electric transition rates for the same multipolarity. For transition of the same type these rates decrease by as much as five orders of magnitude for an increase in multipolarity (11).

The type of the transition is determined by the conservation of parity. If $\pi_i$ and $\pi_f$ are the parities ( $\pi = \pm 1$) of the initial and final nuclear states, then for an electric transition E(L): $\pi_i \pi_f = (-1)^L$ and for a magnetic transition M(L): $\pi_i \pi_f = -(-1)^L$.

Sometimes the transition rates for radiation of two different multipolarities are comparable. These mixed transitions usually occur when the two processes are M(L) and E(L + 1). If this transition is the observed one then the $F_k$ must be replaced by

$$F'_k = \left[F_k (L\ I_f\ I_i) + \delta^2 F_k (L+1,\ I_f\ I_i) + 2\delta F_k (L, L+1,\ I_f\ I_i)\right] / (1+\delta^2) \qquad (1.4)$$

Similarly if the transition is unobserved, the $U'_k$ must be replaced by

$$U''_k = \left[U'_k (L\ I_{n-1}\ I_n) + \delta^2 U'_k (L+1,\ L_{n-1}\ L_n)\right] / (1+\delta^2) \qquad (1\ 5)$$

The parameter $\delta$ is defined such that $\delta^2 = x/(100 - x)$ where x is the percentage of (L + 1) multipolarity present.

## III. The Hyperfine Interaction in Ferromagnets:

There are large hyperfine fields in ferromagnetic materials. ~~This hyperfine interaction is far more complex and less well understood than in ordinary metals~~. The problem was first considered by Marshall (12). A more detailed study has been made by Freeman and Watson (13). The following discussion is concerned only with the elements of the iron group. These are the only ferromagnets used in the experiments

described in this thesis.

There are many contributions to the hyperfine interaction. The Hamiltonian can be written as

$$\mathcal{H} = \mathcal{H}_z + \mathcal{H}_q + \mathcal{H}_o + \mathcal{H}_c \qquad (1.6)$$

The first term is the Zeeman interaction between the nuclei and the local field. This local field is comprised of the external applied field, the demagnetization field (a function of the bulk shape), and the Lorentz field ( a function of the bulk magnetization).

The second term is the electric quadrupole interaction. It is the interaction of the nuclear electric quadrupole moment with the local electric field gradient. This term is zero for nuclei sitting at sites of cubic symmetry and is large for other sites.

The third term represents the orbital and dipolar interactions between the nucleus and its electrons. These interactions arise from the mixing of the electron shells with the neighbouring 3-d electrons and from any residual unquenched orbital momentum.

The last term is the Fermi contact term (14). This is the most important term. It arises from the spin polarization of the s electrons at the nucleus. There are two sources of this polarization. They both give large but opposite effects. The first is called core polarization. It is caused by the exchange interaction between the core s electrons and the 3-d electrons (15). The other is the polarization of the conduction s electron band by the 3-d electrons (16).

IV. Nuclear Magnetic Resonance (N M R):

Using nuclear radiations to detect NMR was first suggested by Bleombergen and Temmer (17) and first used by Matthias and Holliday (18). In this form of NMR a steady rf field ($H_x = 2H_1 \sin \omega t$) is applied perpendicular to the orienting field, $H_o$. When the frequency of the rf field is the Larmor frequency, $\omega_o$, it tends to equalize the population of the magnetic sub-states. This causes the $B_k$ to approach zero. Thus if $H_x$ is swept through Larmor frequency the anisotropy will change when $\omega = \omega_o$. Matthias, Olsen, Shirley, Steffan and Templeton (19) have considered this type of NMR in detail. It has also been considered by Spanfaad and Hartman-Boutron (20) in the case of long relaxation times and by Johnston, Fox and Stone (21) for mixed dipole and quadrupole interactions. NMR is a more powerful method than the anisotropy method (see II), but it does not always work.

When NMR is done in ferromagnetic hosts there are several important consequences. The first is the enhancement of the rf field which allows the resonance to be saturated with a low applied field. When a small transverse field, $H_1$, is applied the magnetization is tipped through the angle $H_1/H_o$. The hyperfine field, $H_{hfs}$, follows the magnetization. The internal transverse field, $H_x^{int}$, is the sum of $H_1$ and the transverse component of $H_{hfs}$, so

$$H_x^{int} = \left(1 + \frac{H_{hfs}}{H_o}\right) H_1 \qquad (1.7)$$

The quantity $( 1 + H_{hfs}/H_o )$ is called the hyperfine enhancement factor and is typically of the order of 100.

The second important property of a ferromagnet is the

inhomogeneity of the internal field (22). This results in a wide resonance, typically 1 MHz wide. In order to have an appreciable change in the anisotropy, as many nuclei as possible must be resonated at the same time. This can be accomplished by a frequency modulation of $H_1$.

Relaxation processes are important in any resonance. In dilute alloys spin-spin interactions are very weak, so only longitudinal relaxation takes place ( $\tau_2 = \tau_1$). This also implies that the spin temperature concept can not be applied to non-equilibrium situations. The dominating longitudinal relaxation mechanism is the hyperfine coupling between the nuclei and the conduction electrons.

A further discussion of NMR, relaxation and spin-temperature is given in part two of this thesis.

V. Thermometry:

Once $W(\theta)$ as a function of temperature has been determined for a particular system it can be used as a thermometer. Two of the most common systems are $^{60}$Co in Fe polycrystalline foil and $^{60}$Co in a hexagonal Co single crystal. Since iron has a cubic structure, the hyperfine field has no preferred direction. Thus, the $^{60}$Co<u>Fe</u> thermometer must be polarized by an external magnetic field. In a Co single crystal, the hyperfine field is aligned along the c-axis. So, a Co single crystal thermometer can be used when no polarizing field is available. Since the hyperfine field for Co is greater in Fe then in Co, the anisotropy for a given temperature will be greater for $^{60}$Co<u>Fe</u> than $^{60}$Co<u>Co</u>.

A $^{60}$Co nucleus emits two gamma-rays when it decays. Both of these have identical $U_k F_k$ coefficients. Thus, both show the same

anisotropy. The following table summarizes the data needed to determine $W(\theta)$ for $^{60}Co$.

Table 1.1

Orientation Data for $^{60}Co$

| | | |
|---|---|---|
| $U_2F_2$ | -0.4205 | |
| $U_4F_4$ | -0.2428 | |
| I | 5 | (ref. 23) |
| $\mu$ | 3.754 n.m. | (ref. 23) |
| $H_{Fe}$ | -287.7 kOe | (ref. 24) |
| $H_{Co}$ | -227 kOe | (ref. 24) |

# Chapter Two: Channelling

## I. Introduction:

In order to interpret the results of hyperfine field measurements, it is necessary to know the location in the crystal lattice of the nuclei being measured. If the impurity is easily soluble in the host, the site is usually assumed to be substitutional. For some systems, this assumption can not be made and some means of locating the impurity site must be used. One such method is channelling.

The concept of the channelling of charged particles in a crystal was first suggested by Stark (25) in 1912. The concept lay dormant until it was independently suggested by Robinson and Oen (26) fifty years later. The process of channelling and its use for atom location has been discussed in detail in the reviews by Alexander (27) and Dearnaley (28).

## II. The Channelling Process:

When a beam of ions enters a crystal parallel or almost parallel to a crystal axis or plane it will be steered along the axis or plane by successive glancing collisions with the lattice atoms. There are two principal results of this. First, the beam will penetrate further into the crystal than otherwise. Second, the flux of ions will be greater in the center of the channel than near the rows of planes of atoms that border the channel. This effect is called flux peaking. For a given channel, the flux peaking is dependent on the angle between the incident beam and the channelling direction. To become channelled, an ion must enter the crystal at an angle less than the critical angle, from an axis

or plane. This angle is typically $1^{\circ}$ for the principal axis and planes.

When a channelled ion is scattered into an angle greater than the critical angle it can leave the channel. This process is called dechannelling. Dechannelling can be caused by a single collision with a crystal defect or an interstitial atom or by multiple scattering caused by thermal vibrations of the lattice atoms or by collisions with electrons. Once an ion has become dechannelled, its motion will be in a random direction. It will behave just as an ion that was never channelled.

III. Atom Location by Channelling:

The technique of locating atoms with channelled ions is dependent on flux peaking. Because of the flux peaking, the yield of any close encounter interaction between a channelled ion and an atom in the crystal is higher for atoms near the center of the channel. In the experiments described in this thesis, the close encounter interaction observed was Rutherford back-scattering. In a typical experiment the ion beam is angularly scanned about several different channelling directions. The yields for both the host and the impurity atoms are normalized to the yield for a random beam. Possible sites for the impurities can be found by comparing the experimental yields to yields calculated on a computer for various sites. There are several 'rules of thumb' to aid this comparison (27).

1. If the impurities are substitutional, their yields will be the same as the host's yield.
2. If the impurities are slightly displaced from a

substitutional site, the impurity's critical angle will be less than the host's, but the minimum yields will be the same.

3. If the impurity lies on an axis or in a plane, the yield for a beam channelled along that axis or plane will appear to be substitutional.

4. If the impurity occupies a site of high symmetry (such as the body center of an FCC lattice), the impurity's yield will show peaks and dips. The higher the symmetry the fewer the peaks.

IV. Rutherford Back-Scattering:

A review of the Rutherford back-scattering technique has been given by Mayer, Eriksson and Davies (29). The energy of an ion back-scattered from a depth x is

$$E(x) = (E_0 - E_1(x))\, k - E_2(x) \qquad (2.1)$$

where $E_0$ is the initial ion energy, $E_1(x)$ is the energy lost by the ion while penetrating to depth x, $E_2(x)$ is the energy lost on the way out, and k is the ratio of the energy before and after the collision. This ratio is given by

$$k = \left[ \frac{M_1 \cos 0 + (M_2^2 - M_1^2 \sin^2 \theta)^{\frac{1}{2}}}{M_1 + M_2} \right]^2 \qquad (2.2)$$

where $\theta$ is the laboratory scattering angle, $M_1$ is the ion mass and $M_2$ is the target mass.

There are several important features of this process. The back-scattered ions span a wide range of energies. The energy spectrum of ions scattered from the host atoms will be continuous

up to the energy $E_o k$, corresponding to the surface of the crystal. If the mass of the impurities is larger than the host's, then its spectrum will continue above the host's. In implanted materials the impurities are localized in a layer near the surface of the crystal. The back-scattering from this layer will produce a peak in the spectrum. So the spectrum from the impurities will be separated from the spectrum of the host if the impurities are heavier than the host and lie in a layer near the surface. This situation makes it possible to do atom location experiments on samples containing low impurity concentrations.

V. Computer Model:

The model used was an analytical model in which the rows or planes of atoms that bound a channel are considered to be strings or sheets of uniform charge density. The calculations are based on the continuum model developed by Lindhard (30) and is essentially the same as that used by Alexander, Callaghan, and Poate (31) and Callaghan (32). In this approximation the standard Lindhard (30) potentials are used. For axial channelling, the potential at a distance r from a single axial row is

$$U(r) = \frac{Z_1 Z_2 e^2}{d} \ln \left[ 3 (a_{TF} / r)^2 + 1 \right] \qquad (2.3)$$

where $Z_1$ and $Z_2$ are the atomic numbers of the ion and target atoms respectively, e is the electronic charge, $a_{TF}$ is the Thomas-Fermi screening radius:

$$a_{TF} = 0.468 \left( Z_1^{2/3} + Z_2^{2/3} \right)^{-\frac{1}{2}} \qquad (2.4)$$

and d is the interatomic spacing along the axis. For planar channelling, the potential at a distance r from a single plane is

$$U(r) = 2\pi Z_1 Z_2 e^2 N d_p \left[ (r^2 + 3a_{TF}^2)^{\frac{1}{2}} - r \right] \qquad (2.5)$$

where N is the atomic density of the crystal and $d_p$ is the distance between planes.

In the continuum model, the transverse energy of an ion is assumed to be conserved. When the ion enters the crystal, its transverse energy is

$$E_\perp = E_o \psi_i^2 + U(\underline{r}_i) \qquad (2.6)$$

where $\psi_i$ is the angle of the incident ion, $\underline{r}_i$ is the location of the point of entry in the transverse plane and U is sum of potentials of all the strings or sheets of charge that bound the channel. After entering, the ion is confined to the region of the channel where $U(\underline{r}) \leq E_\perp$ . From this, $r_m(E_\perp)$, the minimum distance of approach to a string or sheet, can be defined. The ion is assumed to be dechannelled if $r_m \leq a_{TF}$ and thus to contribute only to the random fraction of the beam.

An axially channelled ion is assumed to have a uniform spatial probability distribution within its accessible area. Hence the probability, f, of finding an ion with total transverse energy $E_\perp(\psi_i, \underline{r}_i)$ at position $\underline{r}$ is

$$f(\underline{r}, E_\perp) = \begin{cases} 1/A_m : E_\perp \geq U(\underline{r}),\ E_\perp < U_{TF} \\ 0 \quad : E_\perp < U(\underline{r}),\ E_\perp < U_{TF} \\ 1/A_o : E_\perp \geq U_{TF} \end{cases} \qquad (2.7)$$

where $A_m$ is the area of the channel accessible to the ion, $A_o$ is the total area of the channel and $U_{TF}$ is the potential at a Thomas-Fermi screening distance from a string. Intergrating f over all positions of entry for the ions, gives the normalized

flux at a position $\underline{r}$.

$$F(\underline{r}, \psi_i) = \iint_{A_o} f(\underline{r}, E_\perp (\psi_i, \underline{r}_i)) \, d A(\underline{r}_i) \qquad (2.8)$$

For planar channelling, the spatial probability distribution is assumed to be a simple harmonic distribution. This is a fairly good approximation in the center of the channel where the potential can be approximated as that of a simple harmonic oscillator. It is in this region that flux peaking is most important. Thus, the probability of finding an ion with a minimum distance of approach $r_m$ at a distance r from the center of the channel is

$$f(r, r_m) = \begin{cases} 2/d_p & : r_m \leq a_{TF} \\ 0 & : r_m > \frac{d}{2}p - r,\ r_m > a_{TF} \\ \left[\left(\frac{d}{2}p - r_m\right)^2 - r^2\right]^{-1/2} / \pi & : r_m < \frac{d}{2}p - r,\ r_m > a_{TF} \end{cases} \qquad (2.9)$$

The singularity at $r = d_p/2 - r_m$ is removed by setting $r = d_p/2 - r_m - a_{TF}$ at that point. The normalized flux is

$$F(r, \psi_i) = \int_0^{\frac{d_p}{2}} f\,(r, r_m\,(\psi_i, r_i))\, d\, r_i \qquad (2.10)$$

Equations (2.8) and (2.10) were integrated numerically on a computer. The computed results differed in two important ways from the experimental results. First, the calculated minimum yields for substitutional sites were lower than the experimental ones. Second, the calculated critical angle was also smaller.

The first is assumed to be a result of the imperfections in the crystal. The oxide layer, crystal defects and radiation damage will increase the random fraction of the ion beam. To

account for this the calculated yields were re-normalized to the experimental minimum yield of the host.

The difference in the critical angles is assumed to result from the approximate potentials used. To compensate for this, the calculated yields were re-normalized so that the calculated and experimental host yields have the same angular width.

These are the same corrections that Alexander, Callaghan, and Poate (31) and Callaghan (32) used. These authors also compared this type of computer simulation to a Monte Carlo simulation based on a binary collision model. They found that there was reasonable agreement between the models.

# CHAPTER THREE

## Nuclear Orientation and Channelling Apparatus and Technique

### I. Cryogenics:

The apparatus used in these experiments has been described in detail by Fox (33) and Johnston (34). The required temperatures were achieved by the adiabatic demagnetization of a salt pill. The salt pill was made from 200g of finely ground chrome alum mixed with glycerol and a saturated solution of the alum. The magnetic field for the demagnetization was supplied by a water cooled solenoid, which can produce fields up to 40 kOe. When not in use the magnet can be moved away from the dewar. The heat of magnetization was removed by He exchange gas to a helium bath pumped to 1.3 K by a rotary pump. The pill cools the sample by means of a copper cold finger. The sample is soldered to the cold finger which is hard soldered to a number of copper foils that are immersed in the pill. The sample can be maintained in the region of 10 - 20 mK for up to twelve hours. A superconducting solenoid is used to produce a field of up to 10 kOe on the sample. This field is reduced to less than 100 Oe in the region of the pill by a compensating coil. This magnet is used to saturate the magnetization of the ferromagnetic samples. A pair of rf coils are located on either side of the cold finger. The axis of these coils is perpendicular to the axis of the polarizing magnet. Provision has been made for gamma-rays to leave the apparatus in directions parallel and perpendicular to the polarizing field.

The sample and a $^{60}$CoFe thermometer are soldered to the

cold finger. Either Wood's metal or soft solder are used. The apparatus is then assembled. Care is taken to ensure that the magnets and rf coils are properly located. The samples, which are thin foils or crystals, are aligned normal to the axis of the rf coils. After pre-cooling with liquid nitrogen the jacket containing the pill is pumped and filled with a few torr of exchange gas. The nitrogen is blown out and replaced with liquid helium. The helium is pumped to $\approx 1.3$ K and the magnet is manoeuvred into place. The pill is magnetized and allowed to come to thermal equilibrium with the helium bath. Then the exchange gas is pumped away until the pressure is $\lesssim 10^{-5}$ torr. The pill is then demagnetized in 15 minutes at an approximately exponential rate. At the end of the demagnetization the large solenoid is removed, the gamma-ray detectors are positioned and the polarizing field is swept up.

II. Gamma-Ray Spectroscopy and NMR:

A Ge(Li) detector and a multi-channel annalyzer were used in the orientation experiments. The system is shown schematically in fig. 3.1. The overall resolution was 2.2 keV. With this system, the anisotropy of all but the weakest gamma-rays could be measured. The biggest draw-back is the low efficiency of the detector, necessitating long counting times at each temperature to get good statistical accuracy. For the geometry used the solid angle corrections were calculated by the method given by Rose (35).

In the NMR experiments shorter counting times were desired, so a wide range of frequencies could be searched before the pill warmed up. In these experiments a 3" x 3" NaI detector was used.

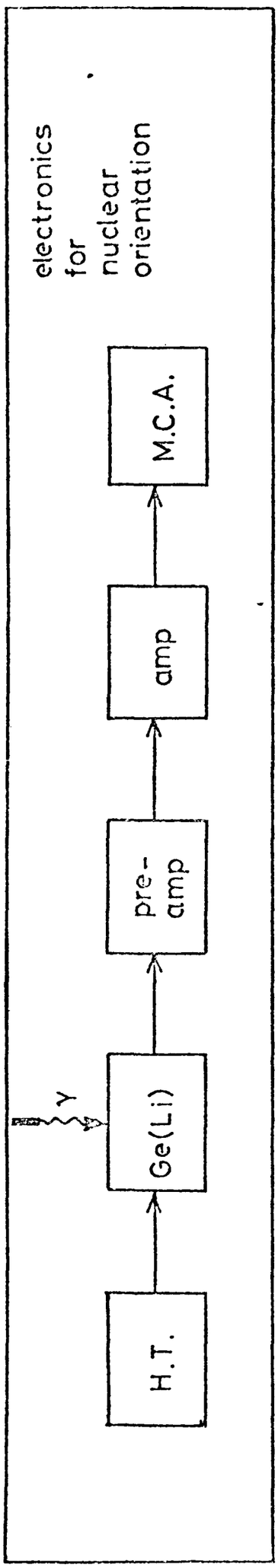

electronics
for
nuclear
orientation
M.C.A.
amp
pre-
amp
Ge(Li)
γ
H.T.

Fig. 3.1

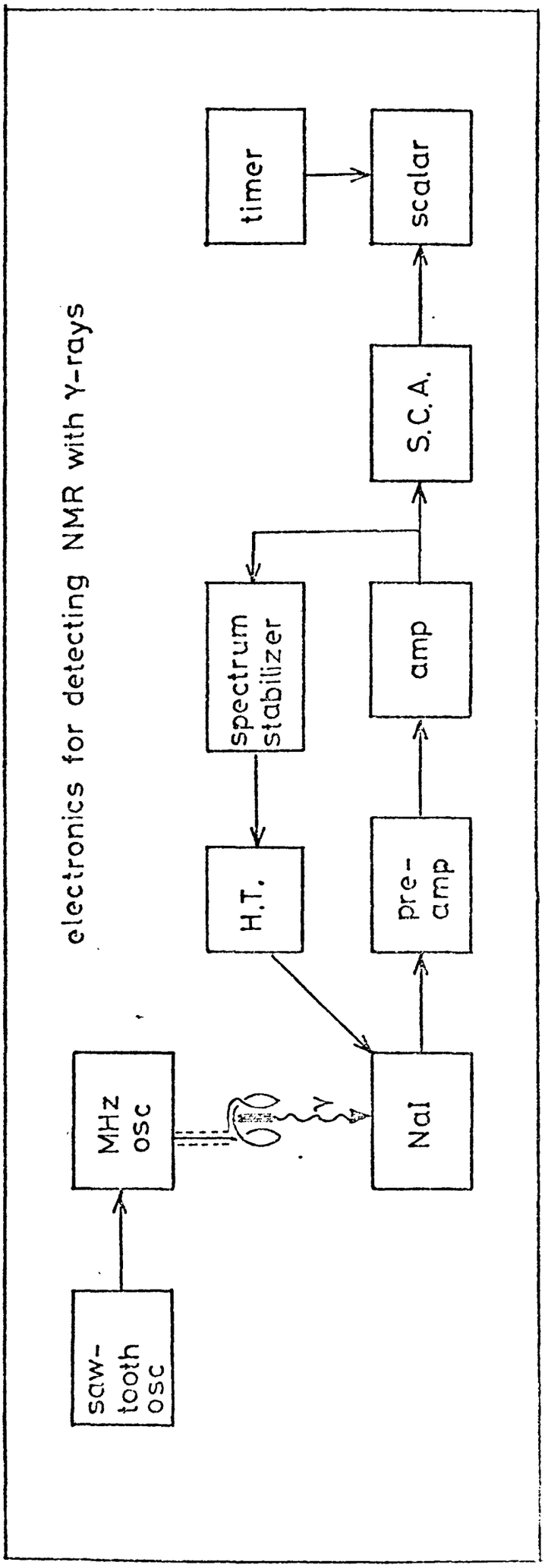

electronics for detecting NMR with γ-rays
timer
scalar
S.C.A.
spectrum
stabilizer
amp
H.T.
pre-
amp
MHz
osc
γ
NaI
saw-
tooth
osc

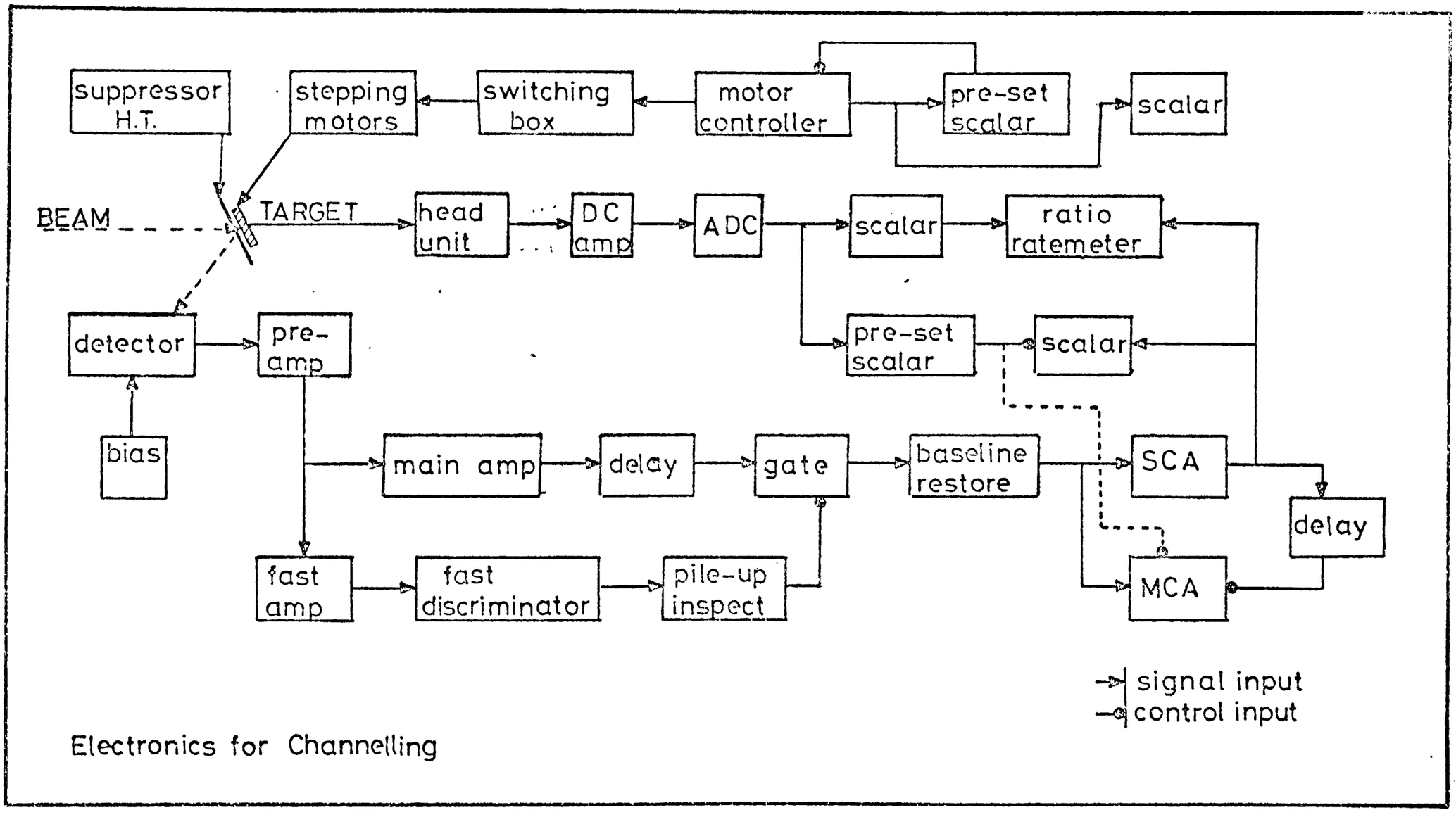
Fig. 3.2

These detectors are ~ 15 times more efficient but have a resolution of only 200 keV. The anisotropies of several gamma-rays were monitored with a single channel analyzer. The rf was supplied by a Schlumberger FSM 500 frequency synthesizer. The frequency could be modulated externally by $\pm$400 kHz with a saw-tooth generator. The modulation was done at 10-100 Hz. The accuracy of the system was better than 1 part in $10^5$. The system is shown schematically in fig. 3.2.

III. Channelling:

The apparatus was the same one described by Alexander (27), Callaghan (32) and Alexander, Callaghan and Poate (31). A beam of 3.5 MeV $^{14}N^{+}$ ions was used. This beam was obtained from the Harwell 5 MeV Van de Graaff accelerator. After acceleration the beam was bent $90^{\circ}$ by an analyzing magnet. The beam was then focused and collimated. The half-angle divergence was $\approx 0.03^{\circ}$. The target chamber was adjustable both vertically and horizontally to align the sample with the beam. The chamber was pumped to a pressure $\lesssim 10^{-6}$ torr by an oil diffusion pump. A liquid nitrogen trap was used to reduce the hydrocarbon contamination of the sample. The sample could be rotated with respect to the beam with a goniometer. The goniometer could be independently rotated about three axes. The maximum rotations were $360^{\circ}$ about a vertical axis, $360^{\circ}$ about an axis normal to the target and $\pm 20^{\circ}$ about a horizontal axis in the plane of the target. The rotations were controlled by stepping motors. Each step corresponded to $0.01^{\circ}$. The backlash was approximately $0.05^{\circ}$. The target chamber is shown in fig. 3.4.

To compare back-scattered spectra they must be normalized




Electronics for Channelling

Fig. 3.3

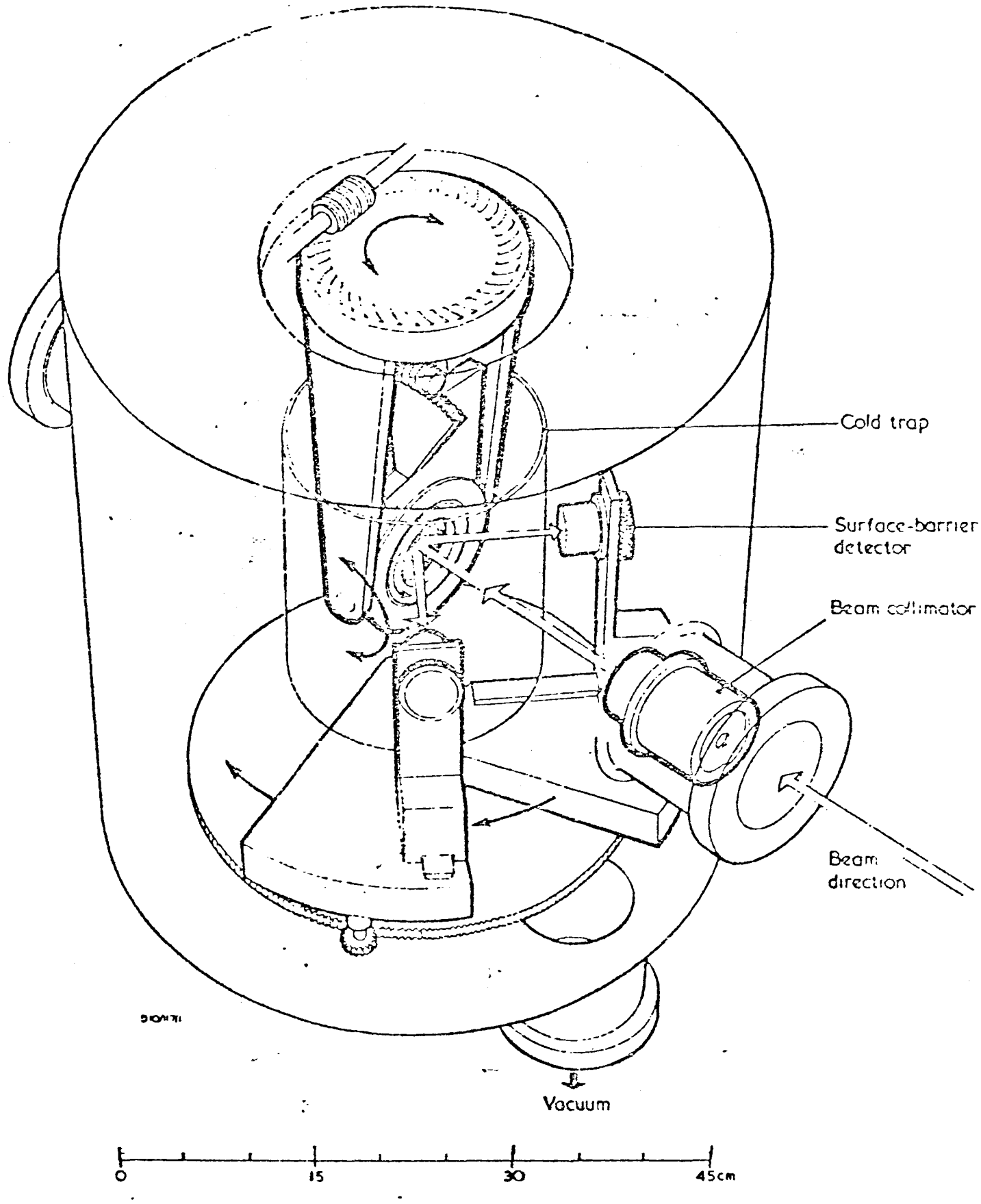

Cold trap
Surface-barrier detector
Beam collimator
Beam direction
Vacuum
0
15
30
45cm

Fig. 3.4

to the same incident charge. This was accomplished by integrating the beam current and taking counts for constant charge. The emission of secondary electrons was suppressed by placing -1.5 kV on a loop wire of 1 cm in front of the sample. Silicon surface barrier detectors with a surface area of 100 $mm^2$ were used. They had a resolution of $\simeq$ 70 keV for 3.0 Mev $^{14}N$ ions. The detectors were located between $160^{\circ}$ and $170^{\circ}$ to the beam direction. The particular angle used was chosen to avoid enhancement of the signal by channelling of the scattered ions. After amplification, the signal was analyzed by a multi-channel analyzer. A system of fast electronics was used to reduce pile-up. The beam current was adjusted to keep the dead time of the system approximately constant. The electronics is shown schematically in fig. 3.3.

The orientation of the crystal axes and planes were found by scanning a few degrees about the horizontal and vertical axes of the goniometer. During this process the back-scattering rate normalized to constant beam current was monitored. The planes and axes were found by plotting the location of the minimums of this rate. The identification of the planes and axes was facilitated by cutting the sample normal to a major axis.

# Chapter Four

## Orientation of $^{74}As$ in Iron

### I. Introduction:

The nucleus $^{74}As$ was chosen for several reasons. As nuclei had never been oriented in thermal-equilibrium and the magnetic moment of $^{74}As$ was unknown. The simple shell model (36) of this nucleus gives the ground state as $(\pi f_{5/2})^1 (\nu g_{9/2})^1$. This is in agreement with the known spin and parity of $2^-$ (37). The nucleus $^{86}Rb$ has the same spin and parity arising from the configuration $(\pi f_{5/2})^{-1} (\nu g_{9/2})^{-1}$. The moment of $^{86}Rb$ has been measured as -1.6915 n.m. by Braslaw, Brink and Kahn (38). The question was, if there was a correspondence between the moment due to the odd particles in $^{74}As$ and that due to the odd holes in $^{86}Rb$.

The half life of $^{74}As$ is 17.9 days. It decays by $\beta^-$ emission (32%) to $^{74}Se$ and by electron capture (39%) and $\beta^+$ emission (29%) to $^{74}Ge$. The principal decay paths and intermediate states are shown in fig. 4.1 (37). Both the $\beta$-decays are first forbidden with log ft values of 7.6 for the decay to Se and 6.9 for Ge. Both the principal gamma-rays (635 and 596 keV) are $2^+ \rightarrow 0^+$ transitions of E2 character. They should show the same anisotropy. If there were any differences between the types of $\beta$ decay or any reorientation effects in the electron capture they should show up as differences in the anisotropy.

Iron was chosen as a host because As is highly solubile in Fe (43) and because the hyperfine field in Fe is larger than in

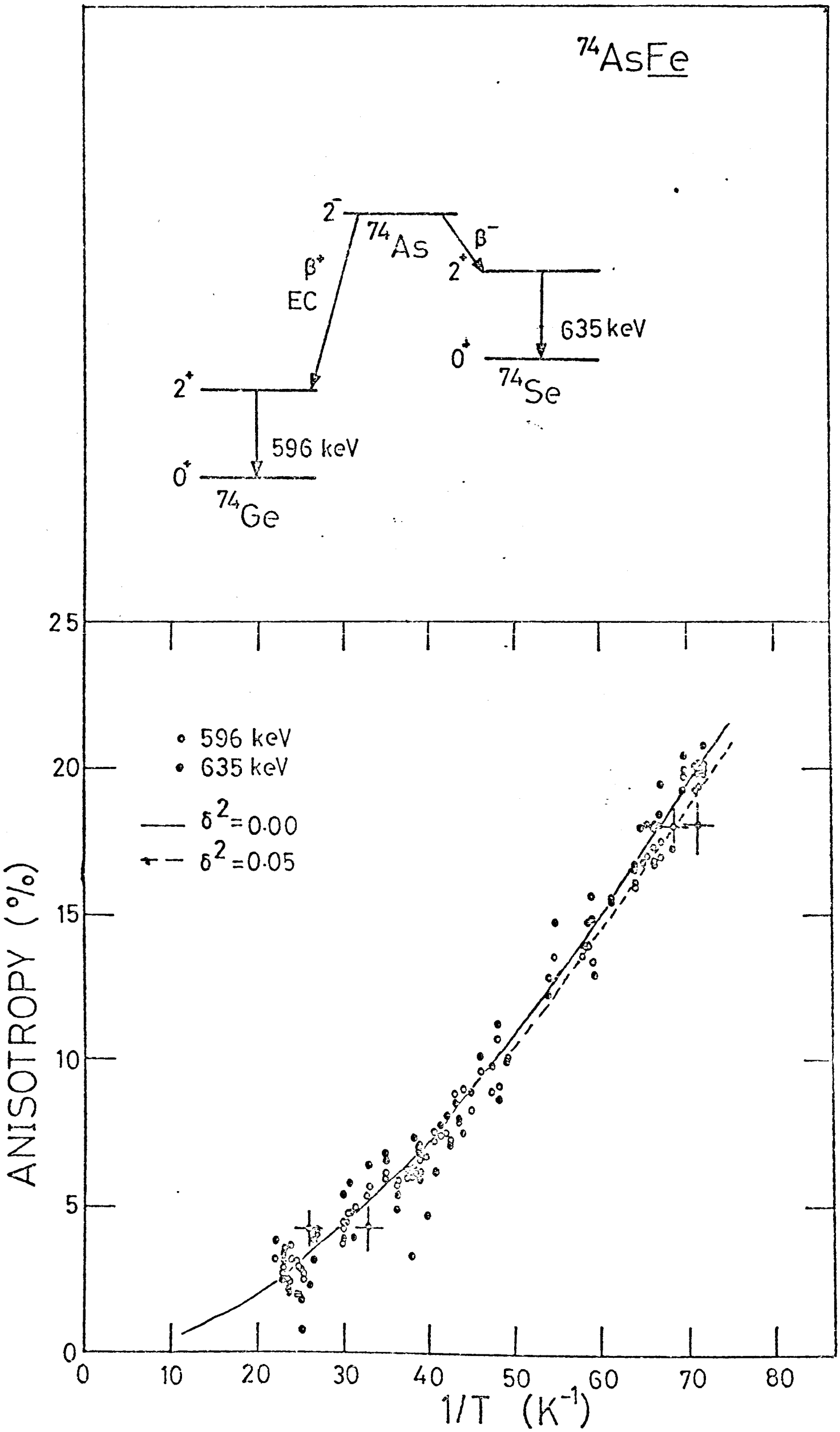

$^{74}$AsFe
2⁻
$^{74}$As
β⁺
EC
β⁻
2⁺
635 keV
0⁺
$^{74}$Se
2⁺
596 keV
0⁺
$^{74}$Ge
25
20
15
10
5
0
ANISOTROPY (%)
596 keV
635 keV
δ² = 0.00
δ² = 0.05
0
10
20
30
40
50
60
70
80
1/T (K⁻¹)

Fig. 4.1

other ferromagnetic hosts. The results of the experiments described in this chapter have been published (39).

II. Sample Preparation:

The samples were prepared from carrier free $^{74}As$. The activity came as sodium arsenate in aqueous solution. The samples were prepared by simultaneously electroplating the As and some Fe onto thin Fe foils. The As was then diffused into the foils in an oven. The simultaneous electroplating was to prevent the As from vaporizing (b.p. 633°C) during diffusion.

The samples used for the orientation runs were electroplated onto 100 - 200 μm thick foils. These foils had been rolled from 99.98% pure Fe. The surface was cleaned in toluene and electropolished before plating. The electroplating solution was made from a dilute solution of $FeSO_4$ in water. $H_2SO_4$ was added to adjust the pH to ~ 1 - 2. The activity was then added. The foil was electroplated at 100 ma for 15 minutes. This resulted in ≈ 70 μCuries on a 1 $cm^2$ foil. The thickness of the plated layer was ≤ 1 μm. The sample was diffused in a hydrogen atmosphere for 10 hours at 800°C. After diffusion, about 72% of the activity remained on the foil. The sample was etched in dilute $HNO_3$ to remove any surface activity. Very little activity was lost by the etching.

A 2 μm foil was used on the NMR run. This was to ensure that most of the activity was within the skin depth. The foil was electroplated in the same way as the others, except about three times as much activity was used. This foil was diffused for 1.5 hours at 800°C

III. Results:

The results of the orientation experiments are shown in fig. 4.1. It contains the results of three runs. The anisotropy was found to be identical for both gamma-rays, indicating that there is no difference between the two types of decay and that there are no reorientation effects. Since the $B_k$ and $F_k$ coefficients are identical for both gamma-rays, the data shows that the $U_k$ for the beta-decays are the same. Since the beta-decays are first forbidden, they can be a mixture of $j = 0$ and $j = 1$ transition, where $j$ is the angular momentum of the electron-neutrino field. Two curves are plotted in fig. 4.1 representing $\delta^2 = 0.00$ and $\delta^2 = 0.05$, where is the ratio of the amplitudes of $j = 1$ to $j = 0$ present. $\delta^2 = 0.05$ corresponds to a mixture of 95.2% $j = 0$ and 4.8% $j = 1$. The values of the relevent parameters are given in table 4.1. The data indicates that $\delta^2 = 0.00$ is a very good fit and $\delta^2 = 0.05$ is the outside limit of agreement. Thus the transitions are predominantly ($> 95.2\%$) $j = 0$.

Table 4.1

Orientation Parameters for $^{74}As$

| | k = 2 | k = 4 |
|---|---|---|
| $U_k(j=0)$ | 1.000 | 1.000 |
| $U_k(j=1)$ | 0.500 | -0.667 |
| $F_k$ | -0.598 | -1.069 |
| $Q_k$ | 0.960 | 0.885 |

The results of the NMR experiments are shown in fig. 4.2. They were carried out at a temperature of approximately 0.02 K with a frequency modulation of ± 400 kHz. The data was taken alternately with and without FM at each frequency to establish the baseline of zero resonance effect and to allow the nuclei to relax back to thermal-equilibrium. The experiment was performed in two different polarizing fields and with both increasing and decreasing frequency sweeps. No dependence on sweep direction was found. The shift in resonance frequency with polarizing field indicates a positive hyperfine field. The curves in fig. 4.2 are calculated assuming a full line width of 1.0 MHz and taking into account the ± 400 kHz modulation. This results in an apparent line width of 1.3 MHz, which is in agreement with the data. The curves are fitted by eye to help determine the centre frequency.

Using $^{75}$As, Koi, Kawakami, Hihara and Tsujimura (40) found the hyperfine field of 1 at .% As in Fe to be 342.9(3) kOe. The data for $^{74}$As yields a Larmor frequency of 209.88(15) MHz at $H_0$ = 1.79 kOe. This gives the magnetic moment of $^{74}$As as

$$|\mu| = 1.597(3) \text{ n.m.}$$

This is in good agreement with the data for the shifted resonance. The experiment does not determine the sign of the magnetic moment. By comparison with other nuclei, it is expected to be negative. Table 4.2 compares the magnetic moments of several doubly odd nuclei closely related to $^{74}$As. The table shows that there is a correspondence between the moments of $^{74}$As and $^{86}$Rb, but not for the other moments listed.

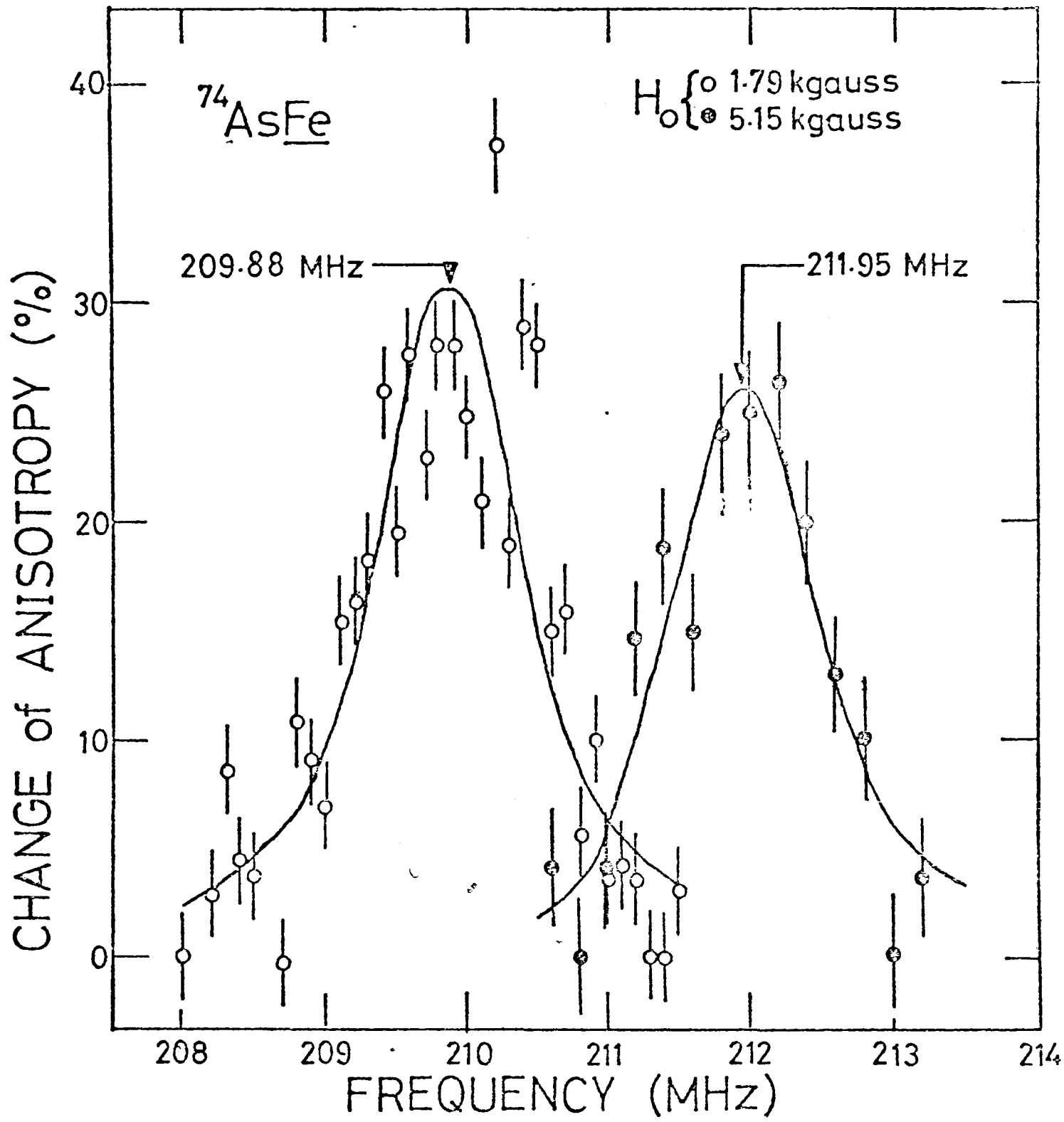



Fig. 4.2 (top)

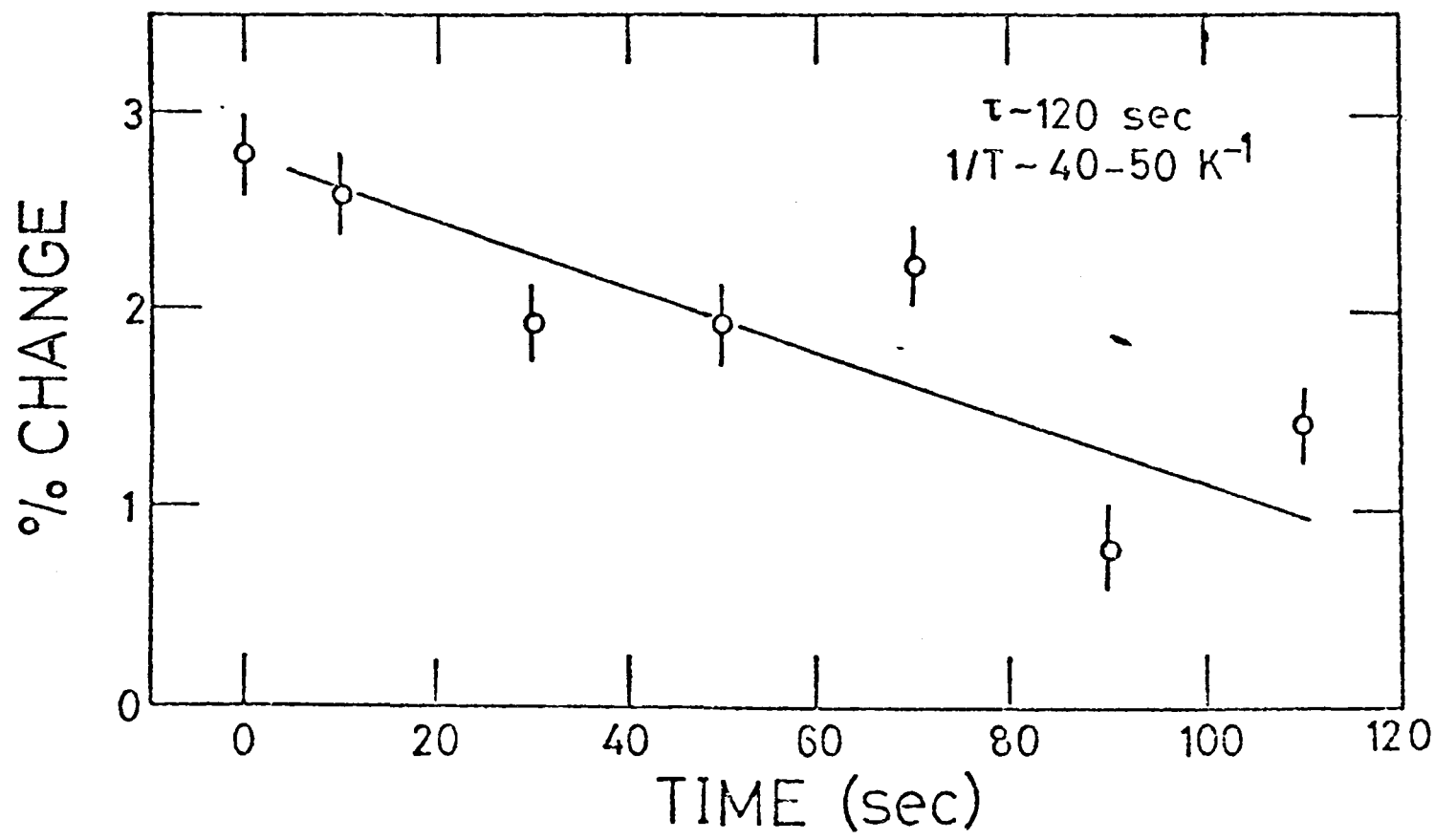



Fig. 4.3 (bottom)

Table 4.2

Magnetic Moments of Some Doubly Odd Nuclei

| Nucleus | Configuration | (n.m.) | ref |
|---|---|---|---|
| $^{74}As$ | $(\pi f_{5/2})^1(\nu g_{9/2})^1$ | (-) 1.597(3) | this work |
| $^{74}As$ | $(\pi f_{5/2})^1(\nu g_{9/2})^3$ | - 0.903(5) | 41 |
| $^{84}Rb$ | $(\pi f_{5/2})^1(\nu g_{9/2})^{-3}$ | - 1.32 (2) | 42 |
| $^{86}Rb$ | $(\pi f_{5/2})^1(\nu g_{9/2})^{-1}$ | - 1.6915(14) | 38 |

An attempt was made to measure $\tau_1$. The $^{74}As$ nuclei were first resonated with FM for 100 sec at a temperature of 0.02 K. The FM was turned off and the relaxation was observed by counting the gamma-rays over 20 sec intervals. The result of ten such runs were added together. These are shown in fig. 4.3. They indicate a relaxation time of

$$\tau_1 = 120(30) \text{ sec.}$$

This value is consistent with the empirical relation found by Reid, Scott and Stone (76). These authors found that

$$\tau_1 \, T \gamma_n^2 \, H^2 = \text{constant} \qquad (4.1)$$

where the constant is $2 \times 10^{18}$ $Oe^2$ sec K within a factor of 2. For $^{74}$AsFe the data gave a value of $4(1) \times 10^{18}$ for this constant. Each of the contributions to the hyperfine interaction (sec 1.III) can contribute to the relaxation process. Campbell(77) has found that eq. 4.1 can be justified if the predominate relaxation mechanism is the interaction between the s conduction electrons and the nuclei. Thus, this probably is the predominate relaxation mechanism of As in the AsFe system.

# CHAPTER FIVE

## Bismuth in Nickel Experiments

### I. Introduction:

This set of experiments was motivated by the desire to investigate the discrepancy in the reported values of the hyperfine fields at Bi and Pb atoms in Fe, Co, and Ni hosts. In recent years, several groups have measured these fields. They have used a variety of preparation methods and have found a variety of results. Their findings are summarized in Table 5.1.

This table suggests that the observed field is dependent on the method of preparation. This view is supported by the channelling experiments of Feldman, Kaufmann, Mingay and Augustyniak (51). These authors looked at the ratio of the yields for aligned and unaligned $^{4}He^{+}$ beams in the Pb Fe and Bi Fe systems. They concluded that Pb and Bi implants are primarily substitutional and that samples annealed at temperatures $\geq 800^{\circ}C$ are interstitial. This means that the substitutional sites have a lower hyperfine field than the interstitial ones.

Two groups of nuclear orientation experiments are reported in this chapter. They are the orientation of $^{206}Bi$ diffused into nickel and of $^{206}Bi$ implanted into nickel. To aid in the interpretation of these experiments, a group of channelling experiments on the BiNi system was also done. A similar set of experiments on the BiFe is reported in the next chapter. $^{206}Bi$ has a known magnetic moment and decay scheme. It should occupy the same crystal site as $^{204}Pb$ and $^{207}Pb$, used in most of the PAC experiments,

Table 5.1

Reported Values of the Hyperfine Fields on Bi and Pb

| System a) | H(kOe) | method of measurement b) | method of preparation | heat treatment | ref |
|---|---|---|---|---|---|
| $^{207}$PbFe | 250(15)<br>273(23) | PAC | electroplate<br>diffused | -<br>5hr @ 800°C | 44 |
| $^{207}$PbFe | 0(70) | PAC | diffused | 1hr @ 600°C | 45 |
| | 480(70) | | | 3hr @ 800°C | |
| | 680(70) | | | 13hr @ 800°C | |
| | 670(70) | | | 31hr @ 800°C | |
| Co | 430(32) | | | 24hr @ 800°C | |
| Ni | 115(15) | | | 24hr @ 800°C | |
| $^{208}$PbFe | 280(70) | PAC | implant by | | 45 |
| Co | 280(70) | | α-recoil | | |
| Ni | 125(35) | | | | |
| $^{207}$PbFe | 610(37) | PAC | diffused | 24hr @ 600°C | 46 |
| $^{204}$PbFe | ≈ 300 | PAC | implant by isotope separator | | 47 |
| $^{207}$PbFe | 650(60) | PAC | diffused | 30hr @ 800°C | 43 |
| $^{204}$PbFe | 262(5) | PAC | diffused | melt,quench | 49 |
| $^{204}$BiFe | 1180(130) | NO | | | |
| Ni | 325(35) | | | | |
| $^{211}$BiNi | 160(30) | PAC | implant by α-recoil | | 50 |

a) $^{204}$Pb and $^{207}$Pb are daughter nuclei of Mismuth isotopes.

b) PAC: perturbed angular correlation, measures field at daughter nuclei.
NO: nuclear orientation, measures field at parent nuclei.

since these lead nuclei are daughters of bismuth nuclei. Nickel was chosen as a host because bismuth is soluble in it. The results of the orientation of $^{206}Bi$ diffused into nickel have been published (52, 53, 54).

The nucleus $^{206}Bi$ decays by electron capture (EC) to $^{206}Pb$ with a half-life of 6.2 days. The decay scheme has recently been studied by Manthuruthil, Camp, Ramayya, Hamilton, Penajian and Doornebos (55) and by Kanbe, Fujioka and Hisatake (56). The results of these two groups are in essential agreement, except the former found more transitions than the latter. In the analysis of the orientation experiments the intensities and log ft values found by Manthuruthil et.al. was used. A simplified decay scheme is shown in fig. 5.1. The transitions studied in this work are shown in bolder lines. The other transitions shown, are those needed for calculating the $U_k$ coefficients. The fractional parentage of the observed transitions are given in the following table.

Table 5.2

Fractional Parentage of the Observed Transitions

| E (keV) | Feeds (keV) | (%) | E (keV) | Feeds (keV) | (%) |
|---|---|---|---|---|---|
| 343 | 314 | 0.4 | 803 | 537 | 31.3 |
| | 516 | 44.7 | | 881 | 68.1 |
| | 1098 | 14.4 | | 1844 | 0.6 |
| | 1595 | 5.5 | 881 | 314 | 0.4 |
| | 1719 | 34.9 | | 516 | 44.7 |
| 398 | 234 | 0.8 | | 1098 | 14.4 |
| | 497 | 61.0 | | 1595 | 5.5 |
| | 620 | 22.8 | | 1719 | 34.9 |
| | EC a) | 15.4 | 895 | EC b) | 100 |
| 497 | EC b) | 100 | 1019 | EC c) | 100 |
| 516 | 184 | 97.0 | 1098 | 234 | 0.8 |
| | 582 | 3.0 | | 497 | 61.0 |
| 537 | 345 | 91.2 | | 620 | 22.8 |
| | 657 | 7.3 | | EC a) | 15.4 |
| | 1904 | 1.5 | 1720 | EC c) | 100 |

a) log ft = 8.5 b) log ft = 6.7 c) log ft = 6.2

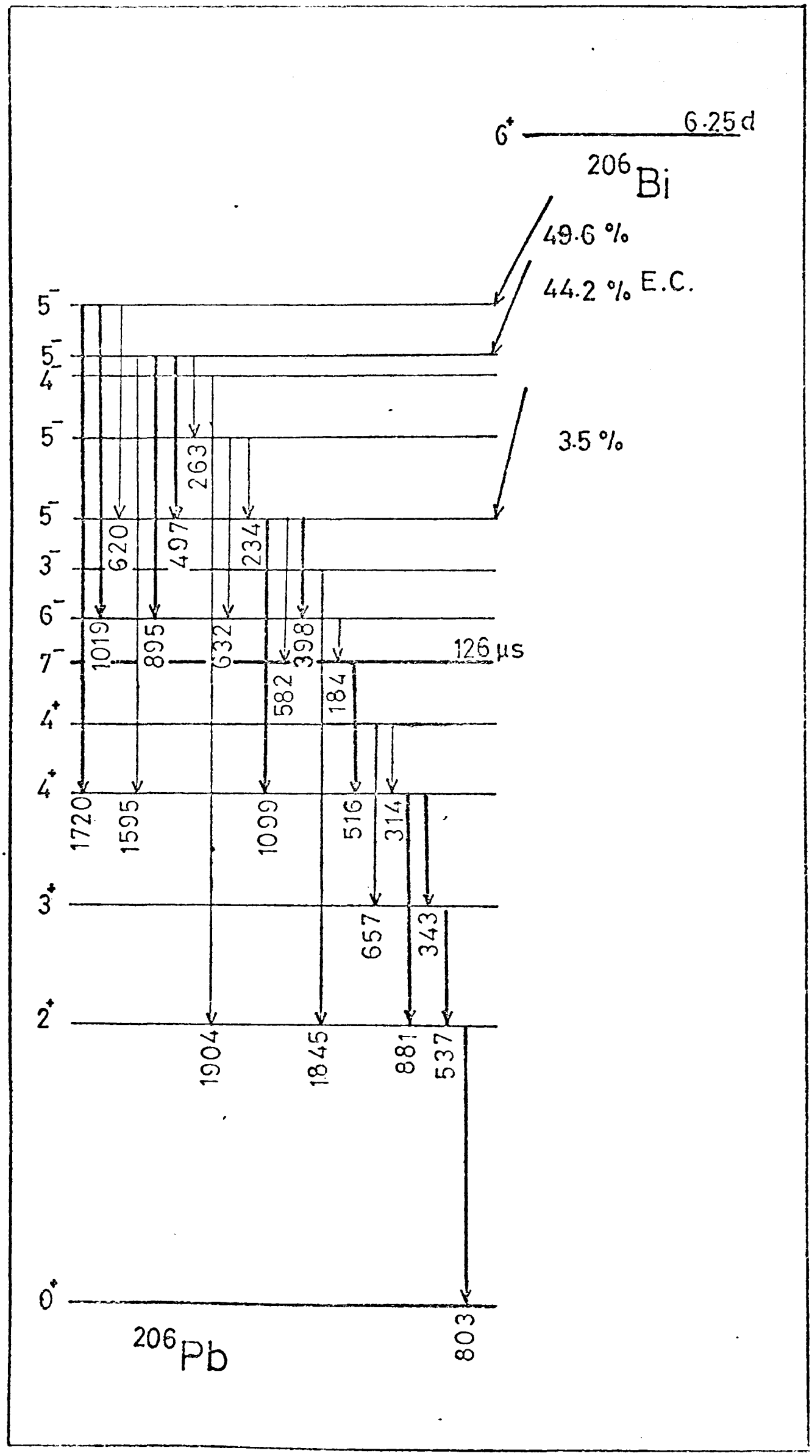

6+
6.25 d
206 Bi
49.6 %
44.2 % E.C.
3.5 %
5-
5-
4-
5-
5-
3-
6-
7-
4+
4+
3+
2+
0+
126 µs
1019
895
632
620
497
263
234
398
582
184
1720
1595
1099
516
314
657
343
1904
1845
881
537
803
206 Pb

Fig. 5.1

An interesting feature of the decay is the 126 μs 2.2 MeV state of $^{206}$Pb. Since the spin-lattice relaxation time is expected to be very much longer than this time, no reorientation effects are expected. One of the aims of these experiments was to confirm this assumption.

## II. $^{206}$Bi Diffused into Nickel

### A. Sample Preparation

The activity came as carrier free $^{206}$BiCl in 1 M HCl. This was diluted with water and electroplated on to 99.9% pure nickel foils. After plating the foils had ≃ 50 μCuries on them, except one which had three times as much. They were then sealed into quartz ampoules containing ~0.1 atm of hydrogen. The foils were melted at 1500°C. Some of the samples were allowed to cool slowly while others were quenched by extracting them from the hot oven and dumping them into a bucket of water. The quenching process took about ten seconds. The samples were etched in dilute $HNO_3$ to remove any surface activity that may have formed. To reduce the demagnetizing field the samples were flattened, first by hammering and then by rolling.

### B. The Hyperfine Field

The anisotropy of eleven gamma-rays were measured in an applied field of 5 kOe over the temperature range 0.15 to 0.015 K. The results were the same for all the samples. This implies that the site occupied by the bismuth atom was independent of the concentrations and heat treatments used. The data indicated that many of the transitions were of mixed multipolarity, as predicted by Kanbe et. al. (56). The data also showed that some reorientation

took place in the 2.2 MeV state, which had not been expected.

The first problem in analyzing the data was to find the hyperfine field. This is a simple procedure if a transition can be found for which the $Q_k U_k F_k$ coefficients are known and if the hyperfine term of the spin Hamiltonian is known. The 1720 keV transition is a suitable one. It is fed by an electron capture transition. The electron capture has a log ft value of 6.2 and can thus be considered to be pure j = 1. The internal conversion measurements of Kanbe et.al.(56) show that the 1720 keV gamma-ray is pure E1. Based on these assumptions, the theoretical orientation parameters are $Q_2U_2F_2 = 0.270$ and $Q_4U_4F_4 = 0.000$. Using these values and assuming that the interaction is pure magnetic, the data was fit for a value of $\mu H$. This is shown in fig. 5.2. From this fit and the known magnetic moment of 4.56 n.m. (57) and correcting for the applied field, the hyperfine field was found to be

$$H = +390(15) \text{ kOe.}$$

This field is assumed to be positive.

Several attempts were made to confirm this field by NMR measurements. However, no resonance was found in either polycrystalline or single crystal samples. The most likely reason for not finding the resonance is that the line was split by a large electric quadrupole interaction. Johnston, Fox and Stone (58) have shown that an electric quadrupole interaction has several important effects on nuclear orientation experiments. They showed that the temperature dependence of the anisotropy can be accurately reproduced by considering a Hamiltonian with an apparent magnetic field of

$$H = H + (2I-1)\ IP/\mu \qquad (5.1)$$

where P is a measure of the quadrupole interaction.

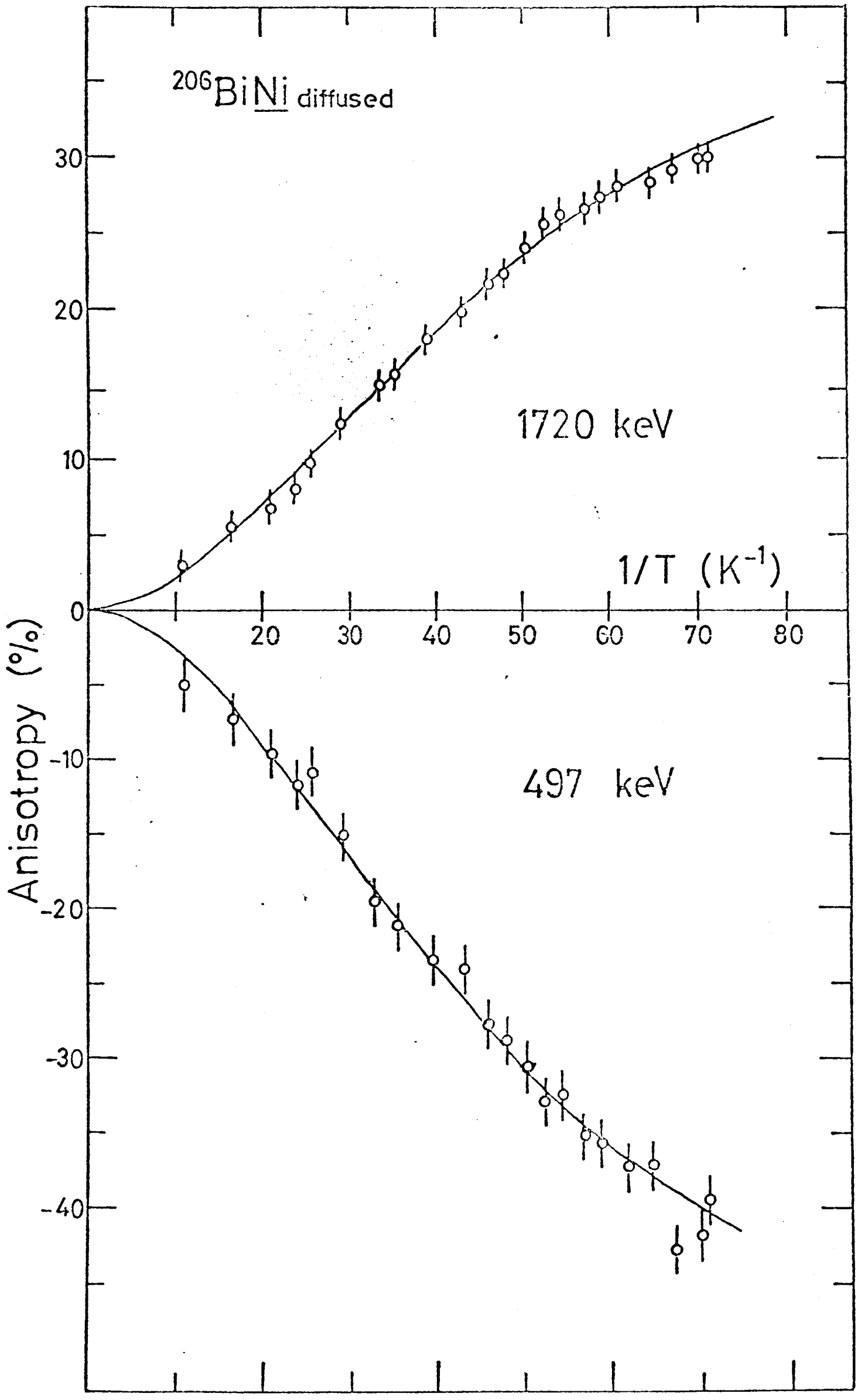

$^{206}$BiNi diffused
1720 keV
497 keV
1/T (K$^{-1}$)
Anisotropy (%)
30
20
10
0
-10
-20
-30
-40
20
30
40
50
60
70
80

Fig. 5.2

$$P = -\frac{3eQ}{4I\,(2I-1)}\,\frac{d^2V}{dz^2} \qquad (5.2)$$

where eQ is the nuclear quadrupole moment and $d^2V/d\,Z^2$ is the electric field gradient. This has the effect of shifting the resonance by the amount (2I-1)P from the frequency expected from the anisotropy data. The resonance is also split into 2I resonances. This splitting combined with the inhomogeneous broadening can completely mask the resonance.

C. Multipolarity Studies.

While the hyperfine field of 390 kOe may only be an average field, the good agreement between the data and the anisotropy calculated for this field, demonstrates that it can be used for the purpose of comparing the other transitions to the 1720 keV one. On this basis, the anisotropies of the other transitions were analyzed by a least squares fitting procedure. Some were analyzed using the multipolarity mixing ratio, $\delta$, as the only parameter, and others by using $Q_2U_2F_2$ and $Q_4U_4F_4$ as independent parameters. The results are summarized in table 5.3 and the mixing ratios are compared to those found by others in table 5.4.

Table 5.3

$Q_2U_2F_2$, and $Q_4U_4F_4$ and $\delta$ fits for H = +390 kOe

| E(keV) | Multipolarity[a] | $Q_2U_2F_2$[c] | $Q_4U_4F_4$[c] | $\delta$ | %[b] |
|---|---|---|---|---|---|
| 343 | M1/E2 | 0.237(4) | -0.007(20) | 0.027(3) | 0.073(15) |
| 398 | M1/E2 | 0.200(3) | -0.013(15) | 0.045(4) | 0.144(20) |
| 497 | M1/E2 | -0.352(4) | 0.000 | -0.09 (2) | 0.8 (3) |
| 516 | E3 | -0.339(6) | -0.006(30) | | |
| 538 | M1/E2 | 0.240(4) | 0.015(15) | 0.033(5) | 0.11(3) |
| 803 | E2 | -0.288(2) | -0.073(10) | | |
| 881 | E2 | -0.292(2) | -0.059(16) | | |
| 895 | M1/E2 | 0.107(3) | 0.040(20) | -0.030(3) | 0.09 (2) |
| 1019 | M1/E2 | 0.127(4) | -0.003(20) | -0.018(3) | 0.032(10) |
| 1099 | E1 | 0.255(5) | 0.005(20) | | |
| 1720 | E1 | 0.271(4) | 0.000(20) | | |

a) L-subshell and internal conversion measurements (56)
b) admixture of higher multipolarity
c) $Q_2 = 0.955$ $Q_4 = 0.860$

Table 5.4

Comparison of M1/E2 Mixing Ratios [a]

| E(keV) | $\delta$[b] | $\lvert\delta\rvert_{max}$[c] |
|---|---|---|
| 184 | | 0.10 |
| 234 | | 0.20 |
| 263 | | 0.11 |
| 343 | 0.027(3) | 0.09 |
| 398 | 0.045(4) | 0.22 |
| 497 | -0.09 (2) | 0.15 |
| 538 | 0.033(5) | 0.17 |
| 620 | | 0.26 |
| 632 | | 0.31 |
| 657 | | 0.48 |
| 895 | -0.030(3) | 0.38 |
| 1019 | -0.018(3) | 0.53 |

a) Using internal conversion measurements Allan (59) found these transitions to be M1.
b) this work
c) L-subshell and internal conversion measurements (56)

The analysis of the transitions that are not fed from the metastable state was straightforward. These are the 1720, 1098, 1019, 895, 497 and 398 keV transitions.

The 1720 and 1019 keV gamma-rays are fed by the same electron capture transition. As already mentioned, the 1720 keV gamma-ray was used to find the hyperfine field. The EC decay was assumed to be pure j = 1 and the 1720 keV to be pure E1. The latter assumption can not be made about the 1019 keV gamma-ray. It was found to be a mixed M1/E2 transition.

The 895 and 497 keV gamma-rays are fed predominantly by an EC decay. This decay has a log ft value of 6.7 and is assumed to be a j = 1 transition. Both gamma-rays show a mixed M1/E2 multipolarity. As an example of the data for these transitions, the data for the 497 keV trnasition is shown in fig. 5.2 with the theoretical curve corresponding to $\delta = -0.09$.

The 1099 and 398 keV transitions fed by three gamma transitions and one EC transition. The unobserved are all predominantly of M1 multipolarity. The $U_k$ coefficients for these transitions are not sensitive to small admixtures of E2 multipolarity since the admixture term is proportional to $\delta^2$. The EC transition has a log ft value of 8.5. This transition, like the other two EC transitions, is assumed to be pure j = 1. Since it has a higher log ft value than the other two, there could be a small admixture of j = 2; but this would not noticably effect the $U_k$. The 398 keV transition was found to be mixed M1/E2 multipolarity. The 1099 keV transition is pure E1, with known $F_k$ coefficients.
The data can therefore be used to check the decay parameters used in the $U_k$ calculations and as a check on the field. The slight

discrepency between the theoretical estimate of 0.246 and the experimental value of 0.254(5) for $Q_2U_2F_2$ is probably due to the difficulty in establishing a reliable background under this peak because of the proximity of the Compton edge from the 1173 keV $^{60}Co$ gamma-ray used in the thermometry. Any admixture of multipolarities of the feeding transitions would result in a reduction of the theoretical $Q_2U_2F_2$ value. It was concluded that the admixtures were small and that the estimate of the field was good.

The $\delta$'s found for all of these transitions were well within the limits found by Kanbe et.al. (56). These are compared in table 5.4.

D. Reorientation of the 2.2 MeV State of $^{206}Pb$:

The transitions that are fed from the metastable state could not be analyzed by the above method. These transitions are the 343, 538, 516, 881, and 803 keV ones. An attempt was made to analyze these gamma-rays in terms of mixing ratios. The data for the 516 keV gamma-ray (fig. 5.3) can be fitted if the transition is assumed to be mixed E3/M4 multipolarity with a mixing ratio of $\delta = 0.51(5)$. This mixing ratio is in conflict with the L-subshell measurements of Kanbe et.al. (56). They found that the 516 keV transition was pure E3. Further evidence against this mixing ratio comes from the analysis of the 881 and 803 keV transitions. These transitions are both pure E2 and have almost identical $U_k$ coefficients. The theoretical anisotropy for these transitions, based on the 516 keV transition being of mixed multipolarity, does not agree with the experimental data (fig. 5.4).

A possible explanation has been put forward by Johnston

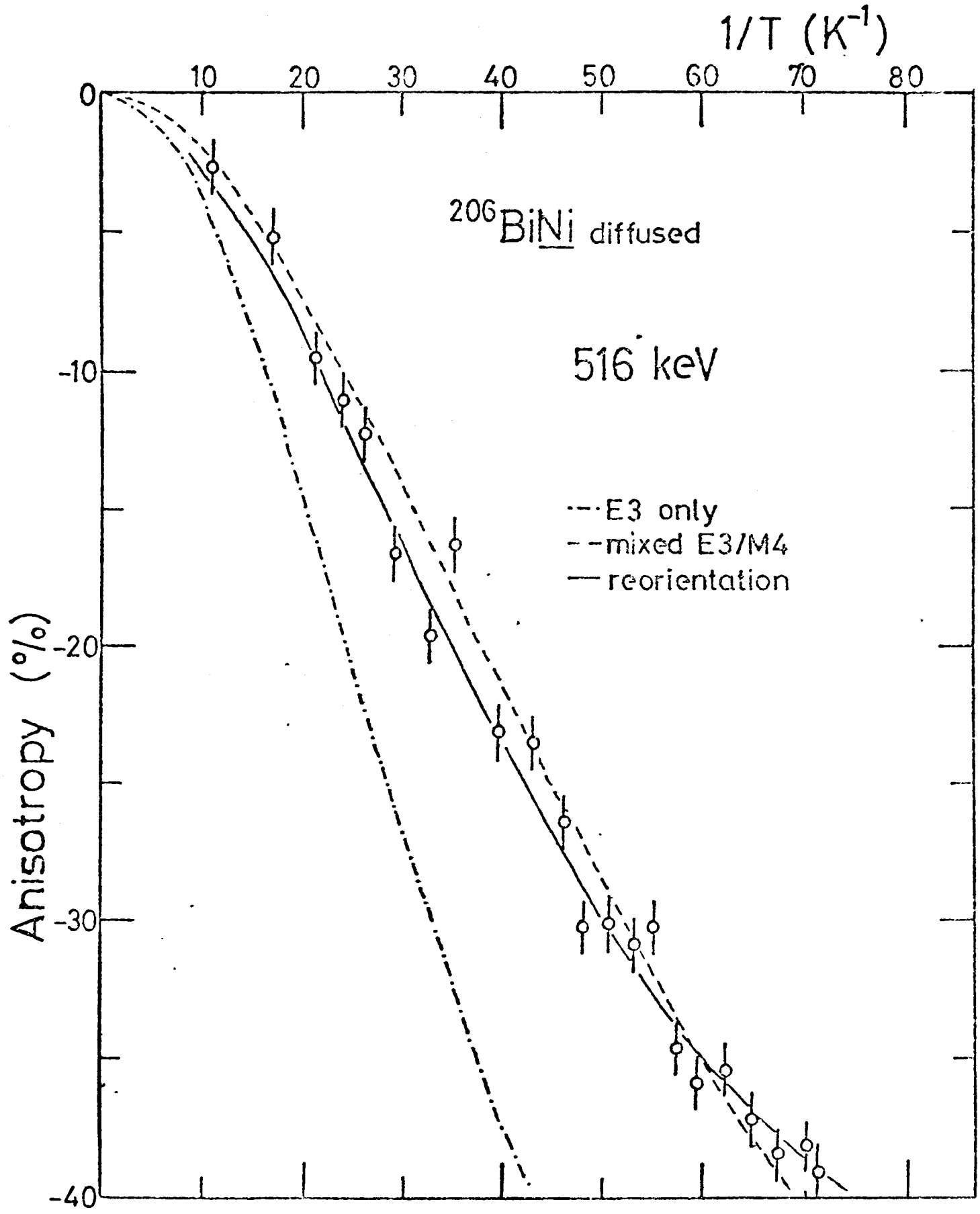

1/T (K$^{-1}$)
10
20
30
40
50
60
70
80
0
-10
-20
-30
-40
Anisotropy (%)
$^{206}$BiNi diffused
516 keV
E3 only
mixed E3/M4
reorientation

Fig. 5.3

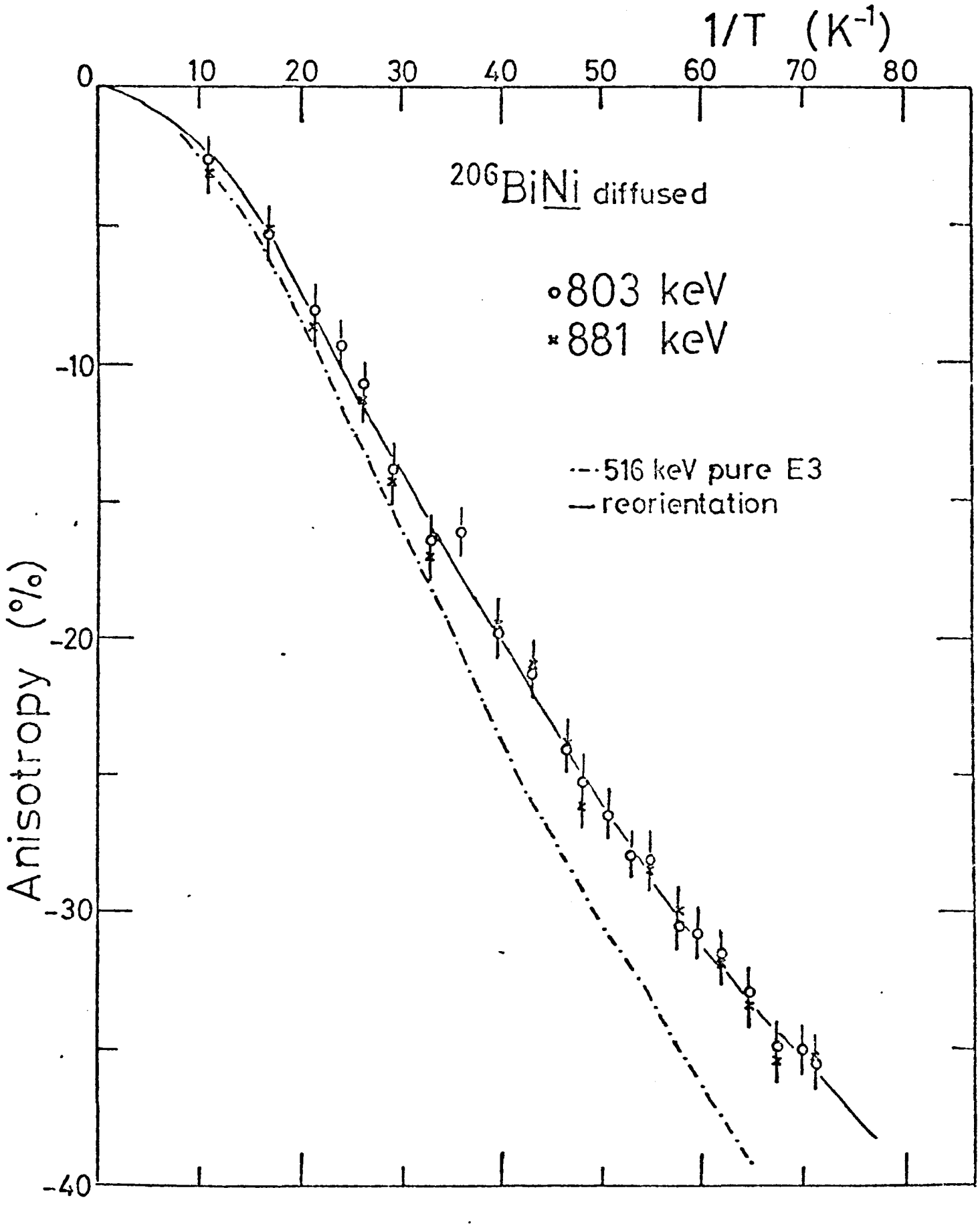

1/T (K⁻¹)
0
10
20
30
40
50
60
70
80
$^{206}$BiNi diffused
•803 keV
×881 keV
---516 keV pure E3
—reorientation
Anisotropy (%)
-10
-20
-30
-40

Fig. 5.4

and Stone (60). They explain the results in terms of a reorientation in the metastable state by an electric quadrupole interaction orientated at random with respect to the magnetic interaction. The metastable state is particularly susceptible to such a perturbation because it has a small Zeeman splitting. The nuclear g-factor for this state is -0.0217 (ref. 61) and the hyperfine field is 115 kOe (45). This results in a Larmour frequency of only 2.3 MHz, two orders of magnitude smaller than typical for impurities in ferro-magnetic hosts.

Johnston and Stone looked at the effect of the Hamiltonian

$$\mathcal{H} = \frac{-\mu_n H I_z}{I} + \frac{3eQV_{zz}}{2I(2I+1)} \left\{ \frac{1}{2}(3\cos^2\phi - 1)\left(I_z^2 - \frac{I(I+1)}{3}\right) \right.$$

$$+ \sin\phi\cos\phi\left[I_z(I^+ + I^-) + (I^+ + I^-)I_z\right]/2$$

$$\left. + \sin^2\phi\,(I^{+2} + I^{-2})/4 \right\}$$

(5.3)

where eQ is the electric quadrupole moment, $\phi$ is the angle between the magnetic axis and the symmetry axis of the electric field gradient and $V_{zz}$ is the electric field gradient along the latter axis. They assumed that the electric field gradient has axial symmetry. This Hamiltonian can be diagonalized to give a set of eigenfunctions $\psi_\lambda$. These can be written in terms of the eigenfunctions, $\chi_n$ , of the Zeeman interaction.

$$\psi_\lambda = \sum_n a_{\lambda n}\chi_n \qquad (5.4)$$

At the instant of formation, the metastable state can be described in terms of the $\chi_n$ states. These states have populations $P_n$, given by the orientation parameters of the preceding decay.

$$P_n = \sum_k (-1)^{k-I-n}\, U_k B_k\, C(I\ I\ -n\ n,\ k0)\ /\ (2I+1)^{\frac{1}{2}} \qquad (5.5)$$

At this time, the population of the $\Psi_\lambda$ states are

$$P_\lambda = \sum_n (a_{\lambda n})^2 P_n \qquad (5.6)$$

Since the $\Psi_\lambda$ are eigenstates of the system, the $P_\lambda$ do not change in time, but the $P_n$ do. Since the lifetime of the metastable state is long compared to the precession period of the nuclear spin, the orientation parameters are determined by the average populations of the $\chi_m$ states, $\overline{P}_m$. This is given by

$$\overline{p}_m = \sum_{\lambda n} (a_{\lambda m})^2 (a_{\lambda n})^2 P_n \qquad (5.7)$$

In terms of the orientation parameters, this is

$$\overline{U_l B_l} = \sum_{\substack{mn \\ \lambda k}} (a_{\lambda m})^2 (a_{\lambda n})^2 U_k B_k \, C(II-nn,k0) \times C(II-mm,l0)(-1)^{k+l-m-n} \qquad (5.8)$$

where $\overline{U_l B_l}$ are the average orientation parameters at the time the state decays. From this, a reorientation coefficient can be defined:

$$A_k(\phi) = \overline{U_k B_k} \,/\, U_k R_k \qquad (5.9)$$

In the temperature region of interest the $A_k$ are not very temperature dependent.

In polycrystalline materials, $\phi$ takes on all values. So, an average reorientation coefficient must be defined:

$$A_k = \tfrac{1}{2} \int_0^\pi A_k(\phi) \sin\phi \, d\phi \qquad (5.10)$$

The data was analyzed in terms of the $A_k$ (tables 5.5 and 5.6, also figs. 5.3 and 5.4). The results for the 516, 803 and 881 keV transitions are consistant. This theory has also been used to account for the reorientation observed in the metastable states

of $^{206}$Pb in the $^{206}$Bi<u>Fe</u> system (see chapter 6) and of $^{207}$Pb in the $^{207}$Bi<u>Ni</u> system (63) by Johnston, Kaplan, and Stone.

Table 5.5

Analysis of 516, 803, and 881 keV Transitions

| E(keV) | Comment | $Q_2U_2F_2$ | $Q_4U_4F_4$ |
|---|---|---|---|
| 516 | Theory, pure E3 | -0.555 | 0.044 |
| | Experiment | -0.339(6) | -0.006(30) |
| 803 | Theory, 516 keV pure E3 | -0.339 | -0.095 |
| and | Theory, 516 keV mixed E3/M4 | -0.331 | -0.085 |
| 881 | Theory, 516 keV with $A_k$ | -0.289 | -0.044 |
| | Experiment | -0.290(2) | -0.066(10) |

Table 5.6

Comparison of $A_k$'s

| E(keV) | $A_2$ | $A_4$ |
|---|---|---|
| 516 | 0.610(12) | -0.11(55) |
| 803 | 0.602(5) | 0.28(30) |
| 881 | | |

The 803 and 881 keV transitions are pure E2 multipolarity. The 343 and 537 keV transitions, which form a parallel feed for the 803 keV transition, are predominantly M1 multipolarity (see below). Thus the 803 and 881 keV transitions have the same orientation parameters. Since these transitions are partially fed by the 516 keV transition, they can be used as an independent check on the reorientation analysis. The data (fig. 5.4 and table 5.6) confirms this analysis.

The 343 and 537 keV transitions were analyzed on the basis of the reorientation of the 2.2 MeV state. They were both found to be mixed M1/E2 transitions (table 5.3). The mixing ratios are within the limits set by Kanbe et.al. (56).

## III. $^{206}$Bi Implanted into Nickel:

### A. Sample Preparation:

The activity was implanted into 99.999% pure nickel single crystals on the Harwell Mk. I electromagnetic separator. Before implantation, the crystals were spark-cut to a size of approximately 1 x 5 x 10 mm. The surface of the crystal was approximately parallel to a {111} plane. The crystals were then electropolished and mounted in the separator. The ion beam was $\simeq 7^{\circ}$ from the surface normal. This was to minimize channelling during the implantation. The bismuth was implanted at 80 keV. The beam current was between 10 and 100 na. The total dose was $\sim 5 \times 10^{14}$ ions/cm$^2$ over the whole crystal. Only a small fraction of the beam was $^{206}$Bi. The beam was probably contaminated with various lead isotopes. The net activity was ~10 μCuries. Two crystals were prepared. One was run without any further preparation. The other one was heat treated before it was run. This crystal was sealed into a quartz ampoule containing ~0.1 atm of hydrogen and heated to 600°C for one hour. This treatment was sufficient to allow the bismuth atoms to move in the crystal but not sufficient to anneal out much of the radiation damage caused by the implantation. About half the activity was lost during the heat treatment.

B. Results:

The data of the nuclear orientation runs was analyzed to find the hyperfine field and the reorientation parameters. The data could not be fit for a unique field, but it could be fit reasonably well if it was assumed that a fraction of the bismuth atoms saw a small field and the others saw the same field as in the diffused samples. The data for the 497 and 1720 keV transitions are shown in fig. 5.5 and for the 516, 803 and 881 keV transitions in fig. 5.6. The data for the 803 and 881 keV transitions have been combined since they have almost identical $Q_k U_k F_k A_k$ coefficients. Each of these and several other transitions were analyzed by a least squares fitting procedure for the fraction in the high field site. The results are given in table 5.6

Table 5.6

Percent in High Field Sites

| E(keV) | un-heated sample (%) | heated sample (%) |
|---|---|---|
| 343 | 68(8) | 15(10) |
| 497 | 85(12) | 25(10) |
| 516 | 78(7) | -20(15) |
| 538 | 85(11) | |
| 803 | | |
| 881 | 79(3) | 20(5) |
| 1720 | 67(7) | 20(5) |
| mean | 77(3) | 20(5) |

The scatter of values for the fraction in high field sites is caused by the weakness of the sample. This results in large statistical errors both in the peaks and in the background under the peaks. Stronger samples were not used because it was

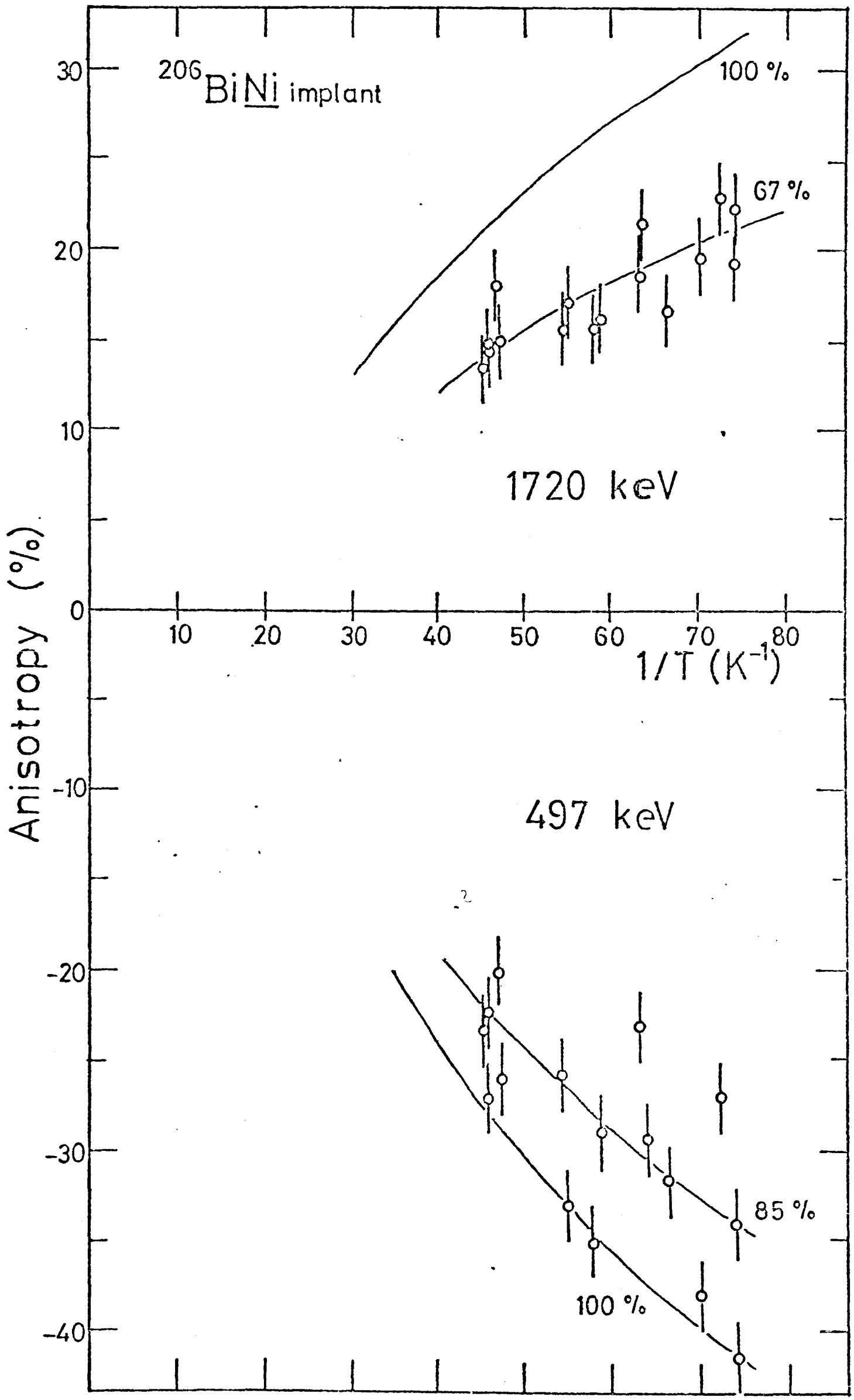

$^{206}$BiNi implant
100 %
67 %
1720 keV
497 keV
85 %
100 %
Anisotropy (%)
1/T (K$^{-1}$)
30
20
10
0
-10
-20
-30
-40
10
20
30
40
50
60
70
80

Fig. 5.5

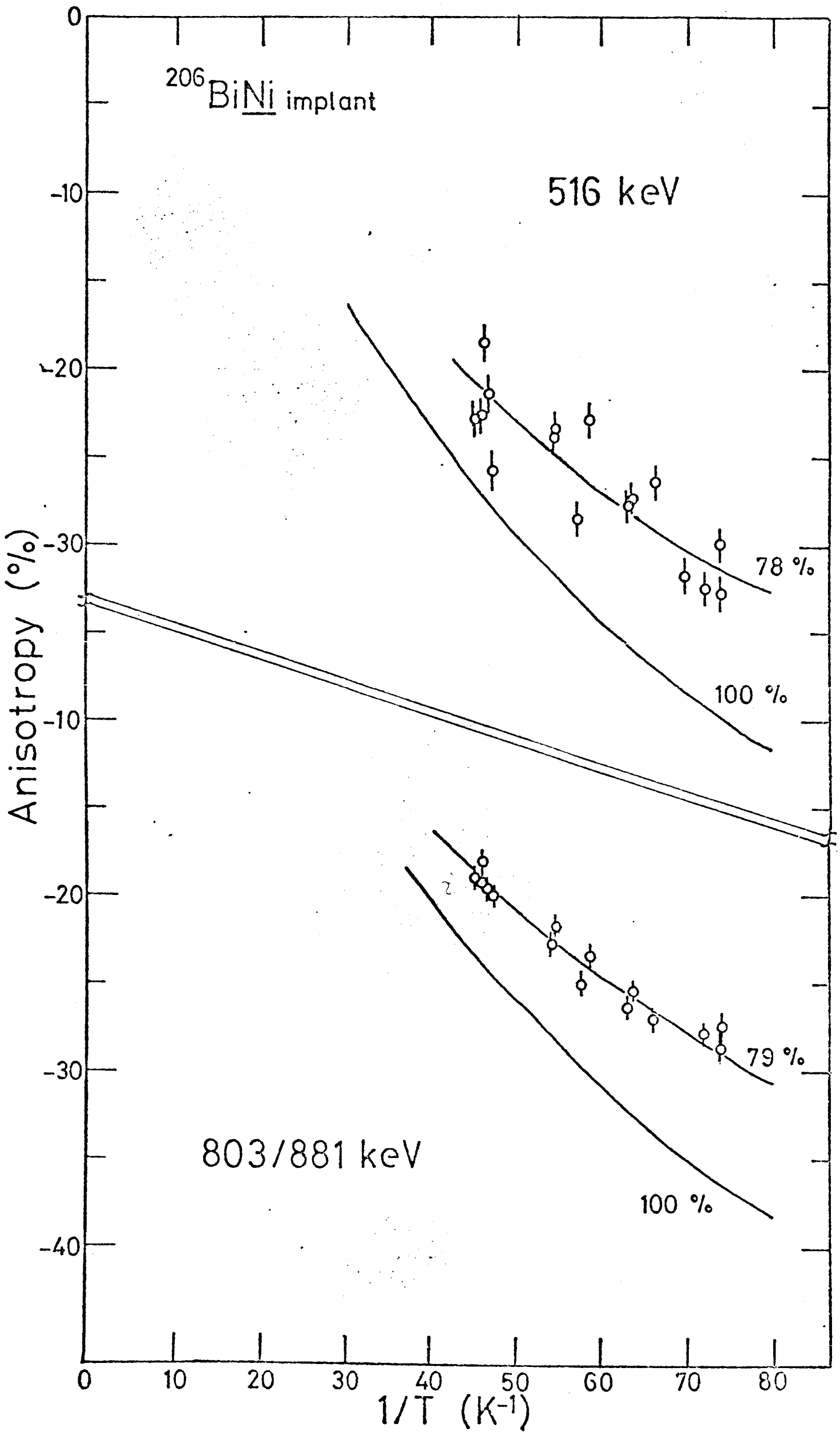

$^{206}$BiNi implant
516 keV
78 %
100 %
79 %
803/881 keV
100 %
Anisotropy (%)
0
-10
-20
-30
-10
-20
-30
-40
0
10
20
30
40
50
60
70
80
1/T (K$^{-1}$)

Fig. 5.6

desired to have the same concentration of impurities in these experiments as in the channelling experiments.

The results are interpreted as indicating that 77% of the implanted ions sit in the same site as in the melted sample. The other 23% are in a low field site. On heating, the bismuth migrates to the low field sites. Approximately 50% of the bismuth left the crystal during the heat treatment. Approximately 20% of the remaining fractions were in high field sites and the other 80% in the low field sites.

## IV. Channelling in Nickel;

### A. Sample Preparation:

Both implanted and diffused samples were studied in these experiments. The implantation was done with stable bismuth at 200 keV. Before the implantation, the nickel single crystals were prepared in the same manner as for the active implants. The diffused samples were made by sealing a piece of bismuth metal along with a nickel crystal into a quartz ampoule containing 0.1 atm of hydrogen. The ampoule was then heated in an oven. After heating the ampoules were allowed to cool slowly. Some of the implanted samples were also heat treated in a similar manner. A summary of the bismuth content and heat treatment used for each sample is given in table 5.7.

Table 5.7

Samples used for Channelling

| Bi Content | | Heat Treatment | Channels Scanned |
|---|---|---|---|
| Implants: | Dose (ions/cm$^2$) | ($^o$C for 1 hr) | |
| | $1 \times 10^{14}$ | none | ⟨111⟩ ⟨110⟩ |
| | $5 \times 10^{14}$ | none | ⟨111⟩ ⟨110⟩ |
| | | 300 | ⟨111⟩ |
| | | 600 | a) |
| | $1 \times 10^{16}$ | none | a) |
| | | 600 | ⟨111⟩ ⟨110⟩ |
| | | 700 | a) |
| Diffused: | Concentration (at %) | ($^o$C for 12 hr) | |
| | 1 | 1200 | a) |
| | | 1400 | a) |

a) quick scans about several directions.

B. The Back Scattering Spectrum:

The channelling was done with 3.5 MeV $^{14}N^+$ ions. For each angular scan, the dead time of the electronics was kept approximately constant by varying the beam current between 1 and 10 nA. The larger currents were used for counts taken near the center of the channel. The counts were taken for a net incident charge of 1 microcoulomb.

The multichannel annalyser was calibrated by taking backscattering spectra from an unimplanted nickel crystal and from a piece of bismuth metal. This procedure was used to correlate channel number with energy and thus with depth inside the samples. This procedure also gave an estimate of the background under the bismuth peak. This was negligible.

The spectra from each angular scan were analyzed by summing the counts in two windows, one on the bismuth peak and one on the part of the nickel spectrum corresponding to the same depth. These sums were then plotted as a function of angle. A typical spectrum is shown in fig. 5.7.

One of the first things to emerge from the spectrum for the unheated "1 x $10^{14}$" and "5 x $10^{14}$" samples was the presence of two bismuth peaks. These peaks are shown in fig. 5.8. The points in this figure are the sum of several runs. The upper peak showed no channelling effect. In this region the bismuth atoms are randomly distributed. The fraction of bismuth in the upper peak is given in table 5.8. This fraction is the same as found in the nuclear orientation experiments in the last section. In the analysis of the other channelling effects the window was set to exclude the upper peak.

Table 5.8

Fraction of Bismuth in the Surface Peak

| Dose (ions/$cm^2$) | Fraction (%) | Method of Measurement |
|---|---|---|
| 1 x $10^{14}$ | 18(3) | channelling |
| 5 x $10^{14}$ | 22(3) | channelling |
| 5 x $10^{14}$ | 23(3) | nuclear orientation |

The correspondence between the fraction in the surface region and the fraction in the low field sites suggests that the low field sites are those in the surface region. A similar surface region has been seen for bismuth implanted in iron (next chapter)

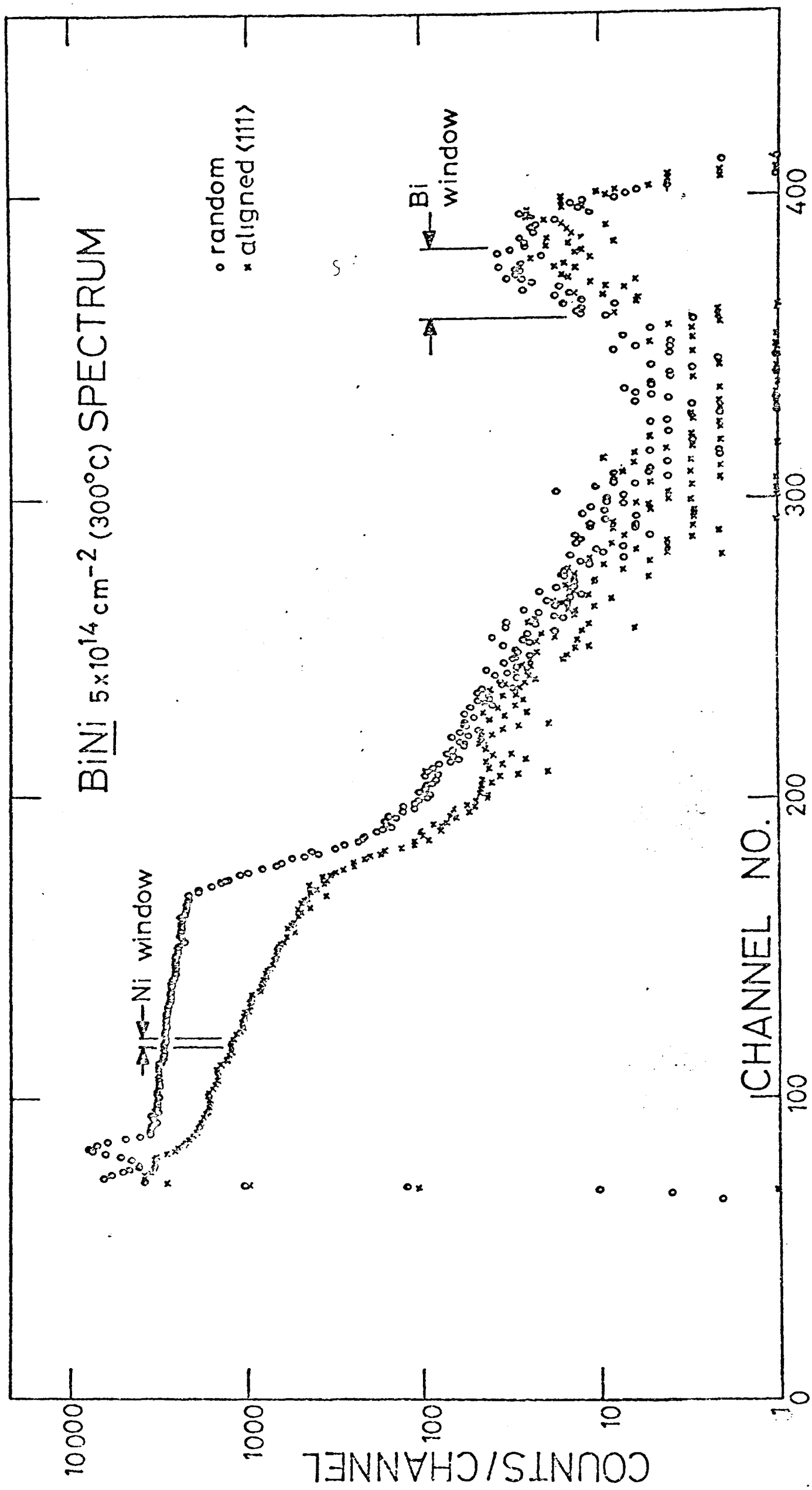

BiNi 5x10^14 cm^-2 (300°C) SPECTRUM
o random
x aligned <111>
Bi window
Ni window
COUNTS/CHANNEL
CHANNEL NO.
10000
1000
100
10
1
0
100
200
300
400

Fig. 5.7

BACKSCATTERING OF 3·5 MeV $^{14}N$ FROM Bi Ni

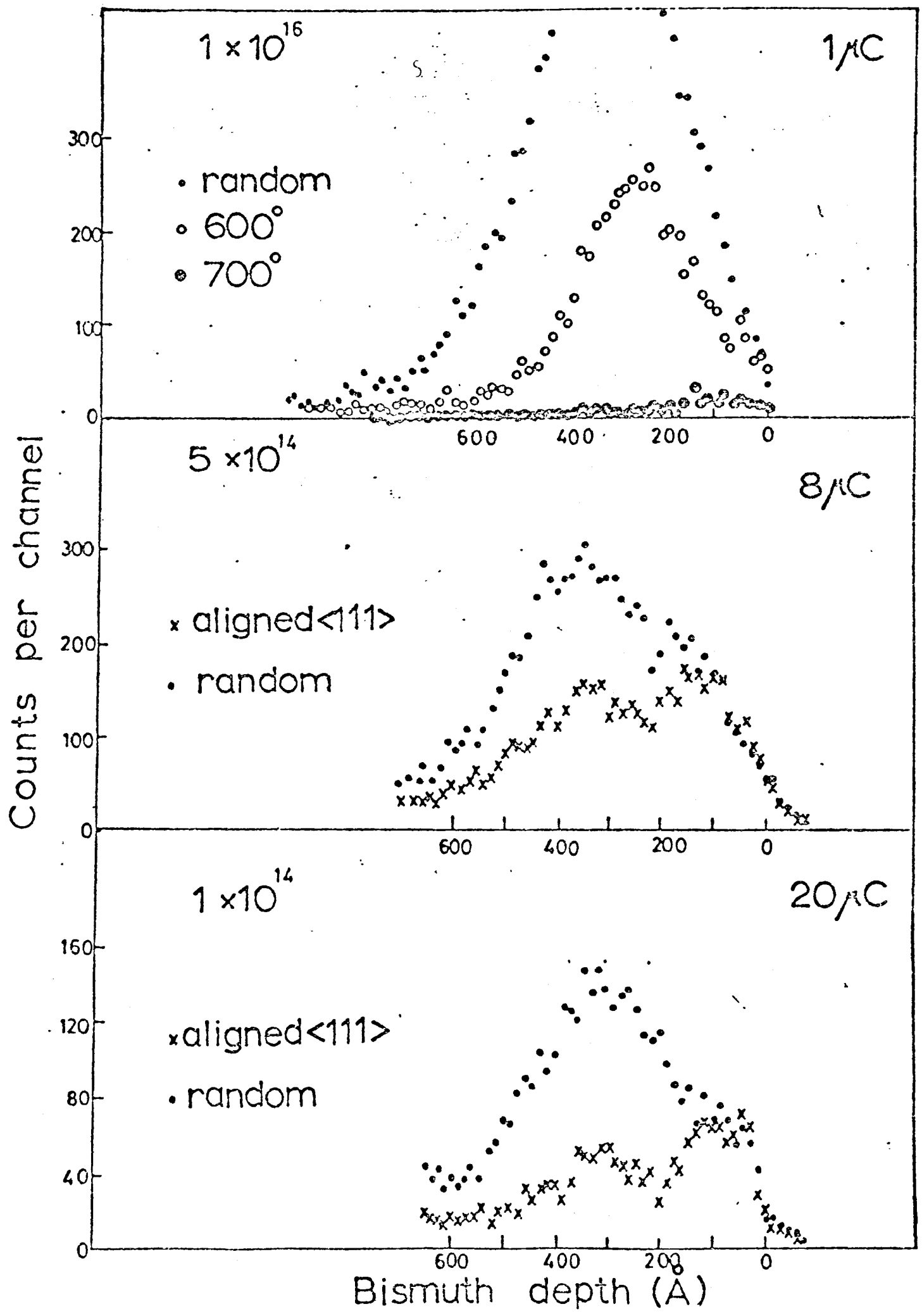



Fig. 5.8

and in copper (63). The absence of this surface region in the melted nuclear orientation sample indicates that this effect is a result of radiation damage.

There are two principal radiation damage mechanisms in ion implantation. One is an internal effect, caused by the stopping of the ion. The other is a surface effect. A review of these damage processes has been given by Nelson (64). The internal damage occurs when the ion is near the end of its trajectory. In this region the ion loses energy by nuclear collisions that displace host atoms. Earlier, the energy loss is by collisions with electrons. This does not cause damage. Thus the region of maximum damage is expected to be the region of maximum ion concentration. So, this mechanism does not explain the bismuth spectrum.

The surface damage mechanism is sputtering. In this process surface atoms are knocked off by incident ions. The number knocked off depends on the type and energy of the incident ion and on the composition of the surface. If the host atoms are preferentially sputtered, the impurities from the region sputtered off can remain to form a surface layer or be driven into the surface where they can form precipitates. Both a surface layer and precipitates would have only a small hyperfine interaction and both would appear to be randomly distributed to a channelled beam. Heating a crystal encourages the formation of precipitates near dislocations. This is especially true when the impurity is very much larger than the host and can not easily fit into the regular lattice. This can be expected for bismuth in nickel, since their Goldschmidt radii

are 1.82 Å and 1.25 Å respectively. The presence of precipitates near the surface would account for both the channelling and the orientation results.

C. The Unheated "1 x $10^{14}$" and "5 x $10^{14}$" Samples:

The results of the scans about the ⟨111⟩ and ⟨110⟩ axes are shown in fig. 5.9 for the 5 x $10^{14}$ ions/$cm^2$ sample and in fig. 5.10 for the 1 x $10^{14}$ sample. The important features of these results are the absence of any structure in the bismuth yields. The yields appear to result from a combination of random and substitutional sites. But, if this were the case the ratio $1 - \chi_{Bi}(0)/1 - \chi_{Ni}(0)$, where $\chi(\phi)$ is the yield at the angle $\phi$, should be the same for all channels. This is not the case, as this ratio of minimum yields is $\simeq 0.5$ for the ⟨110⟩ and $\simeq 0.75$ for the ⟨111⟩ scans. Unique interstitial sites can be ruled out by the lack of structure, and sites slightly displaced from lattice positions can be ruled out since the angular width of the bismuth yields are the same as the nickel yields.

The hyperfine field and channelling results in the XeFe system have been explained by de Waard , (65) in terms of some xenon atoms displaced by nearest and next nearest neighbour vacancies. Computer calculations (66) give the displacement for a nearest neighbour vacancy as $\simeq 1/4$ of the nearest neighbour distance. James (67) has found that this model also explains the effects found in the IFe system. In the FCC nickel lattice the nearest neighbours lie in the [100] directions. In fig. 5.9 the yields calculated for a displacement of 1/4 and 1/5 of the nearest neighbour distance are shown. They show that the single vacancy model does not describe the BiNi system.

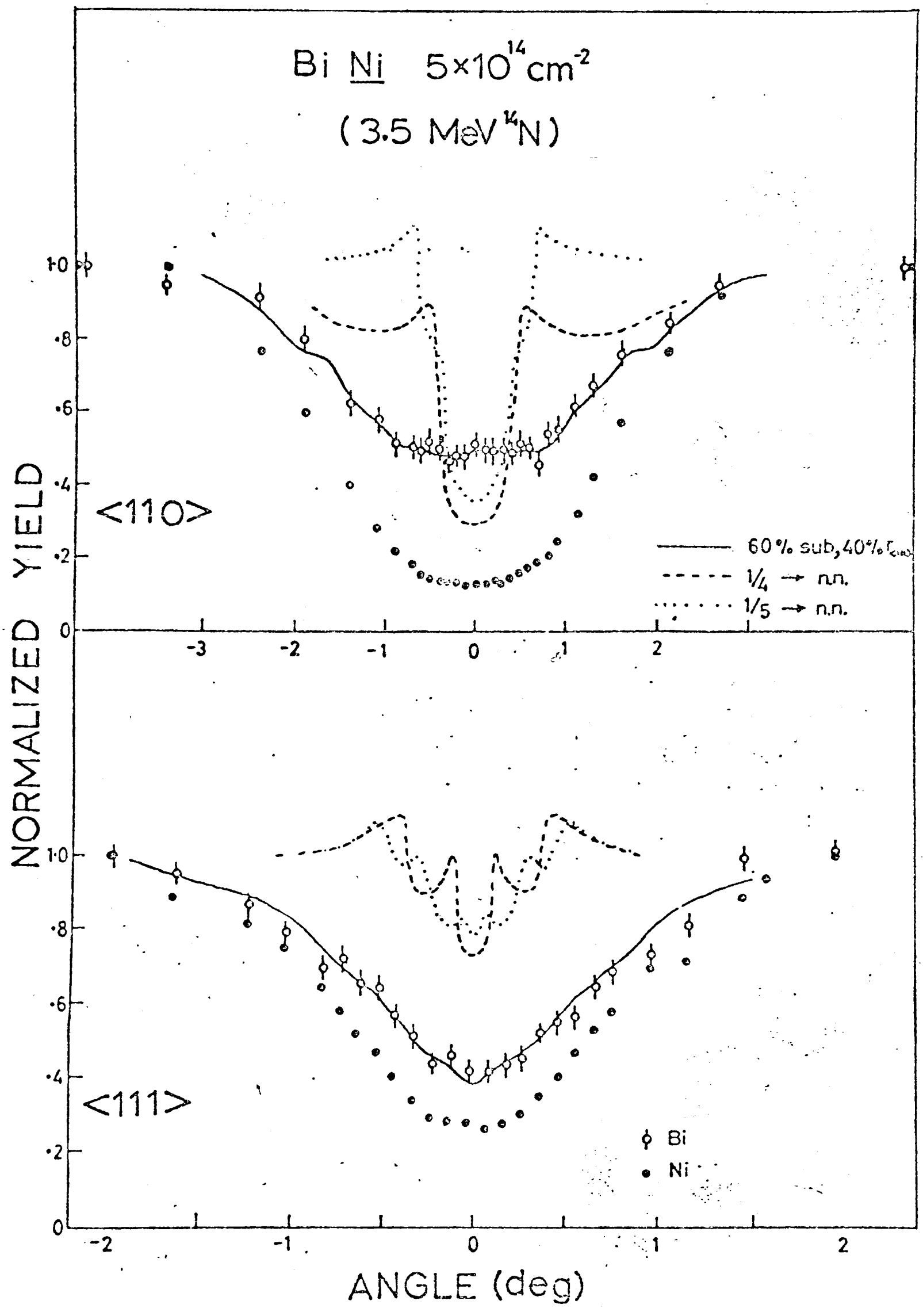

Bi Ni 5×10^14 cm^-2
(3.5 MeV ^14N)
<110>
<111>
YIELD
NORMALIZED
ANGLE (deg)
60% sub, 40% r_rand
1/4 → n.n.
1/5 → n.n.
Bi
Ni
1·0
·8
·6
·4
·2
0
-3
-2
-1
0
1
2

Fig. 5.9

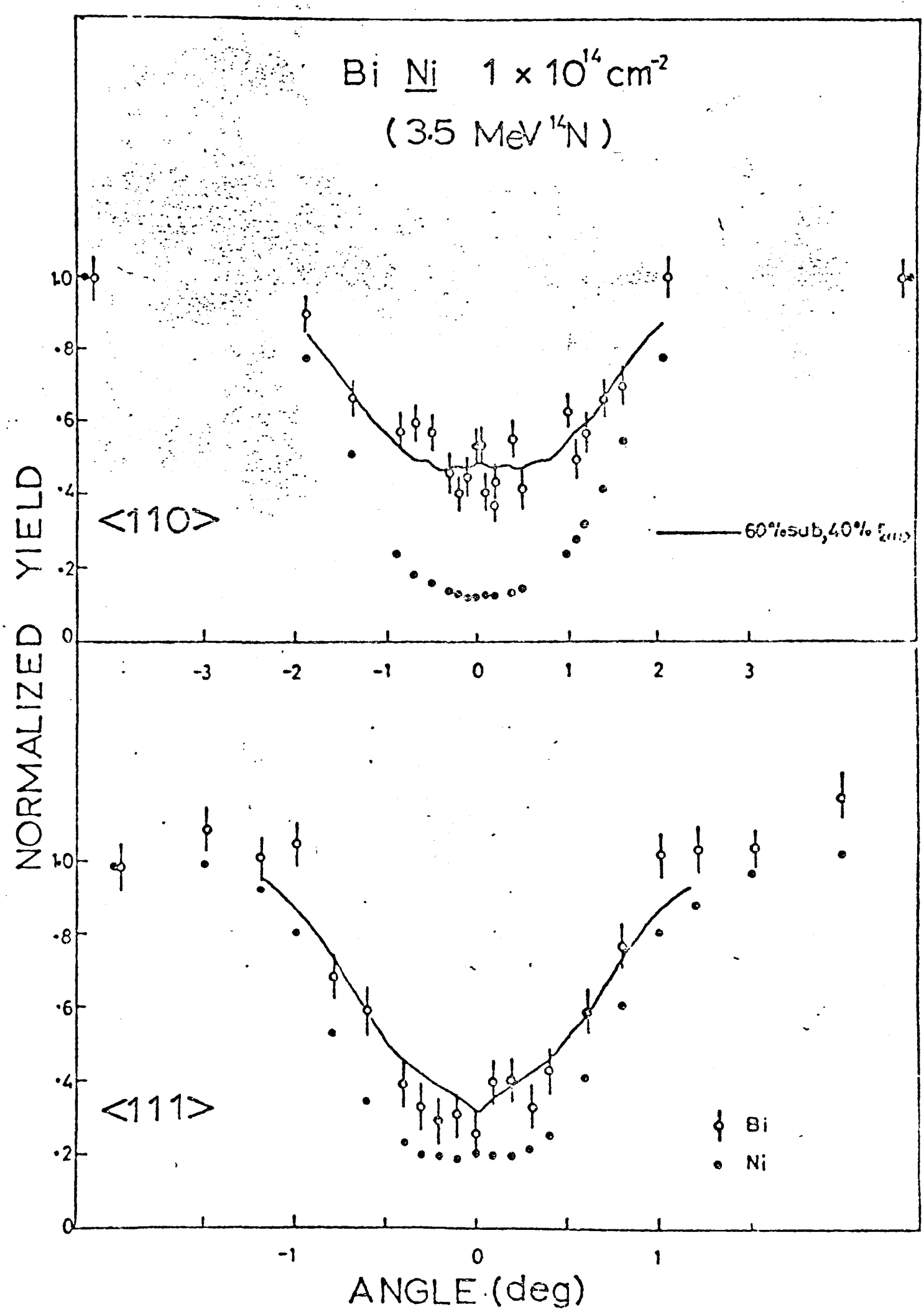
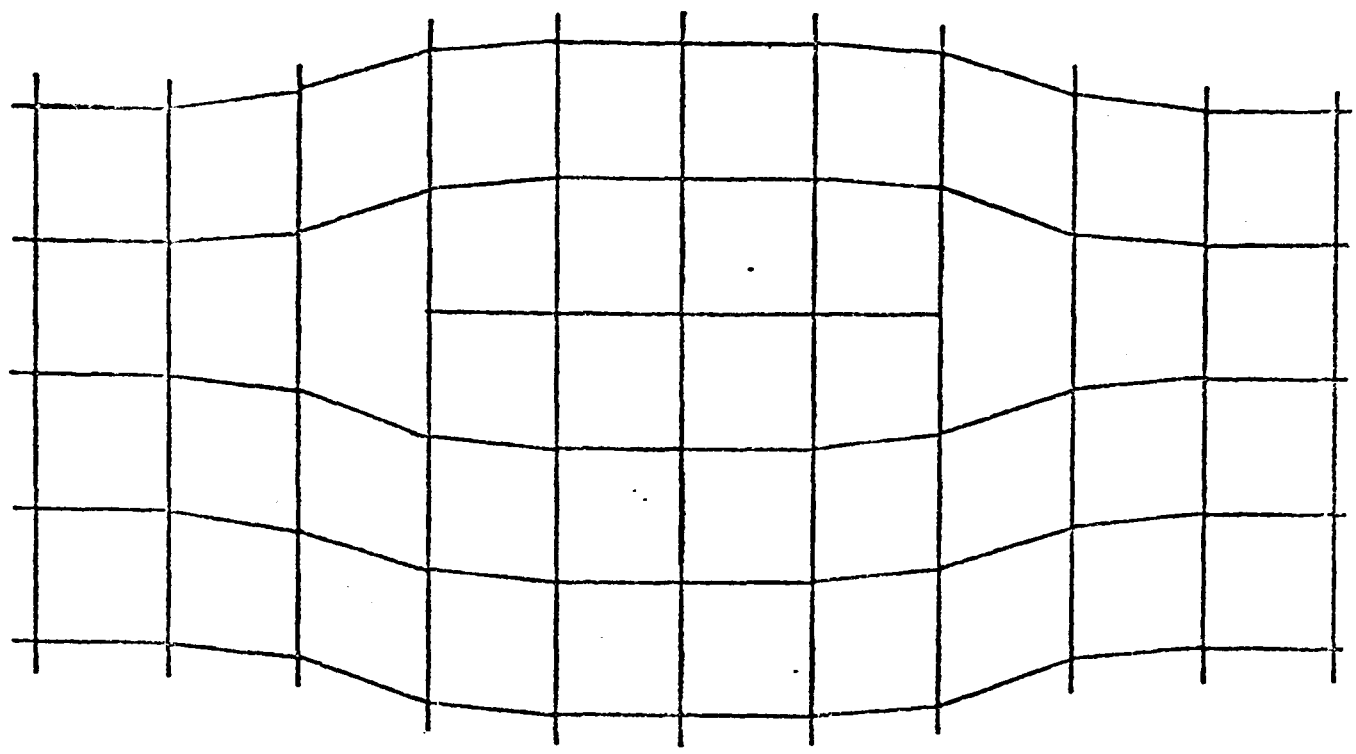

Bi Ni 1 x 10^14 cm^-2
(3.5 MeV 14N)
<110>
60%sub,40% Σ(110)
<111>
Bi
Ni
NORMALIZED YIELD
ANGLE (deg)

Fig. 5.10

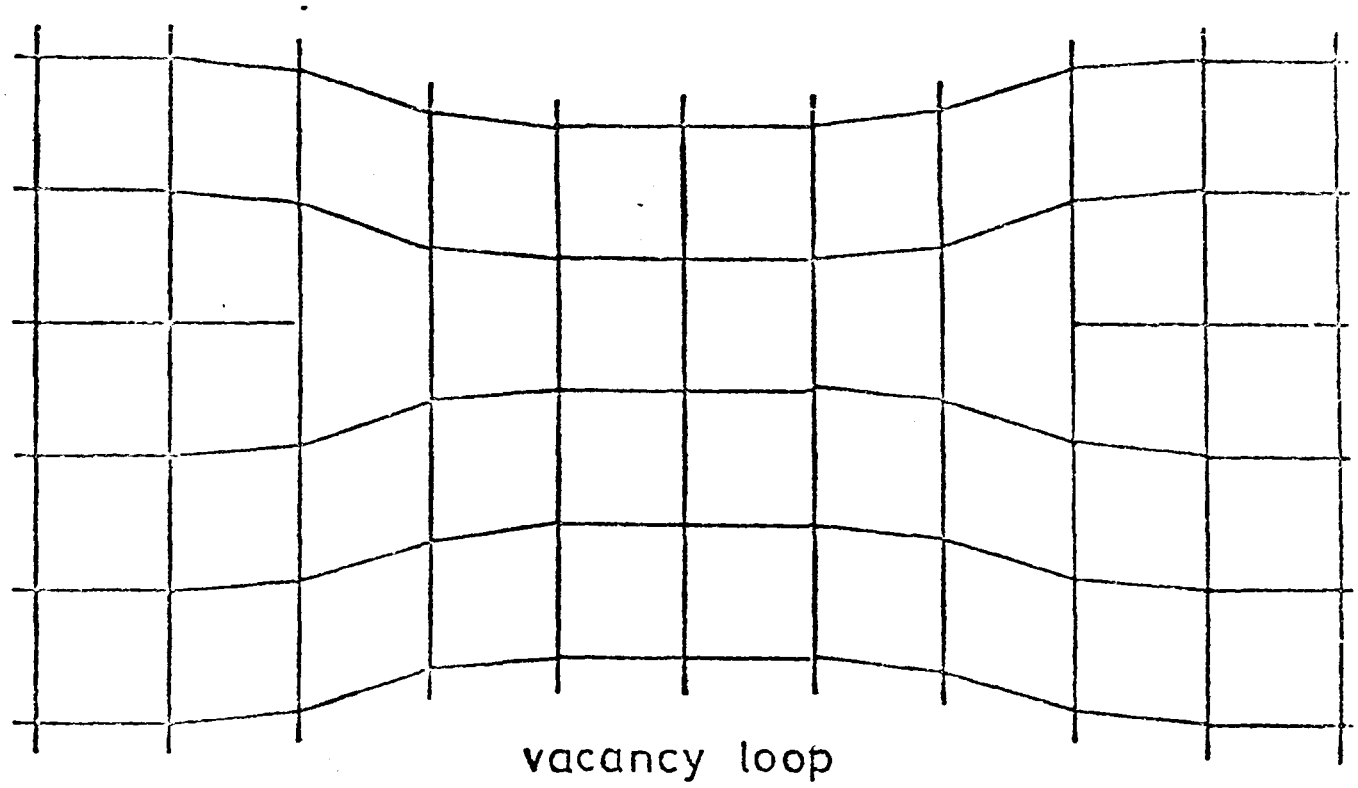
Single vacancies are not the only form of crystal damage present in implanted crystals. Large numbers of dislocation loops are also present. These loops are clusters of interstitials or vacancies. Dislocation loops are shown schematically in fig. 5.11. The properties of these loops have been reviewed by Thompson (68) and by Maher and Eyre (69). Calculations show that these loops have a lower energy than single interstitials or vancancies, and that they form in the close packed planes. These are the {111} planes in a FCC lattice. It has been confirmed that dislocation loops lie in {111} planes by Mazey and Hudson (78) for proton irradiated nickel and by Harbottle (70) for neutron irradiated nickel. The size and number of these loops increases with dose. Dislocation loops are expected in all crystals, no matter what the history of the crystal is.

In the vicinity of these loops the lattice is distorted. This distortion is characterized by a Burgers vector, which represents the displacement of the atoms immediately surrounding the loop from their position in an ideal lattice. For a loop in a {111} plane the Burgers vector is in the [111] direction. The distorted region provides an ideal site for the large bismuth atoms. While the initial position of an implanted ion is substitutional, it is free to move to more favourable sites, by vacancy exchange (64).

Using computer simulations, Morgan and Van Vliet (71) found that a substitutional atom in the distorted region will not appear to be substitutional to a channelled beam. It will appear to be displaced into the channel. The displacement is principally in the direction of the Burgers vector. Atoms near the edge of



interstitial loop



vacancy loop

Dislocation Loops

each line represents
a plane of atoms

Fig. 5.11

the loop, the region of maximum distortion, will have a displacement component parallel to the loop.

In the light of these considerations, the following model is proposed. Most of the bismuth atoms are substitutional in sites more than a few lattice spacings away from a defect. The remaining atoms are substitutional or slightly displaced from substitutional in the distorted region associated with dislocation loops. These sites are displaced principally along a ⟨111⟩ axis from where they would be if the loop did not exist. Computer calculations were made on the assumption that these are distributed uniformly along the ⟨111⟩ axes and in a Gaussian off these axes. The Gaussian was of the form $\exp(-x^2/a^2)$, where x is the distance away from the axis and a is a characteristic distance. Using this model the data could be fit if it was assumed that 60% of the bismuth was pure substitutional, 40% was near dislocation loops, and was characterized by a = 0.35 Å. This distance is small compared to the nearest neighbour distance of 2.49 Å. The calculated yields are shown in fig. 5.9 and fig. 5.10. The calculated yields are not very sensitive to the exact form of distribution assumed. The data could certainly be fit with other distributions as long as such a distribution was predominantly along the ⟨111⟩ axes.

D. The Heat Treated "5 x $10^{14}$" Samples:

On heating, the bismuth migrated away from the inner region and left the crystal. The lower peak in the 300°C sample was reduced to approximately 1/4 of its former heigth. In the 600°C sample the lower peak had completely disappeared. In this sample the only remaining bismuth was in the surface region.

The data for the 300°C sample is shown in fig. 5.12 along with the yields calculated for the model. The calculated yields reasonably fits the data.

E. The "1 x $10^{16}$" Samples:

The unheated sample showed no dips in the bismuth yields. The distribution of bismuth atoms was totally random. This is probably due to the large amount of damage caused by the high dose. Heating the crystal, again resulted in the migration of the bismuth to the surface. Less than half of the bismuth remained after heating to 600°C, and only a small fraction remained in a surface peak after heating to 700°C. This is shown in fig. 5.8.

The sample heated to 600°C did show an effect in the bismuth yields. Heating to 600°C removes some of the damage by increasing the mobility of vacancies and dislocation loops (64,69). The results for this sample are shown in fig. 5.13. Also shown are the calculated yields for 25% pure sutstitutional and 75% along ⟨111⟩ axes. The fit is not as good as for the lower dose samples. In this sample some of the dislocation loops may no longer lie in the ⟨111⟩ planes. Large loops rotate out of the close packed planes by shearing. When this happens in FCC crystals, Bullough and Foreman (72) have shown that the Burgers vector will change from the [111] direction to the [110] direction. This has been observed in aluminium crystals by Makin and Hudson (73) and by Strudel and Washburn (74). The disagreement between the calculated yields and the data for this sample is probably a result of some of the Burgers vectors changing orientation. This would result in some of the bismuth being distributed along the ⟨110⟩ axes.

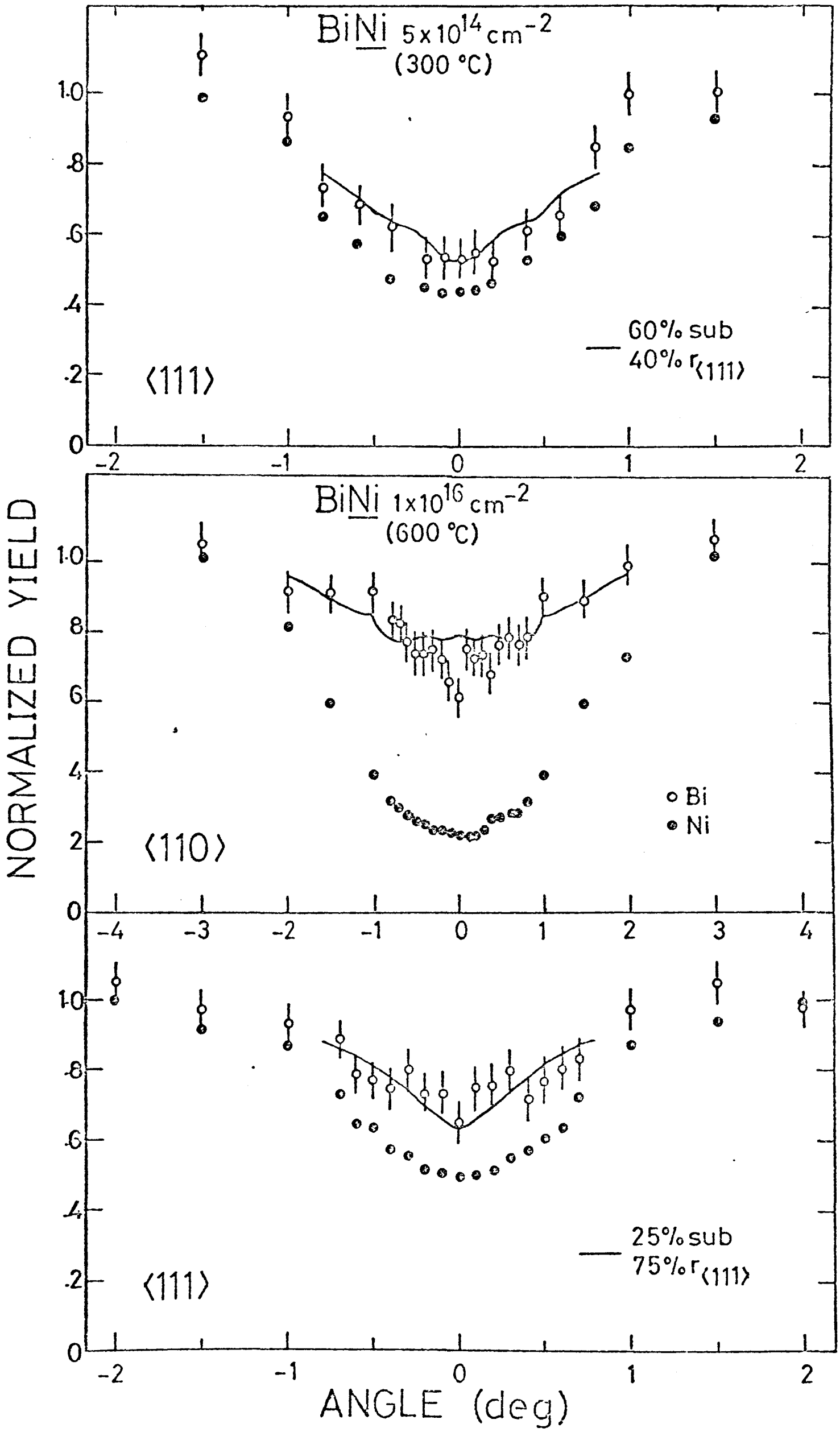



Fig. 5.12 (top)
Fig. 5.13 (bottom)

F. The Diffused Samples:

Dispite the fact that bismuth is supposed to be solubile in nickel (43), the only bismuth seen in the back scattering spectrum of the diffused samples was a surface peak. This peak showed no channelling effect. A mono-layer of bismuth would account for this peak. During the heating process the bismuth was probably in a vapour, which condenses on the surface of the crystal and on the surface of the ampoule while cooling. The large size of bismuth atoms, probably means that it is only soluble in trace amounts in nickel crystals. The nuclear orientation samples were made from melts. So, bismuth must be soluble in melted nickel and these samples cooled faster than the bismuth could diffuse out.

V. Summary:

The hyperfine field on bismuth in nickel was found to be 390(15) kOe for both diffused and implanted samples. This is significantly larger than the value of 325(35) kOe found by Bacon, Hass, Kaindl and Mahnke (49). The discrepancy is outside the range of assigned errors. This is thought to reflect larger uncertainties than assigned by them (75). Reorientation effects were found in the metastable state of $^{206}Pb$. The effect was the same for the diffused and the implanted samples. Johnston and Stone (60) have interpreted this in terms of a quadrupole interaction oriented at random with respect to the magnetic interaction. They found that the reorientation could be accounted for by a quadrupole interaction strength of

$$\frac{3\ eQ\ V_{zz}}{4(2I-1)\ \mu_n H} = +0.112(5) \text{ or } -0.098(5)$$

While they assumed a unique interaction strength, this is not necessary. The reorientation can also be accounted for by applying their theory to a distribution of interaction strengths.

The channelling data indicates that 22(3)% of the bismuth in the 5 x $10^{14}$ ions/$cm^2$ sample were randomly distributed near the surface. This corresponds to the 23(3)% that the orientation runs showed to be in low field sites. The bismuth in the surface region are probably in the form of precipitates or of a surface layer. It was assumed that the measured hyperfine field corresponds to the sites occupied by the atoms not in the surface region. The channelling indicated that these sites were 60% substitutional and 40% distributed along the ⟨111⟩ axes. This distribution could be accounted for by the proximity of dislocation loops. These loops can have both thermal and implantation origins. Similarity between the channelling results for the 1 x $10^{14}$ and 5 x $10^{14}$ ions/$cm^2$ doses, suggests that the loops are not very dose dependent for those doses and that they can be expected to be the same in the thermally prepared samples. The 1 x $10^{16}$ ions/$cm^2$ sample did show a dose dependent effect. In this sample some of the Burgers vectors probably changed direction from the ⟨111⟩ to the ⟨110⟩ direction.

Sites in the distorted region near these loops can be expected to have a large electric field gradient. This would result in a distribution of electric quadrupole interactions. Which, in turn accounts for the reorientation effect. This also implies that the quadrupole interaction strength found by Johnston and Stone is some sort of average. These sites would also be expected to have a different magnetic hyperfine field than the purely

substitutional ones. Thus there is a distribution of fields. This means that the measured magnetic field is also an average. The distribution of magnetic and electric fields would account for the absence of a resonance in the NMR runs.

Both nuclear orientation and channelling experiments were necessary to understand the BiNi system. The two methods were complementary.

# CHAPTER SIX:

## Bismuth in Iron

### I. Introduction:

This set of experiments is a repetition, in an iron host, of the BiNi experiments. Two groups of nuclear orientation experiments are reported in this chapter. They are the orientation of $^{206}Bi$ diffused into iron and of $^{206}Bi$ implanted into iron. To aid in the interpretation of these experiments, a group of channelling experiments was also done. In the analysis of the orientation data, the multipolarity mixing ratios found in the last chapter were used. The analysis was not straightforward in these experiments. There was a difficulty in establishing the background under the peaks in the gamma-ray spectra. Including the two $^{60}Co$ gamma-rays, there are twenty gamma-rays with appreciable intensities. Many of these gamma-rays had a large anisotropy in these experiments. The background under each peak shows an anisotropy which is dependent on the anisotropies of all the higher energy gamma-rays. The background can not be measured under a peak, but only estimated from the background near the peak. All of this, results in a large temperature dependent error in the estimated background. This was less of a problem in the BiNi experiments because the anisotropies were less in those experiments.

The large near saturation of the anisotropies also caused another difficulty. The least squares fitting procedures used in the analysis fitted the data for two parameters at a time. These were either the field and the percentage of Bi nuclei in that field

or the two attenuation coefficients, $A_2$ and $A_4$. The fitting procedures assume that the two parameters are independent of each other. This was not a good assumption for these experiments. This means that the errors calculated from the RMS deviation of the data from the fitted curve are underestimates.

At room temperature bismuth is only soluble in trace amounts in iron. Its solubility is probably the cause of the variety of hyperfine fields reported for PbFe (table 5.1).

II. $^{206}$Bi Diffused into Iron:

The samples were prepared from melts, as the nickel samples had been. Approximately 50 μCuries of activity was electroplated onto 99.98% pure iron foils. The foils were then sealed into quartz ampoules and melted at 1550°C. Some of the samples were allowed to cool slowly, while others were quenched in about 10 seconds by extracting them from the hot oven and dumping them into a bucket of water. The samples were then etched in dilute $HNO_3$ and flattened by hammering and rolling.

Almost all of the activity on the slowly cooled samples was on the surface. There was insufficient activity inside these samples to do a nuclear orientation experiment. It is thought that the bismuth diffused out of the iron as it cooled. This is a result of the room temperature insolubility of bismuth in iron.

The quenched sample did show an effect. The 1720 and 497 keV transitions were analyzed for the hyperfine field and the percent in that field. The 516, 803 and 881 keV transitions were analyzed for the attenuation coefficients. The results are summarized in the following table.

Table 6.1

Quenched $^{206}$BiFe Fits

| $E_{keV}$ | Fraction (%) | Field (kOe) | $A_2$ [a] | $A_4$ [a] |
|---|---|---|---|---|
| 497 | 80(4) | 760(50) | | |
| 1720 | 74(2) | 1030(40) | | |
| 516 | | | 0.97(3) | 3.2(4) |
| 803 | | | | |
| 881 | | | 1.07(17) | 0.8(4) |
| mean | 77(3) | 900(140) | 0.98(4) | 20(12) |

a) The attenuation coefficients were calculated using the mean values for the field and the fraction in that field. The errors shown do not take into account the errors in those mean values.

The data for the 497 and 1720 keV transitions is shown in fig. 6.1. Also shown are the curves for 77% of the bismuth in 900 kOe sites. These curves are reasonable fits to the data. The data for the 516, 803 and 881 keV transitions are shown in fig. 6.2. Also shown are the curves corresponding to the best fit, to the mean attenuation values and to no attenuation. The curve for the mean values is not a goot fit to either set of data. The 803 and 881 keV data can be fit assuming no attenuation. However, this curve does not fit the 516 keV data. The difficulty in finding a fit for both sets of data is probably a combination of the difficulty in estimating a background under the peaks and of the errors in the mean values of the field and fraction in that field. Qualitatively, the data indicates a small amount of reorientation in the metastable state.

III. $^{206}$Bi Implanted into Iron:

The activity was implanted at 80 keV into 99.98% pure iron single crystals. Before theimplantation, the crystals had been spark cut to a size of approximately 1 x 5 x 10 mm. The

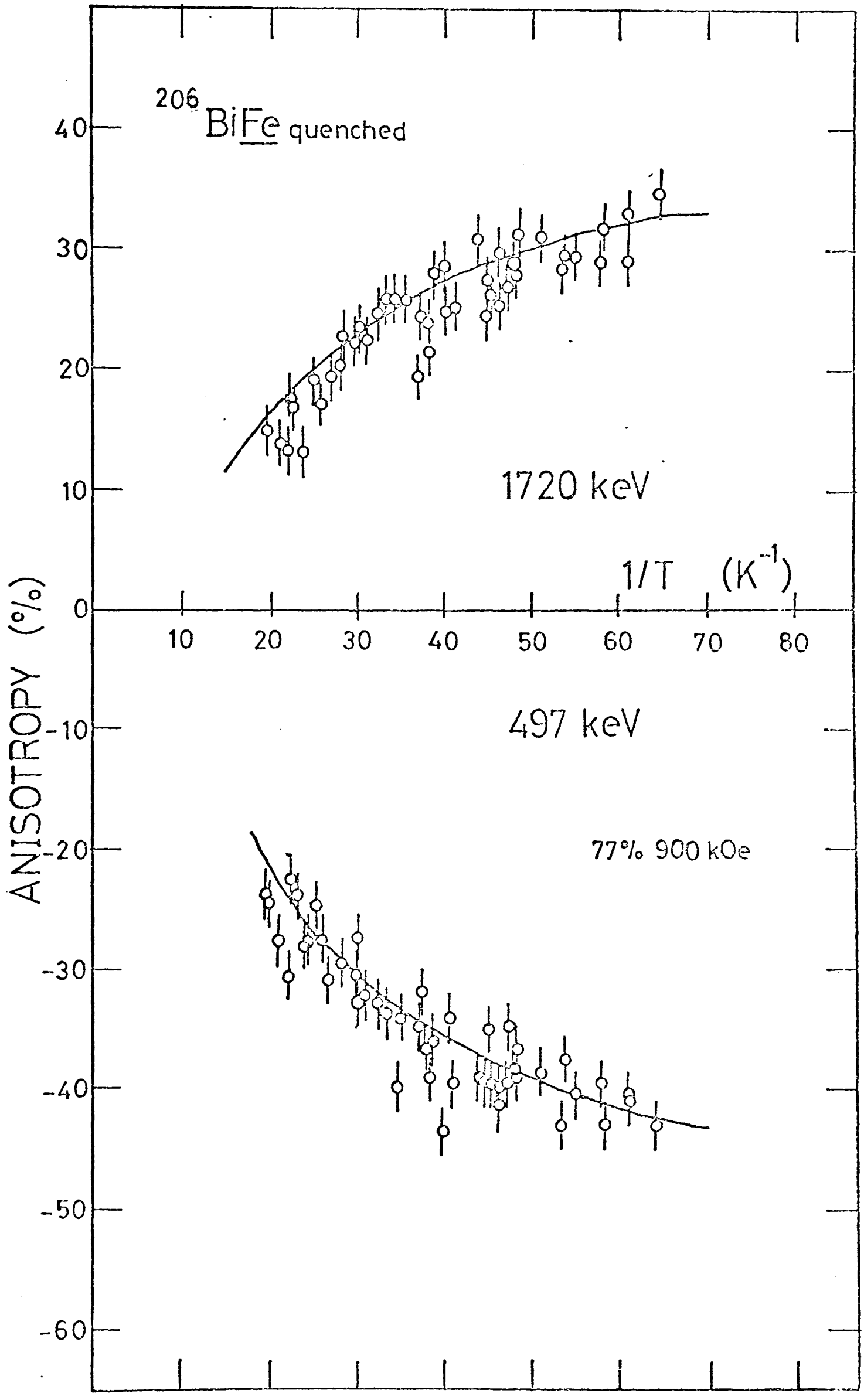

$^{206}$BiFe quenched
1720 keV
497 keV
77% 900 kOe
1/T (K$^{-1}$)
ANISOTROPY (%)
40
30
20
10
0
-10
-20
-30
-40
-50
-60
10
20
30
40
50
60
70
80

Fig. 6.1

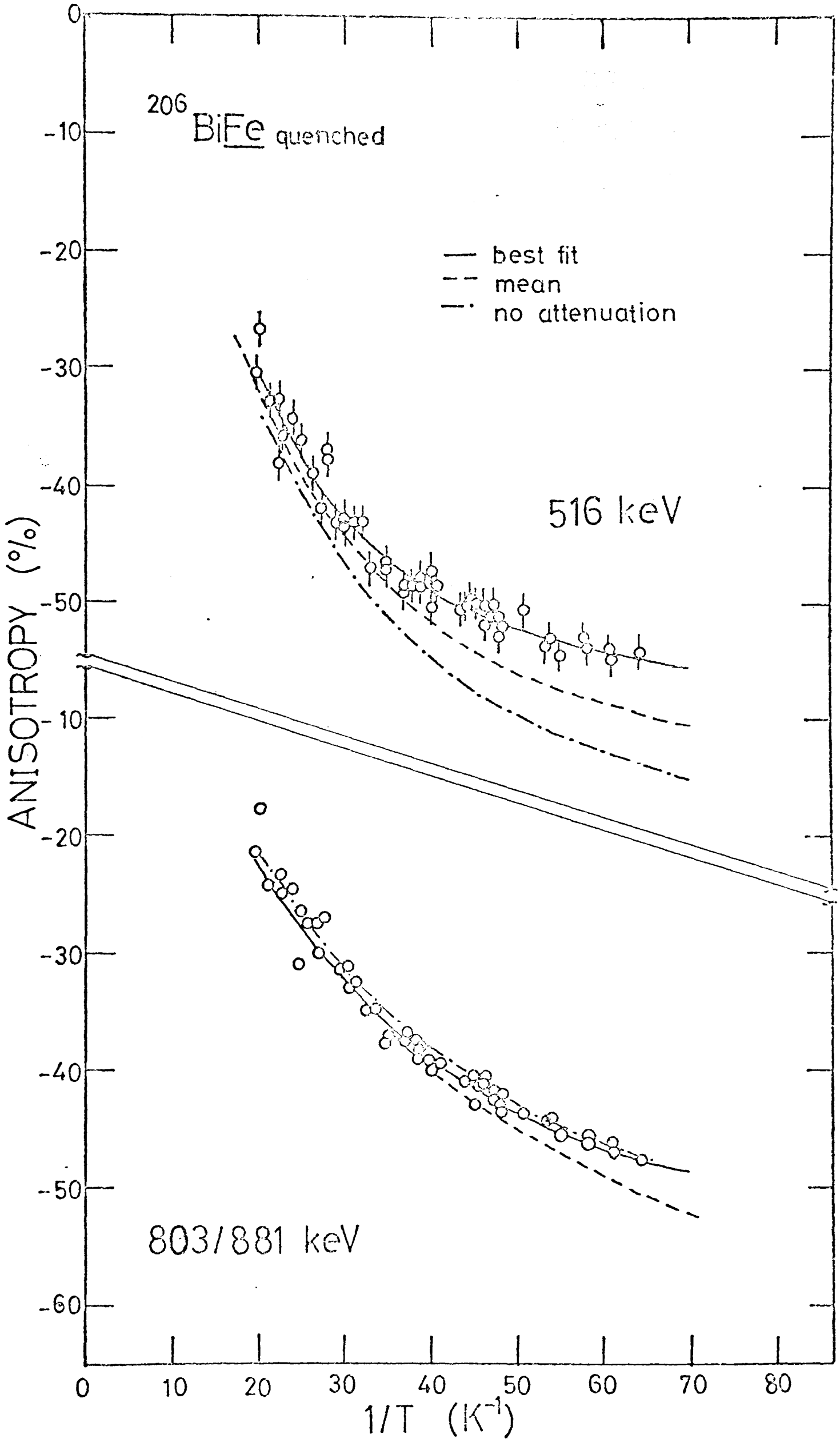

$^{206}$BiFe quenched
— best fit
-- mean
-·- no attenuation
516 keV
803/881 keV
ANISOTROPY (%)
0
-10
-20
-30
-40
-50
-60
0
10
20
30
40
50
60
70
80
1/T (K$^{-1}$)

Fig. 6.2

surface was approximately parallel to a {110} plane. The crystals were then electropolished. The total implantation dose was $\sim 5 \times 10^{14}$ ions/cm$^2$ over the whole crystal and the net activity was ~10 μCuries. Two samples were made. One was run without any further preparation. The other was heated to 600°C for one hour in the usual way. All, but a trace, of the activity was lost during the heat treatment.

The unheated sample showed a large effect. The 497 and 1720 keV transitions were analyzed for the field and percent in that field. The 516, 803 and keV transitions were analyzed for the attenuation coefficients. The results are summarized in the followingtable.

Table 6.2

Implanted $^{206}$BiFe Fits

| E (keV) | Fraction (%) | Field (kOe) | $A_2$ [a] | $A_4$ [a] |
|---|---|---|---|---|
| 497 | 99(5) | 1420(50) | | |
| 1720 | 83(6) | 1370(90) | | |
| 516 | | | 0.64(3) | -0.3(2) |
| 803 } | | | | |
| 881 } | | | 0.33(8) | 2.6(1) |
| mean | 91(8) | 1400(30) | 0.56(16) | 1.6(11) |

a) see note a) Table 6.1

The data for the 497 and 1720 keV transitions is shown in fig. 6.3. Also shown are the curves corresponding to the best fit and to the mean values of the field and percentage in that field. The latter curves are not good fits to either set of data. This is probably a result of the difficulty in establishing a

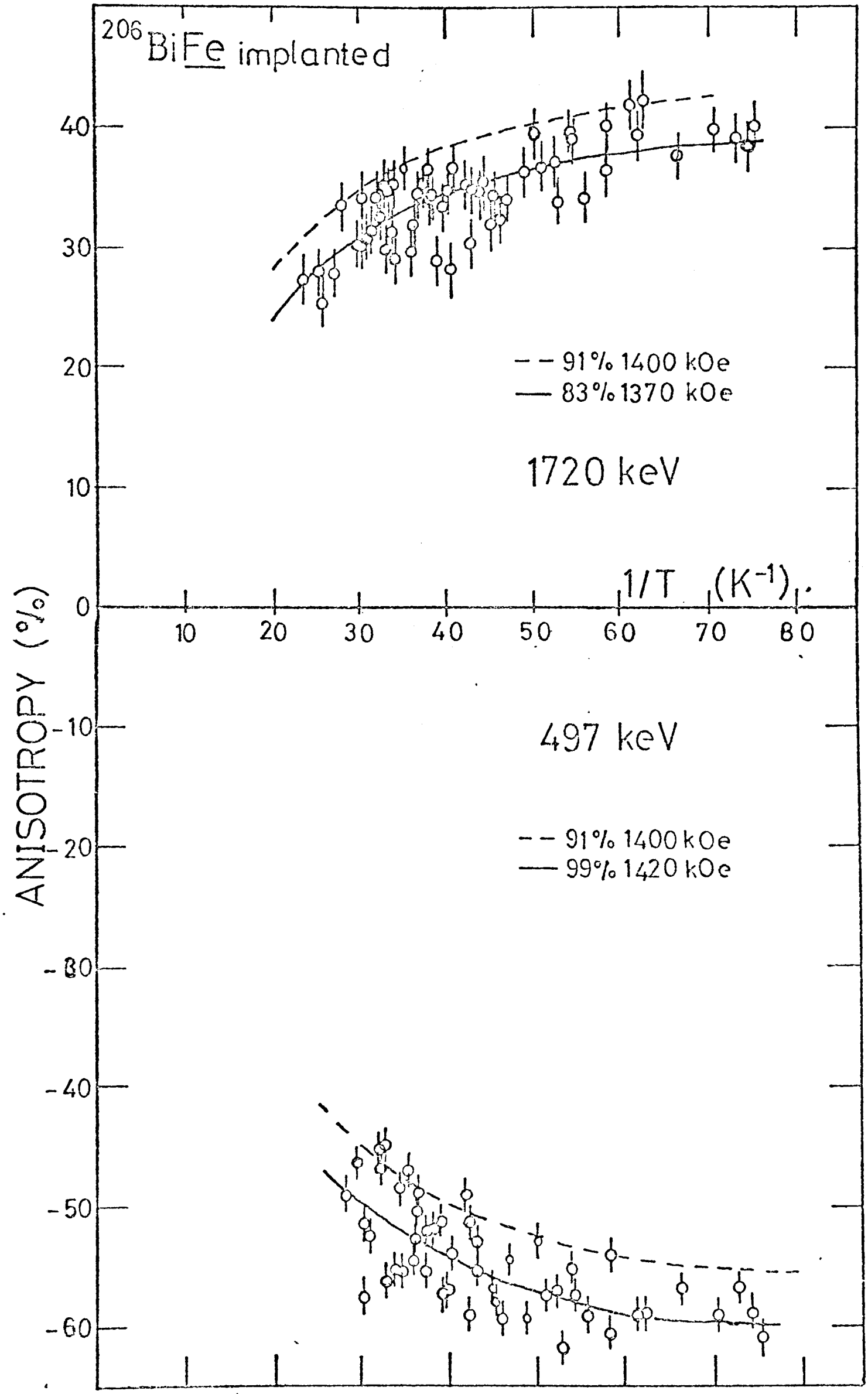

$^{206}$BiFe implanted
40
30
20
10
0
-10
-20
-30
-40
-50
-60
ANISOTROPY (%)
10
20
30
40
50
60
70
80
1/T (K$^{-1}$)
-- 91% 1400 kOe
— 83% 1370 kOe
1720 keV
497 keV
-- 91% 1400 kOe
— 99% 1420 kOe

Fig. 6.3

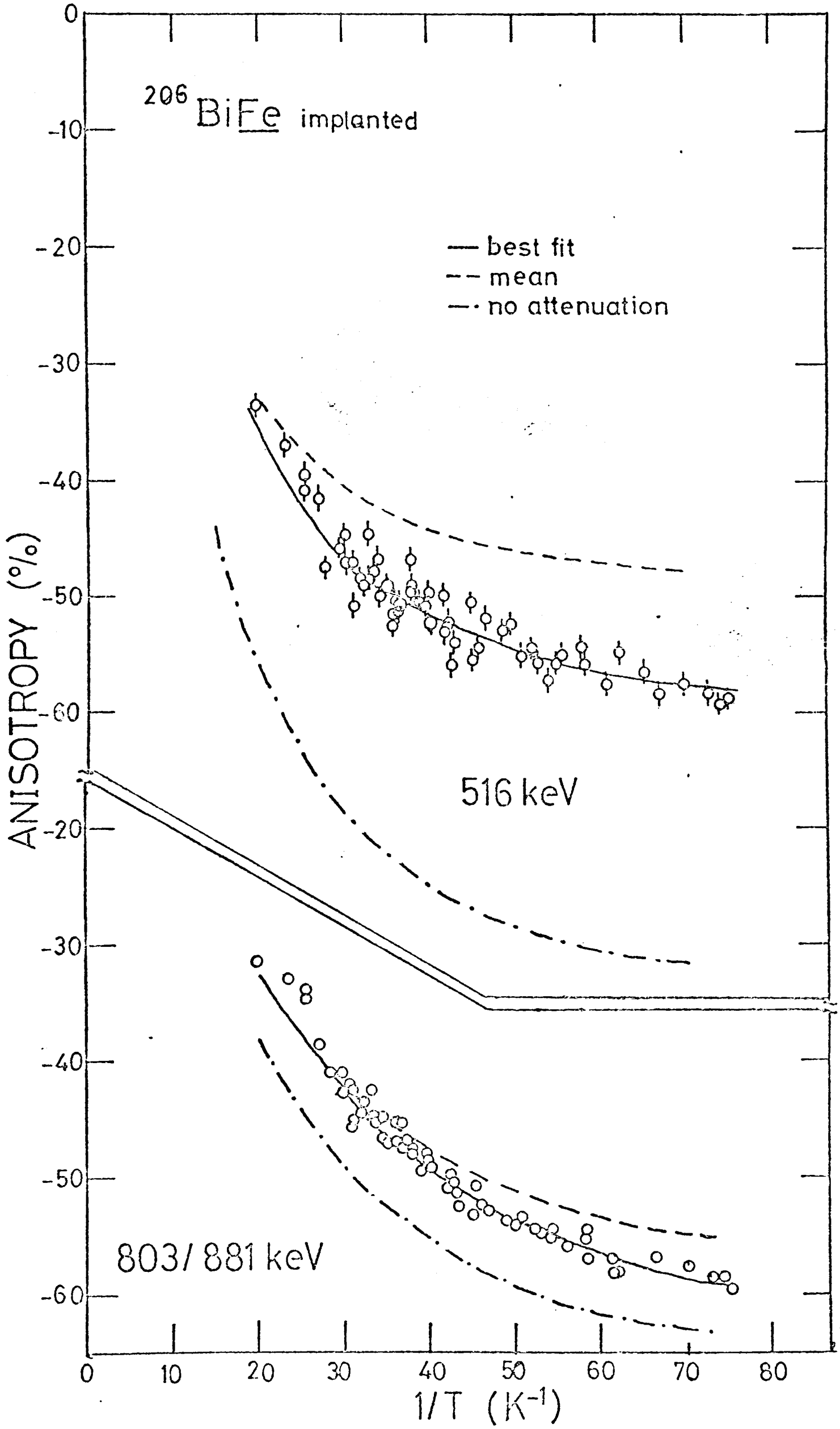

$^{206}$BiFe implanted
— best fit
-- mean
—· no attenuation
516 keV
803/881 keV
ANISOTROPY (%)
1/T (K$^{-1}$)
0
-10
-20
-30
-40
-50
-60
10
20
30
40
50
60
70
80

Fig. 6.4

background. Since none of the transitions with an energy greater than 1720 keV have a significant intensity and since the 497 keV transition is close in energy to two other transitions (516 and 538 keV) of comparable intensities, the data for the 1720 keV transition is probably more reliable.

The data for the 516,803 and 881 keV transitions is shown in fig. 6.4. Again the curves representing the mean values of the best fits does not fit either set of data. All that can be said about the data is that it shows that there is some reorientation in the metastable state and that there is more attenuation in this sample than in the quenched sample.

IV. Channelling in Iron:

Only implanted samples were used in these experiments. The implantation was done with stable bismuth at 200 keV. Before the implantation, the iron single crystals were prepared in the same way as for the active implants. Two crystals were implanted. One with a dose of $1 \times 10^{14}$ ions/cm$^2$ and the other with a dose of $5 \times 10^{14}$ ions/cm$^2$. The ⟨111⟩ and ⟨110⟩ axial channels were scanned in the "$1 \times 10^{14}$ " sample. In the "$5 \times 10^{14}$ " sample the ⟨111⟩, ⟨110⟩ , and ⟨100⟩, channels were scanned. The precedure used in these channelling experiments was the same as that used in the nickel experiments.

A surface peak was seen in the backscattering spectrum. The peak was smaller and less resolved than in the nickel experiments. It was only seen on the ⟨100⟩ scan of the "$5 \times 10^{14}$ " sample. On this scan the beam is incident at an angle of $45^{\circ}$ from the surface normal. Because the implanted ions lie in a narrow layer, the depth

resolution in this layer is improved by a factor of $\cos(45^{\circ})$. This peak contained 12(4)% of the bismuth. This corresponds to the 9(8)% found in the orientation experiments for the amount of bismuth in low field sites. This surface effect is smaller for iron than for nickel. This result is consistent with the experimental findings of Almen and Bruce (80, 81). These authors studied the sputtering of Fe, Ni and Bi by Cu, Kr, Ag and Ta beams. They also studied the sputtering of Fe by Fe beams and of Ni by Ni beams. In all these cases they found that iron was slightly less susceptible to sputtering than nickel. They found that pure bismuth had a very much larger sputtering ratio than either iron or nickel. The sputtering ratio is the number of target atoms knocked off for each incident ion. However, this does not imply that a small amount of bismuth in nickel and iron targets will also have a large sputtering ratio since the sputtering ratio is dependent on the binding energy of the target atoms (82).

For the analysis of the angular scans, the window was set to exclude the surface region. The data for the angular scans is shown in fig. 6.6 and 6.7. The first model chosen to fit the data was the dislocation loop model used to fit the BiNi data. These dislocation loops are expected to form in the close packed planes, which are the {110} planes in iron. These loops would have Burgers vectors in the [110] directions. Eyre and Bullough (83) predicted that the Burgers vectors of large dislocation loops would rotate to the [111] and [100] directions. Dingley and Hale (84) have seen all three types of Burgers vectors in strain deformed iron. Eyre and Bartlett (85) have seen ⟨111⟩ Burgers vectors in neutron irradiated iron and Masters (86) has seen ⟨100⟩ Burgers vectors

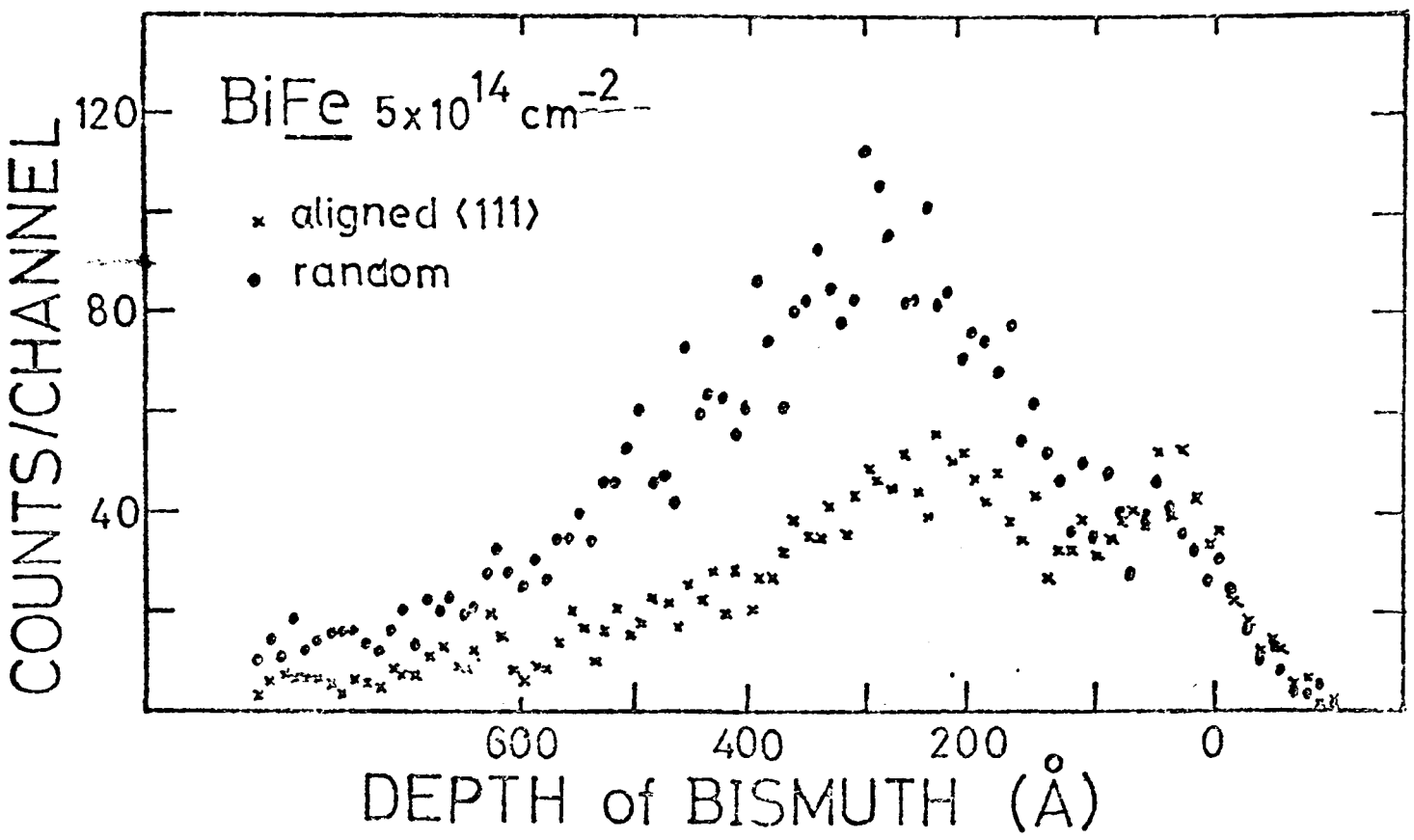



Fig. 6.5 (top)

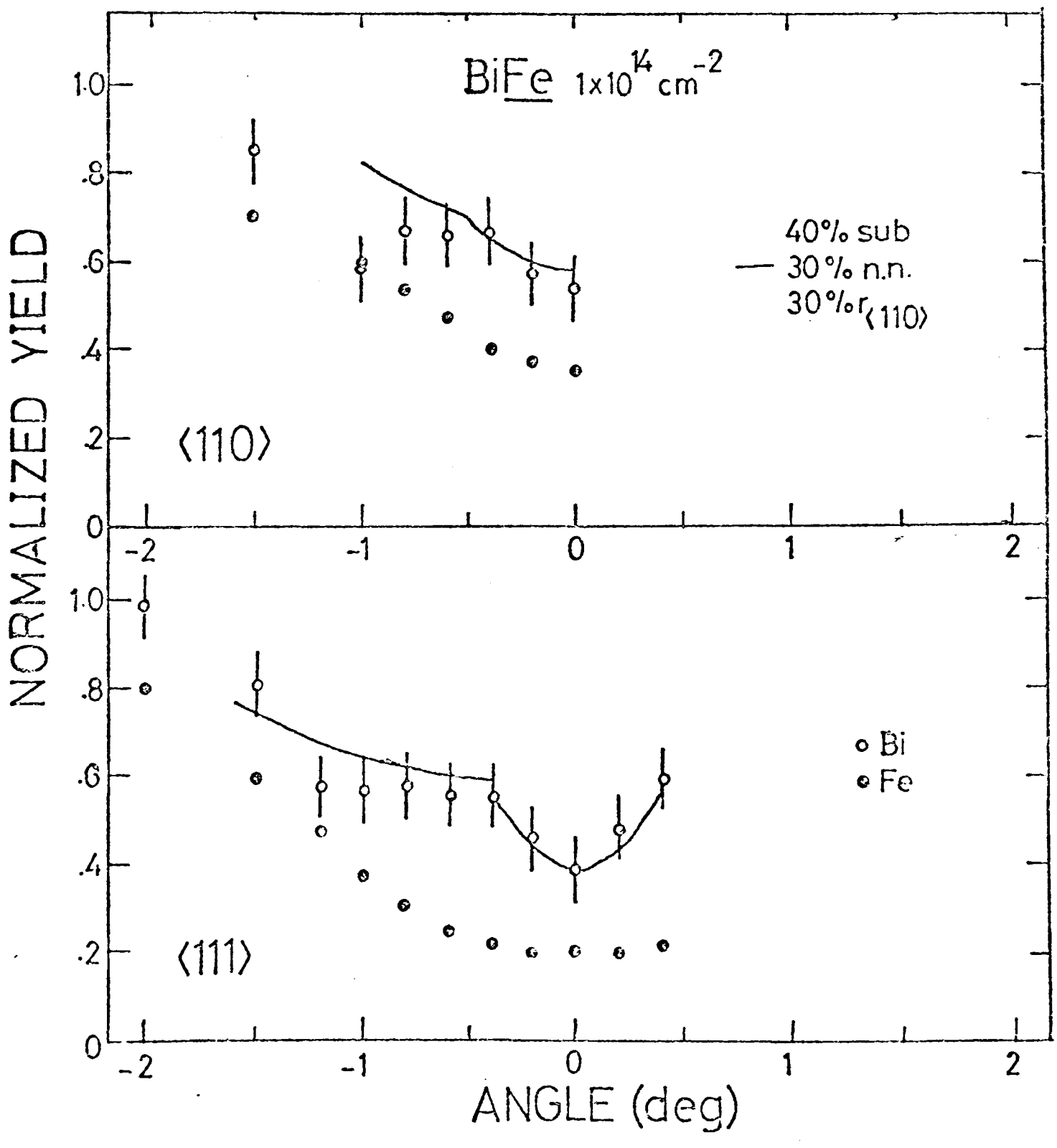



Fig. 6.6 (bottom)

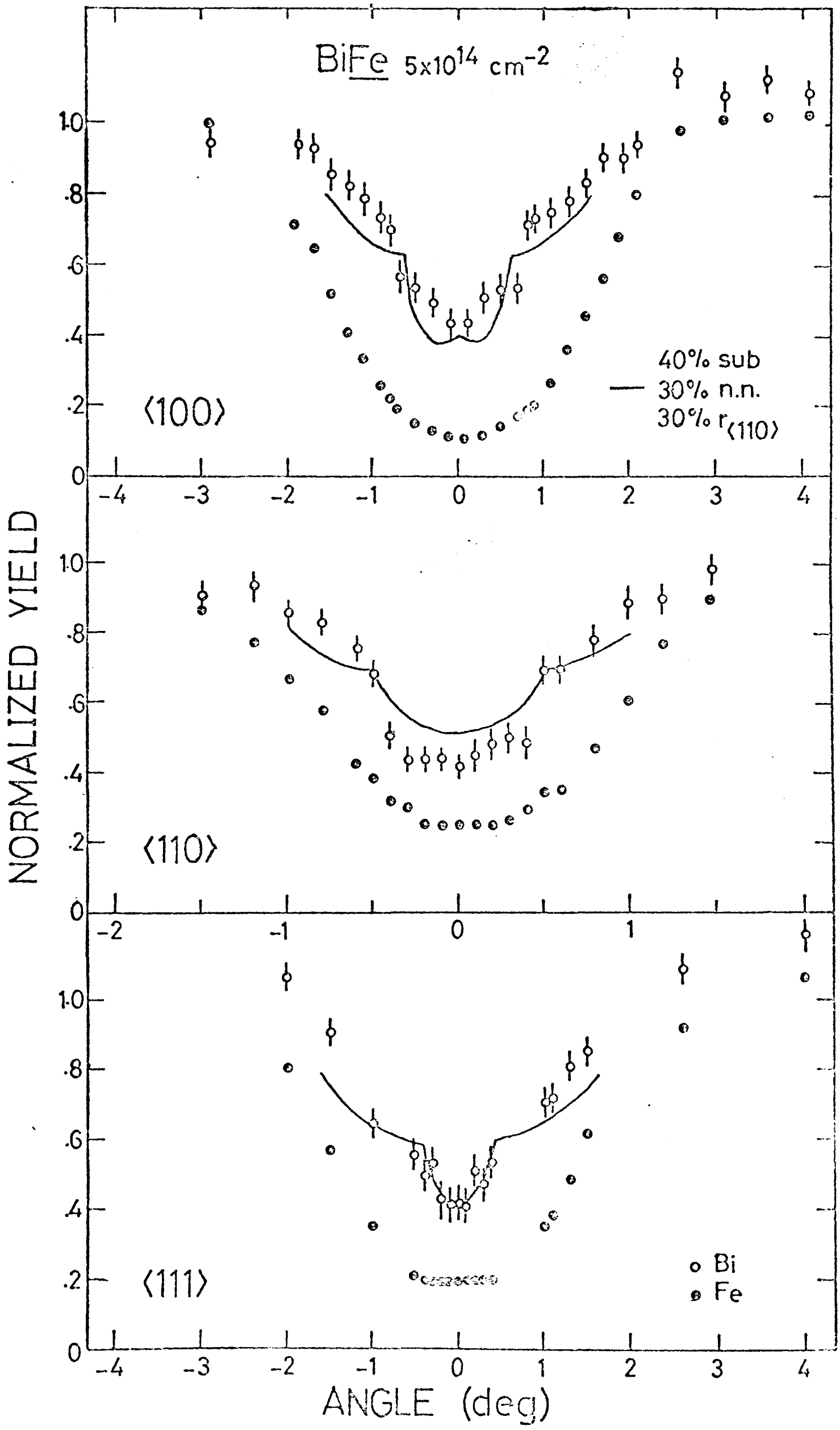

BiFe 5x10^14 cm^-2
40% sub
30% n.n.
30% r⟨110⟩
⟨100⟩
⟨110⟩
⟨111⟩
Bi
Fe
NORMALIZED YIELD
ANGLE (deg)

Fig. 6.7

in iron implanted with iron. Bullough and Perrin (87) have predicted that the Burgers vector will change to the ⟨111⟩ direction in low temperature implants and to the ⟨100⟩ direction in high temperature implants. The data could not be fit by assuming that the bismuth was randomly distributed along any combination of these three directions.

The next model tried was that of nearest neighbour vacancies (see section 5. IV. C.). This produced a reasonable fit if 40% of the bismuth was pure substitutional, 30% was displaced from substitutional by a nearest neighbour vacancy and 30% was randomly displaced along ⟨110⟩ axes by dislocation loops. The displacement caused by the single vacancy was assumed to be the $\frac{1}{4}$ of the nearest neighbour distance calculated for the XeFe system by Drentje and Ekster (66). The 30% assumed to be distributed along the ⟨110⟩ axes could also have been distributed along some combination of the ⟨100⟩ , ⟨110⟩ and ⟨111⟩ axes or completely randomly distributed. The computer model is not accurate enough to make this distinction. Also, the percentages given for the various sites are only approximate.

## V. Summary:

The hyperfine field on bismuth in iron was found to be 900(140) kOe for the quenched sample and 1400(30) kOe for the implanted sample. The former is in agreement with the values of 1180(130) kOe found by Bacon, Hass, Kaindl and Mahnke (49) for a similarly prepared sample. The reported values for the hyperfine field on Pb in Fe (table 5.1) show that the quenched sample should have a field about the same as or less than the field in the implanted sample. This is in agreement with the BiFe results. Table 5.1 also lists the

results of several experiments done on PbFe samples heated to 800°C. An attempt to produce a BiFe sample heated to 600°C resulted in the loss of the activity. So, it was not possible to find out if the field increases in annealed BiFe as it does in PbFe.

The reorientation of the metastable stable state of $^{206}Pb$ was found to be less for the quenched sample than for the implanted sample. This may indicate a different distribution of sites for the two cases or it is possible that the crystal structure in the vicinity of the bismuth is different in the two cases. The quenched sample undergoes two phase transitions during the cooling process. Iron has a FCC structure between 900°C and 1400°C and a BCC structure above and below that region (88). The quenching process might result in a FCC structure in the vicinity of the bismuth. This view is supported by the calculations of Johnston and Stone (60). They account for the reorientation in the quenched sample with an electric quadrupole interaction strength of

$$\frac{3eQV_{zz}}{4(2I-1)\ {}_{n}H} = \pm\ 0.05(1)$$

This means that the ratio of the electric field gradient in iron to that in nickel is 1.1(3). Thus, it is possible that bismuth occupies the same types of sites in quenched iron as it does in nickel.

The channelling experiments showed that the bismuth nearest the surface was randomly located. This region was not as thick as in the nickel samples. As for the nickel samples, this layer probably accounts for the bismuth in low field sites. The channelling experiments also showed that the implanted bismuth was distributed among three sites. These are pure substitutional, displaced by nearest

neighbour vacancies and random. No annealed channelling samples were made; since annealed nuclear orientation samples could not be made. So, it was not possible to confirm the results of Feldman et.al. (51). Also, it was not possible to find the sites for bismuth in the quenched sample. However, on the basis of the reorientation these sites are expected to be more like those for bismuth in nickel than like those in implanted iron.

# R E F E R E N C E S . . . For Part 1.


1a) C. J. Gorter, Physica 14 (1948) 504.

1b) M. E. Rose, Phys Rev 75 (1949) 213.

2a) R. V. Pound, Phys Rev 76 (1949) 1410.

2b) B. B. Bleaney, Proc Roy Soc A64 (1951) 315, and Phil Mag 42 (1951) 441.

3) M. A. Grace, L. E. Johnson, N. Kurti, R. G. Scurlock and R. T. Taylor, Comm. Conf. Phys. Basses Temperatures (Paris, 1955) 261.

4) R. J. Blin-Stoyle and M. A. Grace, Handbuch der Physik 42 (Springen-Verlag, Berlin, 1957) 555.

5) M. J. Steenland and H. A. Tolhoek, Prog. Low Temp. Phys 2 (North-Holland, 1957) 292.

6) S. R. de Groot, H. A. Tolhock and W. J. Huiskamp, Alpha-, Beta - and Gamma - Ray Spectroscopy 2 (North-Holland, 1965) 1199

7) J. M. Daniels and S. K. Misra, Can. J. Phys 44 (1966) 1965

8) L. C. Biedenharm and M. E. Rose, Rev. Mod Phys. 25 (1953)729

9) M. Ferentz and N. Rosenzweig, Argonne Nat. Lab. Report No. Report No. ANL-5324 (1955)

10) H. J. Rose and D. M. Brink, Rev. Mod. Phys. 39 (1967)306.

11) J. M. Reid, The Atomic Nucleus (Penguin Books, 1972)

12) W. Marshall, Phys. Rev. 110 (1958)1280.

13) A. J. Freeman and R. E. Watson, Magnetism (ed: G. T. Rado and H. Suhl) II A (Academic Press, 1965) 167.

14) E. Fermi, Z. Phys. 60 (1930) 320.

15) R. E. Watson and A. J. Freeman, Phys. Rev. 123 (1961) 2027.

16) D. A. Shirley, Phys. Rev. 170 (1968) 363.

17) W. Bloembergen and G. M. Temmer,Phys Rev. 89 (1953) 883.

18) E. Matthias and R. J. Holliday Phys. Rev. Lett. 17 (1966) 897.

19) E. Matthias, B. Olsen, D. A. Shirley, R. M. Steffan and J. E. Templeton, Phys. Rev. A4 (1971) 1626.

R E F E R E N C E S ...to part 1 continued


20) D. Spanfaad and F. Hartman-Boutron, Solid State Comm. 8 (1970)323.

21) P. D. Johnston, R. A. Fox and N. J. Stone, J. Phys. C5 (1972)2077.

22) J. E. Templeton and D. A. Shirley, Phys. Rev. Lett 18 (1967)240.

23) V. S. Shirley, Hyperfine Interactions in Excited Nuclei (ed: G. Goldring and R. Kalish) 4 (Gordon and Breach, 1971)1255.

24) T. A. Koster and D. A. Shirley, Hyperfine Interactions in Excited Nuclei (ed. G. Goldring and R. Kalesh) 4 (Gorden and Breach, 1971) 1239.

25) J. Stark, Z. Phys. 13 (1912) 973.

26) M. T. Robinson and O. S. Oen, Appl. Phys. Lett. 2 (1963) 30; Phys. Rev. 132 (1963)2385.

27) R. B. Alexander, Thesis (Oxford, 1971); U. K. Atomic Energy Authority Report No. AERE-R 6849 (1971).

28) G. Dearnaley, Defects in Crystalline Solids (ed: S. Amelenekx, R. G. Gevers and J. Nikoal) 8 (Ion Implantation) (North-Holland, 1973) 9.

29) J. W. Mayer, L. Eriksson and J. A. Davies, Ion Implantation in Semiconductors (Academic Press, 1970)

30) J. Lindhard, Mat. Fys. Medd. Dan. Vid. Selsk. 34 (1965) No. 14.

31) R. B. Alexander, P. T. Callaghan and J. M. Poate, Ion Implantation in Semiconductors and Other Materials (ed: B. L. Crowther) (Plenum, 1973) 477; U. K. Atomic Energy Authority Report No. AERE-R7469 (1973); and Phys Rev. B9 (1974) 3022.

32) P. T. Callaghan, Thesis (Oxford, 1973).

33) R. A. Fox, Thesis (Oxford, 1970).

34) P. D. Johnston, Thesis (Oxford, 1972).

35) M. E. Rose, Phys. Rev. 91 (1953) 610.

36) H. Hopfermann, Nuclear Moments, (trans: E. E. Schneider) (Academic Press, 1958).

37) C. M. Lederer, J. M. Hollander and I. Perlman, Table of Isotopes, (Wiley, 1967).
J. R. Van Hise and C. Paperiello, Nucl. Phys. A188 (1972) 148.

38) N. Braslau, G. O. Brink and J. M. Kahn, Phys. Rev. 123 (1961)1801.

R E F E R E N C E S ...continued for part 1.


39) M. Kaplan, P. Kittel, P. D. Johnston and N. J. Stone, Nucl. Phys. A193 (1972) 410.

40) Y. Koi, M. Kawakami, T. Hihara and A. Tsujimura, J. Phys. Soc. Japan 33 (1972) 267.

41) F. M. Pipkin and J. W. Culvahouse, Phys. Rev. 109 (1958) 1423.

42) J. C. Hubbs, W. A. Nierenberg, H. A. Shugart, H. B. Silsbee and R. J. Sunderland, Phys. Rev. 107 (1957) 723.

43) M. Hansen, Constitution of Binary Alloys (Mc Graw-Hill 1958).

44) G. C. Pramila, S. G. Cohen and L. Grodzins, Phys. Lett. 24A (1967) 7.

45) J. D. Bowman and F. C. Zawislak, Nucl. Phys. A138 (1969) 90.

46) E. N. Kaufmann, Phys. Lett 35A (1971) 165.

47) E. Bodenstedt,(reported in ref. 46)

48) F. C. Zawislak and J. D. Bowman, Nucl. Phys. A146 (1970) 215.

49) F. Bacon, H. Hass, G. Kaindl and H. E. Mahnke, Phys. Lett. 38A (1972) 401.

50) F. C. Zawislak and D. D. Cook, Bull. Am. Phys. Soc. 14 (1969) 1171.

51) L. C. Feldman, E. N. Kaufmann, D. W. Mingay and W. M. Augustyniak, Phys. Rev. Lett. 27 (1971) 1145.

52) M. Kaplan, P. D. Johnston, P. Kittel, and N. J. Stone, Phys. Lett. 41A (1972) 315.

53) M. Kaplan, P. D. Johnston, P. Kittel and N. J. Stone, Nucl. Phys. A212 (1973) 478.

54) P. D. Johnston, M. Kaplan, P. Kittel and N. J. Stone, Conf. Hyperfine Interactions (Uppsala, 1974).

55) J. C. Manthuruthil, D. C. Camp, A. V. Ramayya, J. H. Hamilton, J. J. Pinajian and J. W. Doornebos, Phys. Rev. C6 (1972) 1870.

56) M. Kanbe, M. Fujioka and Histake,Nucl. Phys. A192 (1972) 151.

57) I. Lindgren and C. M. Johansson, Ark. Fys. 15 (1959) 445.

58) P. D. Johnston, R. A. Fox and N. J. Stone, J. Phys. C5 (1972) 2077.

59) C. J. Allan, Can. J. Phys. 49 (1971) 157.

60) P. D. Johnston and N. J. Stone, Submitted to J. Phys.

R E F E R E N C E S .....to part 1 continued.


61) K. K. Seth, Nuclear Data Sheets B7 (1972) 161.

62) P. D. Johnston, M. Kaplan and N. J. Stone, Phys. Rev. Lett. 32 (1974) 784.

63) H. H. Andersen, Rad Effects 19 (1973) 257.

64) R. S. Nelson, Defects in Crystalline Solids (ed: S. Amelenekx, R. G. Gevers, and J. Nihoul) 8 (Ion Implantation) (North-Holland, 1973) 154.

65) H. de Waard, Proc. Conf. Mossbauer Spectroscopy and Its Applications (Vienna, 1972) 123.

66) S. A. Drentje and J. Ekster, unpublished report, (Nat. Lab. Groningen, 1969).

67) P. K. James, private communication.

68) M. W. Thompson, Defects and Radiation Damage in Metals (Cambridge, 1969).

69) D. M. Maher and B. L. Eyre, Phil Mag. 23 (1971) 409.

70) J. E. Harbottle, Phil Mag. 27 (1973) 147.

71) D. V. Morgan and D. Van Vliet, Proc. Conf. Atomic Collision Phenomenia (Sussex, 1970) 476.

72) R. Bullough and A. J. E. Foreman, Phil Mag. 9 (1964) 315.

73) M. J. Makin and B. Hudson, Phil Mag. 8 (1963) 447.

74) J. L. Strudel and J. Washburn, Phil Mag. 9 (1964) 491.

75) H. E. Mahnke, private communication to P. D. Johnston.

76) P. G. Reid, M. Scott and N. J. Stone, Hyperfine Structure and Nuclear Radiations (ed: E. Matthias and D. A. Shirley, North Holland, 1968) 799.

77) I. A. Campbell, J. Phys. C2 (1969) 1338.

78) P. J. Mazey and J. A. Hudson, J. Nucl. Mater. 37 (1970) 13.

79) R. P. Elliot, Constitution of Binary Alloys, First Supplement (Mc Graw-Hill, 1965).

80) O. Almen and G. Bruce, Nucl. Instr. and Meth. 11 (1961) 257.

81) O. Almen and G. Bruce, Nucl. Instr. and Meth. 11 (1961) 279.

82) P. K. Rol, Thesis (Amsterdam, 1960) quoted in ref. 80 and 81.

R E F E R E N C E S .... to part 1 continued.

83) B. L. Eyre and R. Bullough, Phil Mag. 12 (1965) 31.

84) D. J. Dingley and K. F. Hale, Proc. Roy. Soc. A292 (1966) 55.

85) B. L. Eyre and A. F. Bartlett, Phil Mag. 12 (1965) 261.

86) B. C. Masters, Central Electricity Generating Board Reports RD/B/N245 and RD/B/N321.

87) R. Bullough and R. C. Perrin, Proc. Roy. Soc., A305 (1968) 541.

88) C. J. Smithells, Metals Reference Book, 1 (Butterworths, 1967).

# PART TWO

## Chapter One

## Magnetic Cooling

### I. Introduction:

The method of magnetic cooling was first proposed by Debye (1) and by Giauque (2). They suggested that temperatures below 1 K could be reached by the adiabatic demagnetization of the electronic magnetic moments in paramagnetic salts. The first successful experiments were carried out by three groups: Giauque and MacDougall (3), deHass, Wiersma and Kramers (4), and Kurti and Simon (5). Later Kurti and Simon (6) and Gorter (7) suggested the use of nuclear magnetic moments for magnetic cooling. The first nuclear magnetic cooling experiment was done by Kurti, Simon, Sphor and Robinson (8). Al'tshuler (9) pointed out that the hyperfine field in paramagnets with singlet ground states could be used to enhance theapplied field in nuclear demagnetization experiments. This technique has been successfully used by Andres and Bucher (10).

The adiabatic demagnetization of paramagnetic salts has become a common technique in low temperature research. On the other hand, nuclear cooling experiments are still rare. Recent experimenters have concentrated on using nuclear cooling to refrigerate other systems. March (11) Symko (12), Gylling (13), and Hensel (14) used nuclear cooling to cool conduction electrons. Osgood and Goodkind (15) and Dundon, Stopha and Goodkind (16) used it to cool $^3He$. The nuclear cooling experiments described in this part are concerned with achieving low nuclear spin temperatures

without cooling anything else. The following discussion primarily deals with the latter topic.

## II. The Cooling Process:

The magnetic cooling process has been considered in detail in the review article by de Klerk (17) and in the book by Hudson (18). In this section the highlights of the method will be sketched. For a paramagnetic system, magnetic cooling is a two step process. Starting in zero magnetic field and at temperature $T_i$, the first step is to increase the magnetic field. During this isothermal magnetization heat flows out of the system into a heat reservoir and the entropy of the system decreases. The entropy change is

$$\Delta S = \int_0^{H_f} (\delta M/\delta T)_H \, dH \qquad (1.1)$$

Where M is the magnetization. For an ideal paramagnet the magnetization is given by the well known Brillouin formula

$$M = Ng\mu_o I B_I \, (g\mu_o H/kT) \qquad (1.2)$$

where $B_I(x) = \frac{1}{I}\left\{ (I + \frac{1}{2}) \coth(I + \frac{1}{2}) x - \frac{1}{2} \coth \frac{1}{2}x \right\}$

In the high temperature limit this reduces to the Curie Law $M = CH/T$. From (1.2) it can be seen that $(\partial M/\partial T)_H$ and thus $\Delta S$ is negative. The energy absorbed by the heat reservoir is $-T_i \, \Delta S$.

The second step is an adiabatic and reversible, hence isentropic, demagnetization during which the temperature of the system decreases. The greatest temperature drop occurs when the entropy depends only on the magnetic degrees of freedom of the system. This condition is usually met for temperatures below 1 K. The most important exception is nuclear spin systems in metals.

This case will be treated later.

The cooling is called the magneto-caloric effect and is given by

$$\left(\frac{\partial T}{\partial H}\right)_S = \frac{-T}{C_H}\left(\frac{\partial M}{\partial T}\right)_H \qquad (1.3)$$

Where $C_H$ is the heat capacity in a constant magnetic field.

For an ideal paramagnetic system the entropy is

$$S = Nk\left[\ln \sinh(I+\tfrac{1}{2})\, x - \ln \sinh \tfrac{1}{2}x\right] + \tfrac{1}{2}\coth \tfrac{1}{2}x - (I+\tfrac{1}{2})\, x \coth(I+\tfrac{1}{2})x \qquad (1.4)$$

where $x = g\mu_o H/kT$.

From this, it can be seen that an isentropic process is carried out at constant H/T. Thus the final temperature $T_f$ of an adiabatic demagnetization from temperature $T_i$ and field $H_i$ to a field $H_f$ is

$$T_f = H_f T_i / H_i \qquad (1.5)$$

This is only an approximation since it implies that a demagnetization to zero field results in $T_f = 0$ and $S \neq 0$, which violates the third law of thermodynamics. This discrepency is the direct result of the assumption that the moments are non-interacting.

In order for a system of spins to come to a state of thermodynamic equilibrium, there must be some interaction that allows energy to be exchanged between the spins. This interaction may be either direct (e.g. dipole-dipole)or indirect (e.g. via crystaline field). At temperatures of the order of this interaction ($kT \sim \Delta E$) the higher energy levels become "quenched". This results in a reduction of the entropy. Abragam and Proctor (19) have shown that to first order the interaction can be treated as an internal magnetic field, $H_{int}$. Taking this field into account,

they found that eq. (1.5) becomes

$$T_f = (H_f^2 + H_{int}^2)^{\frac{1}{2}} T_i/H_i \qquad (1.6)$$

III. Spin Temperature:

The discussion so far has assumed that the spin system contains the only degrees of freedom of the total system. This is a good assumption when the spins are in a dielectric salt, where all other degrees of freedom are "quenched". However, for a nuclear demagnetization in a metal the lattice (principally the conduction electrons) still has some degrees of freedom. The entropy and heat capacity of these will in general effect the relations in section (II).

In a demagnetization, only the spins are cooled directly. The spins then relax back to a distribution in equilibrium with the lattice. This distribution is characterized by a temperature $T_L$. The relaxation takes place in a time $\tau_1$. This is called the spin-lattice or longitudinal relaxation time. As mentioned in section (II), there is an interaction between the spins that brings them into a state of mutual thermal equilibrium characterized by a temperature $T_S$. This relaxation takes place in a time $\tau_2$, called the spin-spin or transverse relaxation time. If $\tau_2 \ll \tau_1$ then $T_S$ can differ from $T_L$. $T_S$ is called the spin temperature. The concept of spin temperature has been reviewed in length by Goldman (20) and by Hebel (21).

Spin systems usually used in magnetic cooling experiments meet the condition $\tau_2 \ll \tau_1$. In this case the relations in section (II) will hold if the time taken to demagnetize is very much less than $\tau_1$.

IV. Internal Field:

There are many sources of the internal field. The internal field in ferromagnetic systems has been considered in part one. In this section the internalfield of paramegnetic systems will be considered.

The principal source of the internal field in dielectrics is the classical dipole-dipole interaction. Van Vleck (22) was the first to study these interactions. He considered the interaction Hamiltonian:

$$\mathcal{H} = \sum_{j>i} r_{ij}^{-3} \left[ \underline{\mu}_i \cdot \underline{\mu}_j - 3(\underline{\mu}_i \cdot \underline{r}_{ij})(\underline{\mu}_j \cdot \underline{r}_{ij}) / r_{ij}^2 \right] \qquad (1.7)$$

Van Vleck found that the second moment of the field for a polycrystalline material was (23)

$$\langle \Delta H^2 \rangle = \frac{3}{5} N \varepsilon^2 \mu_n^2 I(I+1) \sum_{j>i} r_{ij}^{-6} \qquad (1.8)$$

where N is the number of particles per $cm^3$. Hebel (21) has shown that the internal field is related to the second moment by

$$H_{int}^2 = \frac{5}{3} \langle \Delta H^2 \rangle \qquad (1.9)$$

This internal field comes from the diagonal terms of the interaction. The off diagonal terms are responsible for spin-spin relaxation, which will be discussed in the next chapter.

In metals there is another internal field which is proportional to the applied field. This field comes from the interaction between the conduction electrons and the nuclear magnetic moments. This interaction is called the Knight shift. Its effect is usually absorbed into the Zeeman term of the Hamiltonian.

V. Nuclear versus Electronic Magnetic Cooling:

In a magnetic cooling experiment a large entropy change on magnetization is desired. This requires $H/T \sim k/\mu$. This ratio is ~1 Tesla/K for electronic moments and $\sim 10^3$ Tesla/K for nuclear moments. The biggest fields that can be easily produced in a laboratory are ~10 Tesla. For these conditions, the necessary initial temperatures are ~1 K for electronic cooling and ~1 mK for nuclear cooling.

There is one advantage to nuclear cooling. The smallness of the nuclear magnetic moment implies a small dipole-dipole field and thus a low final temperature. Electronic systems have ordering temperatures ~10 mK and nuclear systems should show ordering at ~0.1 μK.

# Chapter Two

## Nuclear Magnetic Resonance Thermometry

### I. Introduction:

One of the problems in nuclear cooling experiments is measuring the final spin temperature. Because the spins are not in good thermal contact with their surroundings the temperature can only be measured by measuring a temperature dependent property off the spins, such as the magnetization. In the early experiments the temperature was deduced from the Curie Law behavior of the bulk nuclear susceptibility ( $\chi = C/T$). Kurti, Robinson, Simon and Spohr (8) used a ballistic method and Hobden and Kurti (24) used an AC bridge, to measure $\chi$. Both of these methods are very sensitive to magnetic impurities and require careful calibration at several temperatures to demonstrate that $\chi$ follows Curie's Law. More recently, nuclear magnetic resonance (NMR) has been used to measure the magnetization, $M = \chi H$. NMR has the advantage that it can distinguish between different types of nuclei. It is unaffected by magnetic impurities, since it measures only the magnetization of the nuclei of interest. The first application of NMR thermometry to nuclear cooling experiments was made by Hahn, Walstedt, Froidevaux, and Geissler (25). More recent NMR thermometers have been described by Hensel, and Smith (26) and by Aalto, Berglund, Collan, Ehnholm, Gylling, Krusius, and Pickett (27).

### II. General Principles of Pulsed NMR:

A general review of NMR can be found in the books of Slichter (28) and Abragam (29). The relevent theory will be outlined

below.

A system of nuclear magnetic moments in a steady magnetic field $\underline{H} = H_o \hat{z}$ has an equilibrium magnetization $\underline{M} = M_o \hat{z}$ . In pulsed NMR the non-equilibrium state is of interest. There are various means by which the magnetization can be made to differ from equilibrium. One method is to change the magnitude of the magnetic field quickly. In this case the magnetization decays to its equilibrium value $M_o$ in a time $\tau_1$. During this relaxation there is an exchange of energy between the spin system and its surroundings (the lattice).

It is also possible to tip the magnetization away from its equilibrium direction. This is what is done in pulsed NMR. The tipping is accomplished by pulsing a small transverse rf field. Abragam (29) gives the tipping angle as

$$\cos\theta = 1 - \frac{2H_1^2}{(H_o - \frac{\omega}{\gamma})^2 + H_1^2} \sin^2\left[(\gamma H_o - \omega)^2 + \gamma^2 H_1^2\right]^{1/2} \frac{\Delta t}{2} \qquad (2.1)$$

where $2H_1 \sin \omega t$ is the transverse field and $\Delta t$ is the duration of the pulse. A small pulse will have the greatest effect if $\omega$ is the Larmor frequency $\omega_o = \gamma H_o$. If the pulse tips the magnetization by $90^o$ it is said to be a $90^o$ pulse. After the pulse the transverse magnetization precesses about $H_o$ at the frequency $\omega_o$ and relaxes back to its equilibrium value $M_o^{(o)}$ by a redistribution of energy between the spins. This relaxation occurs in a time $\tau_2$.

In its return to equilibrium, the magnetization undergoes a precession and two types of decay. This rather complicated motion can be described fairly accurately by the Bloch equation (30):

$$\frac{d\underline{M}}{dt} = \gamma \underline{M} \times \underline{H} - \frac{M_x \hat{x} + M_y \hat{y}}{\tau_2} - \frac{M_z - M_o}{\tau_1} \hat{z} \qquad (2.2)$$

One of the important features of this equation is that in general $\tau_1$ is not the same as $\tau_2$. These are the same $\tau_1$ and $\tau_2$ as in section ( 1. III).

III. Spin-Spin Relaxation:

Classically, spin-spin relaxation results from the random phase approximation. Each spin has a different Larmor frequency, since each sees a different local field. This local field is the sum of the applied field and the randomly oriented internal field. If all the spins are precessing in phase at a given time (e.g. there is a net transverse magnetization), then in a time $\tau_2 \sim (\gamma H_{int})^{-1}$ the spins will have drifted out of phase and the transverse magnetization will have disappeared.

Quantum mechanically, spin-spin relaxation occurs because the spin-spin interaction redistributes energy among the spins by mutual spin flips. This process removes the transverse magnetization and establishes an equilibrium among the spins. This is the same interaction discussed in section (1.IV). The resulting time constant is

$$\tau_2 = 1/\gamma H_{int} \qquad (2.3)$$

Another important contribution to $t_2$ comes from the inhomogeneity ($\Delta H$) in the applied field. The observed time constant will be

$$\tau_2^* = \tau_2 \left( \frac{H_{int}}{H_{int} + \Delta H} \right) \qquad (2.4)$$

It is possible to measure $\tau_2$ in the presence of a large $\Delta H$ with spin echo techniques. However, it is easier if $\Delta H$ can be arranged to be small.

IV. Spin-Lattice Relaxation:

Spin-lattice relaxation in metals comes from the coupling of the nuclear magnetic moments with the magnetic moments of the conduction electrons. Only the electrons near the Fermi surface are free to partake in this interaction. The interaction Hamiltonian is

$$\mathcal{H} = \frac{8\pi}{3} \gamma_e \gamma_n \hbar \, \underline{I} \cdot \underline{S} \quad (\underline{r}) \qquad (2.5)$$

Korringa (31) showed that the diagonal terms of this Hamiltonian gave the Knight shift and the off-diagonal terms are responsible for spin-lattice relaxation. In the high field case he found

$$\tau_1 \; T_L = K \qquad (2.6)$$

where $T_L$ is the lattice (the electrons) temperature and K is the Korringa constant, a function of the Knight Shift.

The Korringa relation has been extended to the low field case by Redfield (32), Hebel and Slichter (33) and Anderson and Redfield (34). They found that

$$\tau_1 T_L = K\left[\frac{H_o^2 + (10/3)H_{int}^2}{H_o^2 + \delta(10/3)H_{int}^2}\right] \qquad (2.7)$$

where $\delta$ $(2 \leqslant \delta \leqslant 3)$ is a measure of correlation effects among the electrons.

V. Thermometry:

The pulsed NMR thermometer consists of three mutually perpendicular coils. One produces the steady field in the $\hat{z}$ direction. Another (the transmitter) applies the perturbing pulse in the $\hat{y}$ direction. The third is used as a receiver. The transmitter and the receiver are perpendicular to each other to minimise the mutual coupling.

After the perturbing pulse has been applied, a sinusoidal voltage is induced in the receiver. This voltage oscillates at the Larmor frequency and has the initial amplitude

$$V = 4 \pi \ M_o \omega_o \ AN \eta \ \sin \theta \qquad (2.8)$$

where A and N are the cross-sectional area and the number of turns, respectively, of the receiver, $\eta$ is the filling factor, $\theta$ is the tipping angle (eq. 2.1). This voltage decays in a time $\tau_2$.

The temperature dependence of this voltage is known, since $M_o$ has a known temperature dependence (eq. 1.2). So by measuring V, the spin temperature can be deduced by comparing it to the V of a known temperature. The thermometer can also be calibrated by using the Korringa relation for $\tau_1$. To do this $H_o$ is changed rapidly. Then several successive measurements of V are made. From this, $\tau_1$ is deduced and can be related to $T_L$ which corresponds to the equilibrium value of V.

## Chapter Three

## An Apparatus for Nuclear Cooling Experiments

### I. Introduction:

Copper nuclei have been extensively used in recent nuclear cooling experiments (11-16). There are two naturally occuring isotopes of copper, $^{63}Cu$ and $^{65}Cu$. The properties of these nuclei are given in the following table. In electron paramagnetic substances, usually 10-30% of the entropy must be removed to reach the Néel or Curie point. If we assume, in order to get an estimate, the same to be true for nuclear spins in a metal, then a $H/T \geq 10^3$ T/K is needed. Ordering effects can be expected when $T \sim \mu H/k$. Thus, ordering can be expected to occur at some temperature $< 10^{-6}$ K.

Table 3.1

Properties of Copper

| | $^{63}Cu$ | $^{65}Cu$ |
|---|---|---|
| isotopic abundance (%) | 69 | 31 |
| spin | 3/2 | 3/2 |
| moment (n.m.) | 2.23 | 2.38 |
| $\tau_2$ ($\mu$ s) | 77 | 79 |
| Curie constant per mole (cgs) | 0.32 | |
| Korringa constant (ms K) | | |
| fields > 10 G | 1120 [b] | |
| fields < 1 G | 415 [c] | |
| internal field (Oe) | 3.05 | |
| $\mu H/k$ (K) | $2.6 \times 10^{-7}$ | |
| crystal structure | FCC | |

a) except as noted, these values are taken from ref. 26.
b) ref. 34.
c) ref. 41.

This chapter describes the developement of an apparatus for cooling copper nuclei below $10^{-6}$K. The proposed experiment

was to demagnetize copper nuclei from a large H/T to a field as low as compatable with the measuring procedure used and certainly not more than a field on the order of the internal field. The aim was to reach spin temperatures lower than had been reached before, to see if any spin ordering effects could be observed. In these experiments only the nuclear spin system is cooled to the very low temperatures. After the demagnetization the spin system will warm up with a time constant equal to the spin-lattice relaxation time $\tau_1$. Thus, the time in which measurements can be made is determined by $\tau_1$.

To carry out these experiments an apparatus had to be constructed with the following characteristics (fig. 3.1 shows the apparatus diagrammatically). The nuclear stage has to be magnetized in a field of about 6-8 Tesla provided by a superconducting solenoid. It is in thermal contact with a paramagnetic salt (CMN or CPA) which provide temperatures of the order of 10 mK by adiabatic demagnetization. The starting temperature for this electron paramagnetic demagnetization is provided by a dilution refrigerator (about 200 mK). The necessary field, up to about 0.6 T, is provided by another superconducting solenoid. There is a heat switch between the dilution refrigerator and the paramagnetic salt. The whole assembly (dilution refrigerator, electronic stage and nuclear stage) is enclosed in a vacuum jacket, called the inner jacket (IJ). This jacket is cooled to about 1 K by liquid helium boiling at about 0.5 torr. A second vacuum jacket (outer jacket, OJ) surrounds the $1^{o}$ pot and is immersed in liquid helium boiling at normal pressure (4.2 K). A further vacuum jacket with

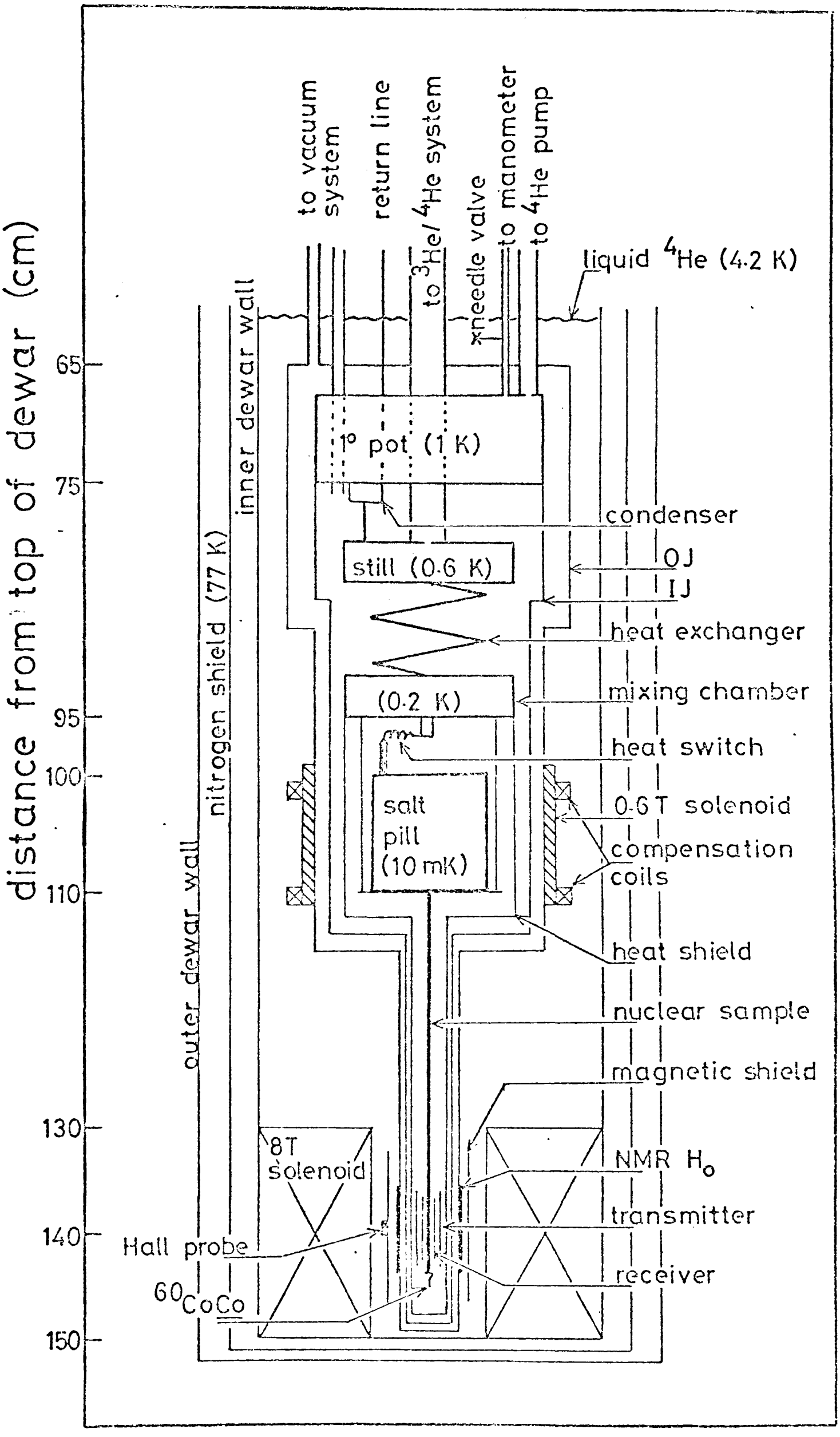

distance from top of dewar (cm)
65
75
95
100
110
130
140
150
to vacuum system
return line
to $^3$He/$^4$He system
needle valve
to manometer
to $^4$He pump
liquid $^4$He (4.2 K)
inner dewar wall
1° pot (1 K)
condenser
still (0.6 K)
OJ
IJ
heat exchanger
(0.2 K)
mixing chamber
heat switch
salt pill (10 mK)
0.6 T solenoid
compensation coils
heat shield
outer dewar wall
nitrogen shield (77 K)
nuclear sample
magnetic shield
8T solenoid
NMR $H_o$
transmitter
receiver
Hall probe
$^{60}$CoCo

Fig. 3.1

a liquid nitrogen shield completes the apparatus.

The majority of my time in Oxford has been spent working on the nuclear cooling apparatus. This has been a very frustrating time as there have been many setbacks. These setbacks are discussed in this and in the succeeding chapter. When I started on D. Phil. work, the design of the whole apparatus, especially of the dilution refrigerator, was already in an advanced state. This was done by a visiting physicist from Czechoslovakia who had previously worked with Professor Neganov, a great authority on dilution refrigerators. Construction of the apparatus had already begun and it was not possible to make substantial alterations.

The design had several drawbacks. In order to reduce the rate of evaporation of the helium from various parts of the apparatus, its length was such that it was not possible to use a separate dewar for the liquid helium. As a result, the cryostat consisted of several demountable parts, most of them made vacuum tight by indium seals. These seals, especially when of large diameter, were not reliable. Similarly, in order to improve efficiency, various parts were put very close together and repairs were difficult to carry out. The conception of this apparatus would have been excellent for carrying out trouble free experiments of long duration (one or two days), but this was too optimistic a concept and did not take into account the need to open the apparatus after relatively brief runs to change samples or experimental conditions. Also, even for a short experiment of a few hours duration, the apparatus needed 20 liters of helium for cooling down and running.

In all, more than two years was spent building and testing this apparatus. Since, moreover, it never worked, it was finally decided to scrap it and build a simpler apparatus compatible with the existing pumping system. The new apparatus is shown in figure 3.1. It has all of the cooling stages that the other had. A hole was knocked in the floor to allow a commercial, one piece dewar to be used. Since the original dilution refrigerator was far too complicated (it had over 100 solder joints in three types of solder which continually leaked) it was replaced with a simpler commercial one. While the new apparatus is simpler than the old one, it is still rather complicated. When a repair or modification has to be made, it takes at least a week to take the apparatus apart, make the change and reassemble the apparatus. So, during the development of this apparatus only one run per week could be hoped for. The various parts of the new apparatus are discussed in the rest of this chapter. Some experiments are discussed in the last chapter.

II. Heat Leaks and Heat Evolution:

In experiments at very low temperatures, extensive precautions must be taken against all sources of heating. In this apparatus, the sample is approximately one gram-ion of copper. If 10% of the entropy of this copper is removed during the magnetization, the total entropy change will be $\Delta S = 0.1\ R \ln 4 \sim 10^{7}$ erg/K. Hence, after a demagnetization to $\sim 10^{-6}$K, the heat needed to restore this entropy change and destroy its degree of ordering is $Q \sim T\Delta S = 10^{-6} \times 10^{7} = 10$ ergs. There are four main causes of

heating at very low temperatures. These are mechanical vibration, conduction along supports and along electrical leads, radiation, and conduction by residual gas desorbed from warmer parts. These problems and methods to overcome them have been reviewed by Mendoza (35) and White (42).

To reduce the amount of vibrations, the apparatus is mounted on a concrete block weighing approximately 1000 kg. This block is supported on a set of springs. The natural periods of vibration are on the order of one second. All connections to the apparatus are flexible. All pumping lines pass through large sand boxes sitting on the floor. The vibration was measured at the top of the apparatus with a Dawe type 1433B vibration meter. This meter has a band width of 1.6 Hz to 10 kHz. With all the equipment on the vibration amplitude was less than 15 μm. This is comparable with the vibration Hensel measured for his apparatus (14). The large booster pump (Edwards 9 B4) used with the dilution refrigerator was responsible for about half of the vibration.

The heat leaks along the supports have been kept low by using low conductivity materials. Electrical leads are manganin or superconducting where ever possible. Radiation down pumping lines is reduced by putting elbows or baffles in them. The desorbtion or gas was a serious problem for the salt pill and nuclear stage. This was corrected by the addition of a heat shield anchored to the mixing chamber. This shield is discussed in more detail in Chapter 4.

III. The Helium Dewar:

The helium dewar is a 200 mm inner diameter conventional liquid nitrogen shielded dewar supplied by the Oxford Instrument Company. The large diameter is needed to accommodate the superconduction solenoids. The liquid nitrogen in the shield will last up to 18 hours. The dewar holds 21 l of liquid helium. The evaporation is typically 350 ml/hr. This will double when a large current is being put into the nuclear demagnetization solenoid. The evaporation is also slightly affected by the current in the salt pill magnet and by the flow of $^3$He in the dilution refrigerator. The vacuum space is usually pumped with an oil diffusion pump during the precooling stages of a run or when the dewar was kept at liquid nitrogen temperatures for an extended period between runs.

IV. The Cryostat:

The cryostat has two brass vacuum jackets, the outer jacket (OJ) and the inner jacket (IJ). The upper part of these jackets has a large diameter (OJ: 133 mm, IJ: 121 mm) to accommodate the salt pill, while the lower part, which contains the nuclear stage, has a smaller diameter (OJ: 43 mm, IJ: 37 mm) so that it can fit into the high field superconducting solenoid. To ensure that the jackets do not touch each other, there is a PTFE cap on the bottom of the IJ. These jackets can be pumped by a 2" oil diffusion pump. The pressure in the jackets can be measured with a set of Hg and oil manometers ($10^3$ to $10^{-1}$ torr), an Edwards pirani gauge (3 to $10^{-3}$ torr) and an Edwards penning

gauge ($10^{-2}$ to $10^{-6}$ torr). These gauges are located near the diffusion pump. The vacuum jackets are demountable, the joints being made with indium seals.

The IJ is attached to the bottom of a one liter container ($1^{o}$ pot). This pot is filled with liquid helium from the main helium bath through a needle valve. It can then be pumped to a temperature of about 1 K (a vapour pressure of about 0.5 torr) by a 900 l/min rotary pump. The biggest heat load on the $1^{o}$ pot is the heat of condensation of the helium returning to the dilution refrigerator. With this heat load the $1^{o}$ pot will maintain a temperature of about 1 K for more than 12 hours on one filling. The vapour pressure of the liquid helium can be measured with a set of manometers connected to the pot by a tube separate from the pumping line.

The process of cooling the apparatus from room temperature usually took two days during which various cryogenic liquids ($N_2$, $H_2$ and He) were transferred into and out of the dewar through a removable vacuum insulated tube (syphon). Inside the dewar, the syphon fits into a tube that goes to the bottom of the helium space. This allows the cryogenic liquids to enter the dewar at the bottom. The purpose of this is to make use of the enthalpy of the gas evaporated in cooling the apparatus. The liquid $N_2$ and $H_2$ are removed from the dewar by blowing them out through the syphon. A heater at the bottom of the dewar supplies the necessary overpressure. When no more liquid comes out of the syphon, the dewar is pumped to just above the triple point (100 torr for $N_2$ and 60 torr for $H_2$). If the pressure were reduced below the triple point, the thermal

contact to the resulting solid would be so poor that it would take a hopelessly long time to evaporate it. A CRT at the bottom of the dewar starts to warm when the last of the liquid is gone. When this happens, the heater is turned off and the dewar filled with helium gas from the laboratory's low pressure helium recovery system, which is contaminated with a small amount of air. At liquid hydrogen temperatures, this air will sometimes block the tube that connects to the syphon. These blocks can be cleared by a heater wrapped around the tube.

On the first day of the cooling process, the apparatus was assembled and the dewar filled with liquid nitrogen. During this and succeeding cooling processes, the temperatures of various parts of the apparatus were monitored with carbon resistor thermometers (CRT). The AC bridge used and the calibration of the thermometer have been described by Hensel (14). The resistors were Speer 470 Ω in the main helium bath and on the $1^{o}$ pot and Speer 220 Ω on the dilution refrigerator and in the salt pill. The calibration of the 220 Ω resistors is shown in fig. 3.2. While cooling to liquid nitrogen temperatures, the jackets were filled with nitrogen at atmospheric pressure. This was to prevent the loss of water from the salt pill. On the evening before the experiment, the liquid nitrogen was removed from the dewar and replaced with liquid hydrogen. At the same time the jackets were pumped and then filled with a few torr of helium exchange gas. On the morning of the experiment, the hydrogen was removed and replaced with liquid helium. There are two liquid helium level indicators in the dewar. One is at the lower end of the needle

# Resistance thermometer calibration

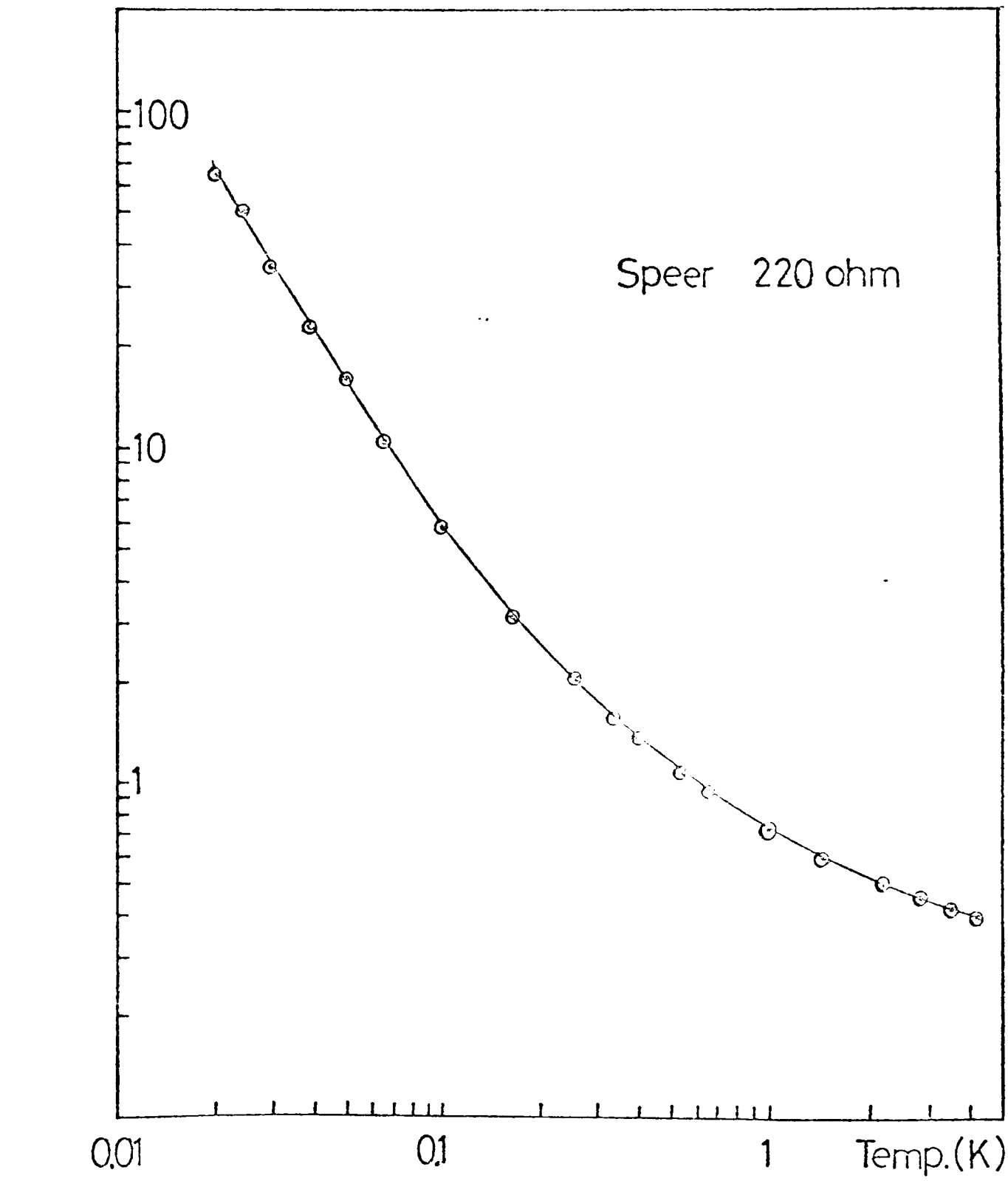



Fig. 3.2

valve, indicating whether there is sufficient helium to fill the $1^{o}$ pot. The other is $\simeq 3$ cm above the top of the OJ, indicating when the dewar is full. The dewar holds 21 l of helium. During the transfer 7 l are boiled off.

V. The Magnets:

Each of the magnetic cooling stages has a NbTi superconducting solenoid. The magnet for the salt pill demagnetization is 120 mm long with an inside diameter of 133 mm. The field at the centre of the magnet is given by 248 G/A. This solenoid has been used up to 6 kG. With dilution refrigerator temperatures down to 200 mK, values of H/T of up to 30 kG/K can be reached as will be seen (sec. VIII), this is more than sufficient for the salt pill demagnetization.

The magnet for the nuclear stage is an 8 T solenoid 180 mm long with an inside diameter of 72 mm. This large diameter is to accommodate eventually a $Nb_3Sn$ insert which would raise the maximum field to 10 T. The magnet is wound in three concentric sections connected in series. Each section is potted in epoxy resin. Also in series are two coils (shown in fig. 3.1) which compensate for the field from this magnet at the salt pill. The central field of this magnet is given by 981 G/A. Thus 8T requires 80A. The field profiles of this magnet, of the compensating coils and of the salt pill magnet are shown in figure 3.3. To prevent a large helium boil off, special care has to be taken with the leads for the large currents used. The leads from the top of the apparatus to the highest position of the helium level are brass

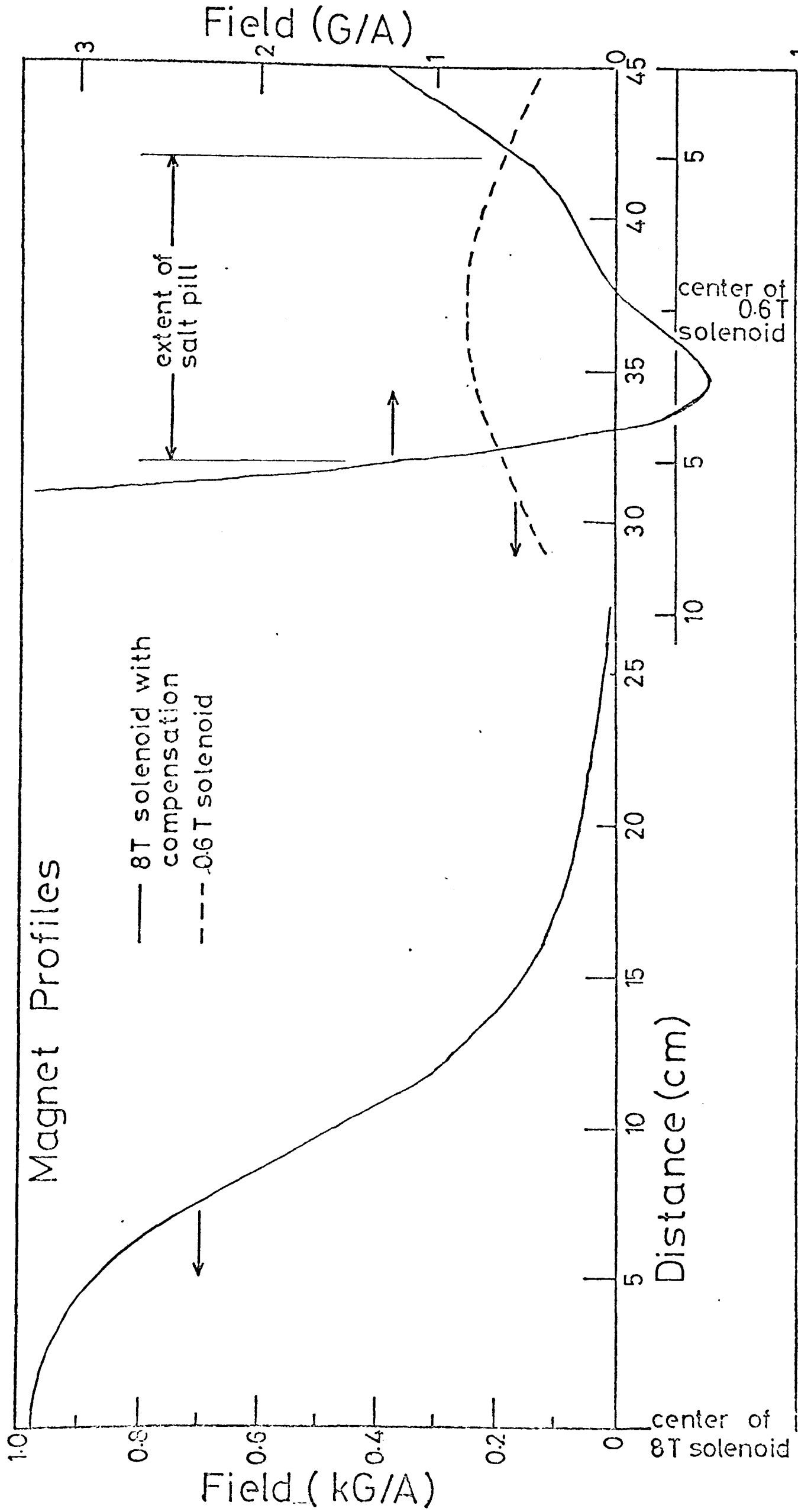

Field (G/A)
3
2
1
0
-1
45
40
35
30
25
20
15
10
5
5
5
10
extent of salt pill
center of 0.6T solenoid
Magnet Profiles
8T solenoid with compensation
0.6T solenoid
Distance (cm)
center of 8T solenoid
1.0
0.8
0.6
0.4
0.2
0
Field (kG/A)

Fig. 3.3

tubes (diameter: 8.7 mm, wall: 0.65 mm). These tubes are inside another tube that carries the evaporated helium which thus cools the leads. Brass rather than copper was chosen because for the same maximum current capacity, it produces a smaller heat leak with no current through the leads.

Before being put into the apparatus the magnet was tested in a separate dewar upto a field of 7.8 T. After the magnet was put into the nuclear cooling apparatus, it was run with a different power supply. With this power supply it was found that the magnet always quenched (went normal) at fields well below 7.8 T, sometimes as low as 2 T. An instability in the power supply was the principal cause of this trouble. With a more stable power supply, the magnet has been run to 7.5 T, although it still sometimes quenches at fields down to 6.5 T. These quenches are thought to have been a result of local strain caused by ice. Since the apparatus is usually taken apart while cold, water condenses on the magnet. This water can penetrate into the cracks in the epoxy resin. On the next run this water will freeze and expand, thus straining the windings. When the magnet is operated at a high field, the large forces between the windings can overcome the strength of the ice. This results in a small local movement in the coil, which causes local heating that quenches the magnet. Since each quench results in the loss of several liters of liquid helium, the field has been limited to 6 T on most runs to be on the safe side. The quenching of the magnet was also found to be dependent on the rate of increase or decrease of the current. After various tests it was decided

to use the following rates, which allow for some safety margin: on magnetization: 120 G/s for 0-10 kG; 60 G/s for 10-40 kG; 20 G/s for 40-60 kG; 10 G/s for 60-80 kG; on demagnetization: 120 G/s for 80-40 kG; 250 G/s for 40-30 kG; 400 G/s for 30-0 kG. To achieve the last rate, the power supply had to be modified to withstand the inductive voltage of about 6 V caused by this rate, since the laboratory's standard power units are designed for 1.5 V. Further difficulties with the magnet and the power supply were found in the low field region. These will be discussed in Chapter 4. The testing of this magnet at high fields took about five months.

## VI. The Dilution Refrigerator:

A detailed discussion of the principles and methods of dilution refrigeration has been given by Wheatly, Vilches and Abel (36). The dilution refrigerator used in this apparatus was supplied by the Oxford Instrument Company. As shown in figure 3.1, this dilution refrigerator is comprised of a condenser, a still, a concentric tube heat exchanger and a mixing chamber. It was designed for a large refrigeration power above 100 mK, rather than a low base temperature. To check the performance of the unit, the refrigeration power was measured by electrically heating the mixing chamber while monitoring its temperature with a carbon resistence thermometer. The results of these measurements are shown in figure 3.4. The cooling power at 100 mK was found to be 800 erg/s instead of the design figure of $2\text{-}3\times10^{3}$ erg/s. No explanation for this discrepancy has been found.

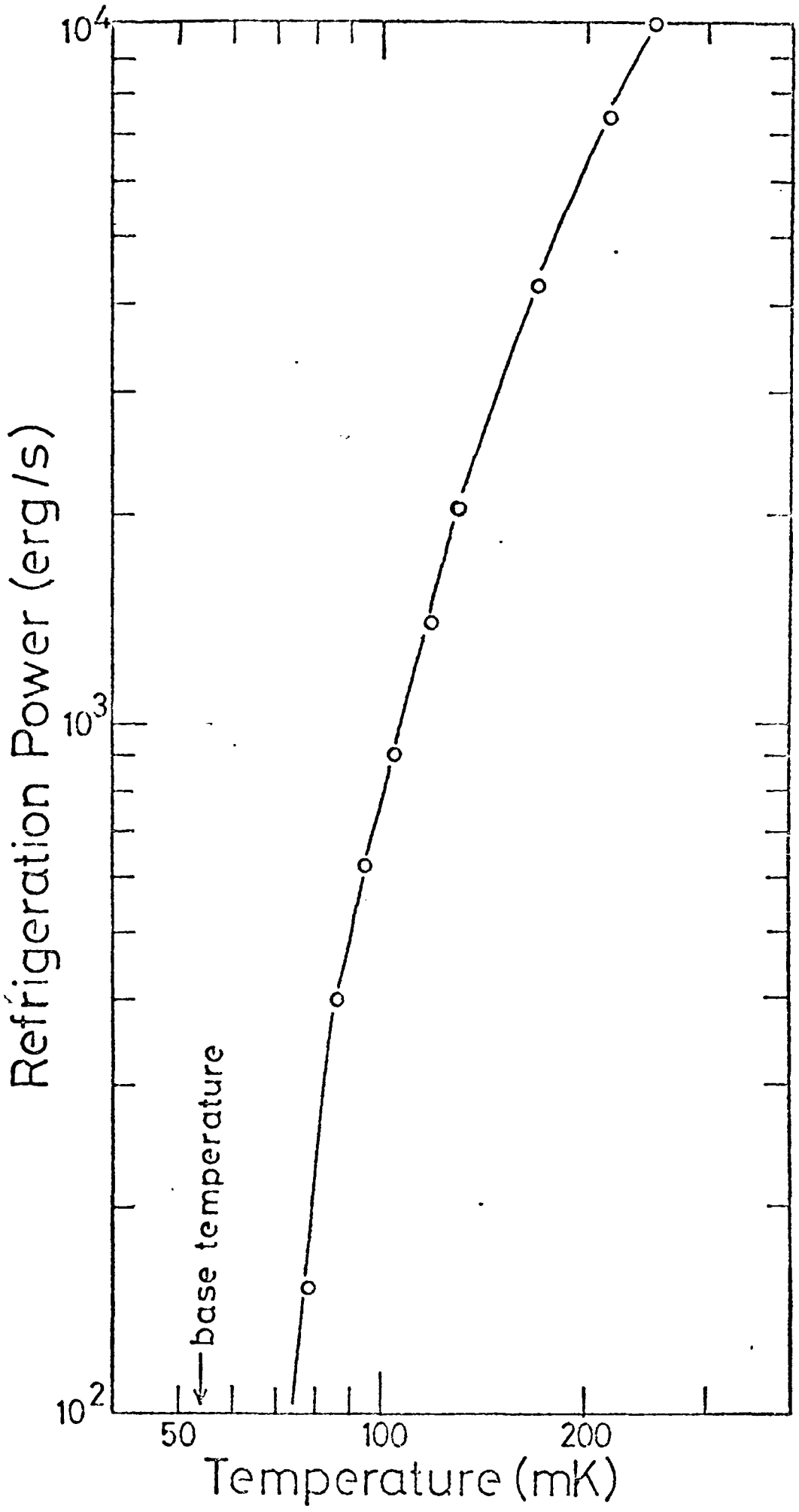

Refrigeration Power (erg/s)
$10^4$
$10^3$
$10^2$
base temperature
50
100
200
Temperature (mK)

Fig. 3.4

The refrigerator is larger than most others used hitherto. It takes a helium mixture of 68 l of $^4$He and 12 l of $^3$He. The gas storage and circulation system is shown schematically in figure 3.5. It has four storage vessels with a total volume of about 100 l. The $^3$He is circulated by an Edwards 9 B4 booster pump backed by a 550 l/min two stage rotary pump. The output side of the latter pump has a volume of about 3 l. To reduce the amount of $^3$He in this part of the system (and thus the total amount needed), this rotary pumped is backed by a 35 l/min rotary pump. Before being returned, the $^3$He is passed through a liquid nitrogen cooled charcoal trap to remove any oil vapour or air that might be in it. The returning helium is condensed in a sintered bronze heat exchanger, which is in contact with the $1^{o}$ pot. The flow rate of the returning helium is measured with a flow meter of the heated tube type. This flowmeter has been described in detail by Niinikoski (37). The flow would be as high as $10^{-3}$ moles/s during the starting up proceedure. This would drop to $\sim 10^{-4}$ moles/s at latter stages. The flow can be increased by applying heat to the still, either electrically or by warming the $1^{o}$ pot. The flow was usually kept $\simeq 3 \times 10^{-4}$ moles/s. There was no significant increase in refrigeration power at higher flow rates. This is thought to be a result of the inefficiency of the heat exchanger. The pressures at both ends of the booster pump are measured with pirani gauges. The pressure of the returning helium is measured with a pair of Bourdon gauges. One of these has a pressure actuated switch in it. If the pressure in the return line exceeds a predetermined value (usually 760 torr),

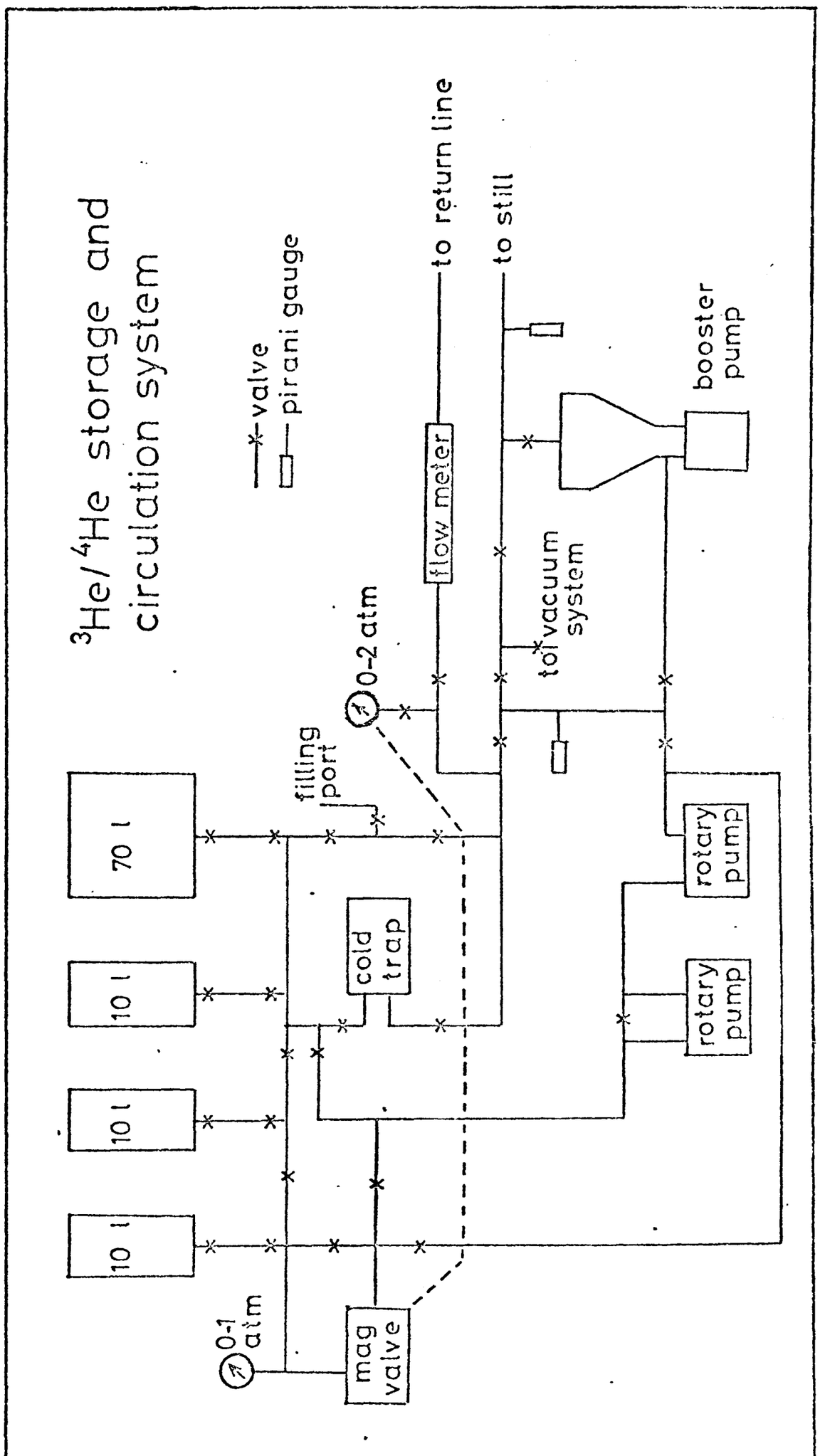

$^3He/^4He$ storage and circulation system
valve
pirani gauge
to return line
to still
booster pump
flow meter
to vacuum system
0-2 atm
filling port
70 l
10 l
10 l
10 l
cold trap
rotary pump
rotary pump
0-1 atm
mag valve

Fig. 3.5

a magnetic solenoid valve will open and release the helium to the storage vessels. This allows the refrigerator to be run unattended without losing any helium if the return line blocks.

The following is the operating proceedure of the dilution refrigerator.

1. Starting from 4.2 K; pump the exchange gas out of the jackets and fill the $1^{o}$ pot.
2. Pump the $1^{o}$ pot.
3. When the $1^{o}$ pot is below the $\lambda$-point, pump the helium mixture into the still.
4. When the pressure in the still is 20 to 40 torr, start circulating the mixture by slowly pumping the still with the rotary pump. During this proceedure the pressure of the returning mixture is kept below 760 torr.
5. When the pressure in the still is $\approx 1$ torr, start pumping with the booster pump.
6. As soon as the mixing chamber starts to cool rapidly, the refrigerator is in its operating mode.

The above proceedure typically takes $1\frac{1}{2}$ hours. At the end of a run, the mixture is pumped into the store. This process can be hastened by warming the $1^{o}$ pot and by putting exchange gas into the jackets.

There were several difficulties encountered during the first months of operating the refrigerator. After the initial few runs the performance of the refrigerator started to degrade. On each successive run, the cooling power became less and the base

temperature became higher. It took seven months to convince ourselves and the manufactures that something was wrong with the refrigerator and not with our apparatus or technique. In the end, the refrigerator was tested on a compatible cryostat at the Rutherford Laboratory and it was discovered that a leak between the two sides of the heat exchanger, which opened gradually after the first few runs, was the cause of the trouble. After the heat exchanger was replaced, the refrigerator was still not behaving properly. The base temperature was $\simeq$200 mK. Two months were spent in trying various helium mixtures and making sure that there was no touch between any part of the refrigerator and the IJ. Even the heat exchanger was replaced, but there was no improvement. It was finally decided to replace the existing condenser with a larger one. The old condenser was a 250 mm length of 0.5 mm wall 2 mm diameter copper tube soft soldered to the bottom of the $1^{o}$ pot. The heat transfer for this exchanger was calculated to be more than necessary and the early experiments with the first heat exchanger had indeed shown it to be sufficient. On removing it from the apparatus, it was discovered that the solder joint between the condenser and the $1^{o}$ pot was of poor quality. Because of inadequate heating, the soft solder had not run. Most of the contact between the two parts was "dry" and there was only a small area of good contact. The thermal contact through the "dry" joint had probably become worse each time it was temperature cycled. This had resulted in the loss of four months. The new condenser is a disc of sintered bronze (6 mm thick, 20 mm diameter) which is a press fit into a brass housing soldered with indium to the

bottom of the $1^{o}$ pot. This condenser has given reliable service for more than a year now.

## VII. The NMR System:

### A. Introduction:

The purpose of the pulsed NMR system is to measure the magnetization of the copper sample. As described in section 2.V, the NMR system can be used as a thermometer for temperatures much greater than the ordering temperature. Spin ordering effects are expected to show up as deviations of the final temperature from $T_f = (H_f^2 + H_{int}^2)^{\frac{1}{2}} T_i/H_i$ (eq. 1.6). One of the purposes of this experiment was to test the usefulness of the integrating NMR thermometer for fields less than 10 Gauss.

The NMR is done in the final demagnetization field. To observe ordering effects, the final field must be $\leq H_{int}$. For this purpose a 10 kHz (8.9 Gauss) system was built. This system can be extended to 3 kHz ( 3 Gauss). However, this low frequency system is not very useful at temperatures above 10 mK because of the very small signals from it. For the preliminary experiments, a more sensitive NMR system was used. This was a 100 kHz (89 Gauss) system. Both of these systems are similar to the one described by Hensel and Smith (26). Both integrate the signal induced by the free precession decay of the nuclei.

### B. The Crossed Coil System:

The crossed coil system is shown diagrammatically in figure 3.6. To observe a sharp resonance, the inhomogeneity of $H_o$ must be a small fraction of $H_{int}$. Since 100 G is the largest field used, the homogeneity must be about or better than 1%. Since this is not a particularly difficult requirement, the

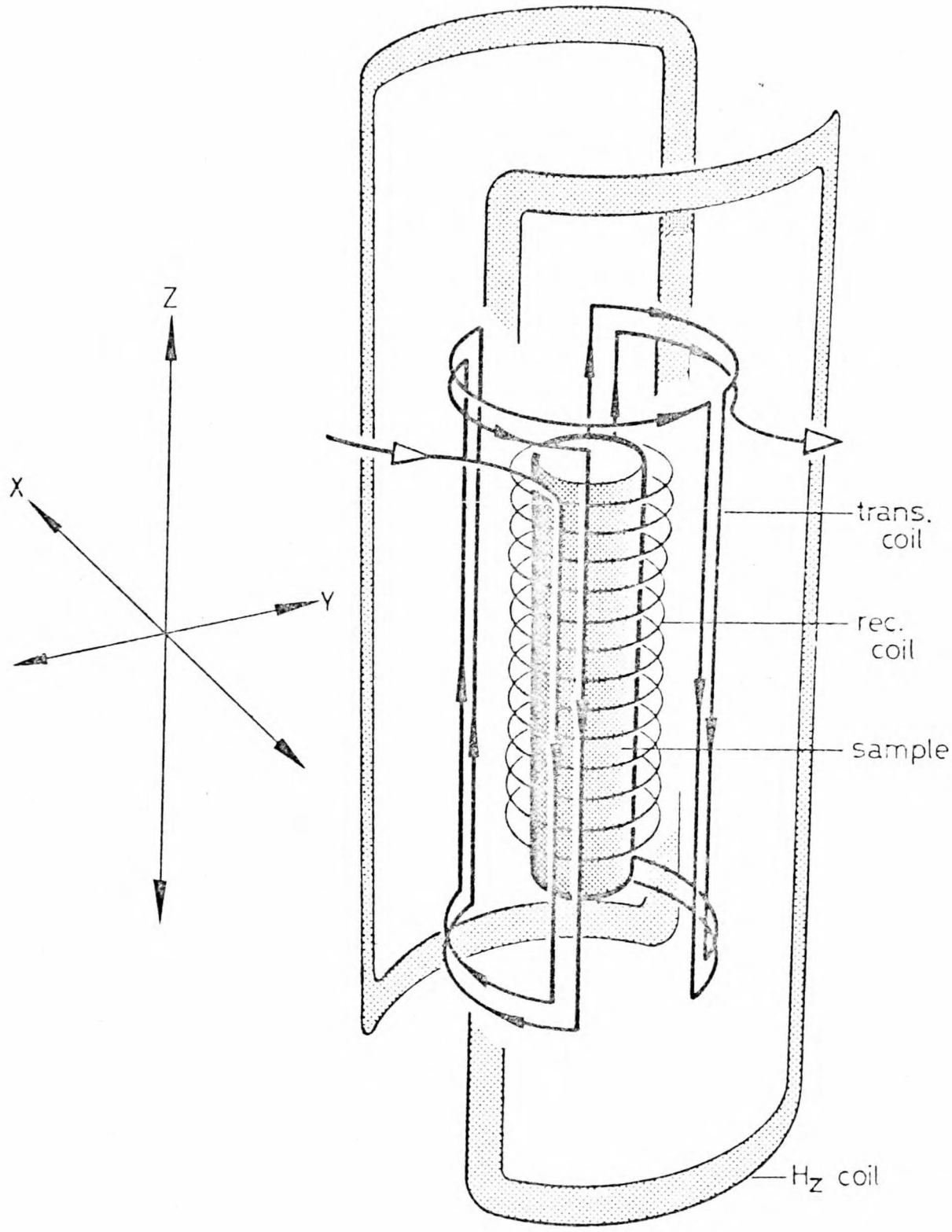



Figure 3.6 The N.M.R. coils

arrangement of the coils was chosen to maximize the received signal. This is done by placing the receiver coil axially in the cryostat so as to maximise the filling factor. The three coils are mutually perpendicular. The axes of the steady field, $H_o$, and the tipping or transmitting field, $H_1$, are in the horizontal plane. All coils are centrally located with respect to the nuclear demagnetization magnet.

The steady field coil is mounted in the liquid helium bath. It consists of a pair of coils arranged in a saddle shaped geometry. Each coil is a 125 mm x 55 mm rectangle containing 30 turns of NbTi superconducting wire. The turns are held together with epoxy resin. The coils are bent around the outside of the OJ and held in place with adhesive tape. The central field of these coils is 11 G/A. The homogeneity is 1% over a cylinder 60 mm long and 15 mm in diameter.

The transmitter coil is made of a copper coated flexible plastic, as used for printed circuits, which had most of the copper etched off so as to produce a pair of suitably spaced rectangular coils of two turns each. The coil is shown full scale in figure 3.7. The coil is wrapped around a plastic tube and mounted inside the IJ by attaching it to the copper sample with nylon threads. The finished coil 165 mm long with a diameter of 21 mm. The calculated field for this coil is 1.3 G/A. The leads to this coil are copper from room temperature to the $1^o$ pot. From there they are superconducting. The leads are thermally anchored to the $1^o$ pot and to the still. The transmitting pulses

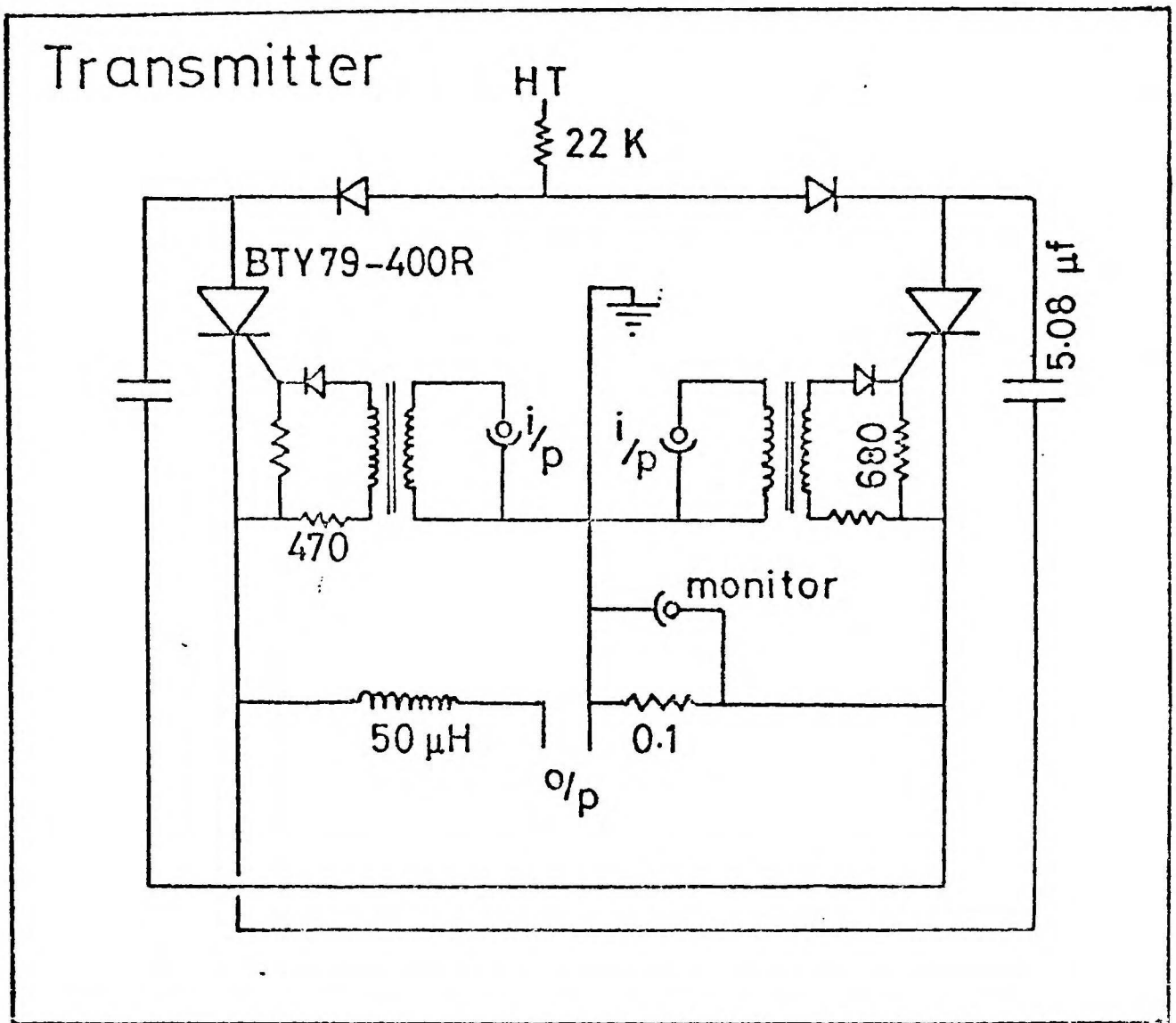

Transmitter
HT
22 K
BTY79-400R
5.08 µf
i/p
i/p
680
470
monitor
50 µH
0.1
o/p
Transmitter Coil

Fig. 3.7

can be expected to heat this coil and cause the evolution of gas. There is no evidence that this causes a significant heat leak into the specimen for the pulses normally used ($\sim$ 10 A). However, on the few occasions when large pulses ($>$ 100 A) have been used the warming-up rate of the pill was increased.

A receiver coil must be designed to have a large response to the NMR signal and a fast recovery from transients induced by the transmitter. A good signal can be achieved by having at least 3000 turns of wire as close to the nuclear sample as possible. Fast recovery requires a Q of about $\frac{1}{2}$ (critical damping). This can be achieved by making a long coil in several sections and with few layers to reduce the self capacitance and by using resistance wire to have a large resistance. To meet these requirements, the receiver coil is wound in 25 circular grooves (1.5 mm wide, 1 mm deep, 0.5 mm separation) cut into a plastic tube (50 mm long, 18 mm diameter, 2 mm wall). The former is a press fit inside the transmitter coil and there is a 2 mm gap between it and the nuclear sample. Each groove contains 125 turns of 0.04 mm diameter enamel coated manganin wire. The coil has a resistance of 47 k$\Omega$ and an inductance of about 400 mH. This gives a Q of about 1 for 100 kHz and about 1/10 for 10 kHz. The leads are thermally anchored to the mixing chamber and the $1^{\circ}$ pot. From there to the receiver amplifier the leads are encased in PTFE sleeving inside a metal tube.

C. <u>The Electronics</u>:

A block diagram of the electronics is shown in figure 3.8. The 100 kHz system has been described in detail by Hensel and Smith (26).

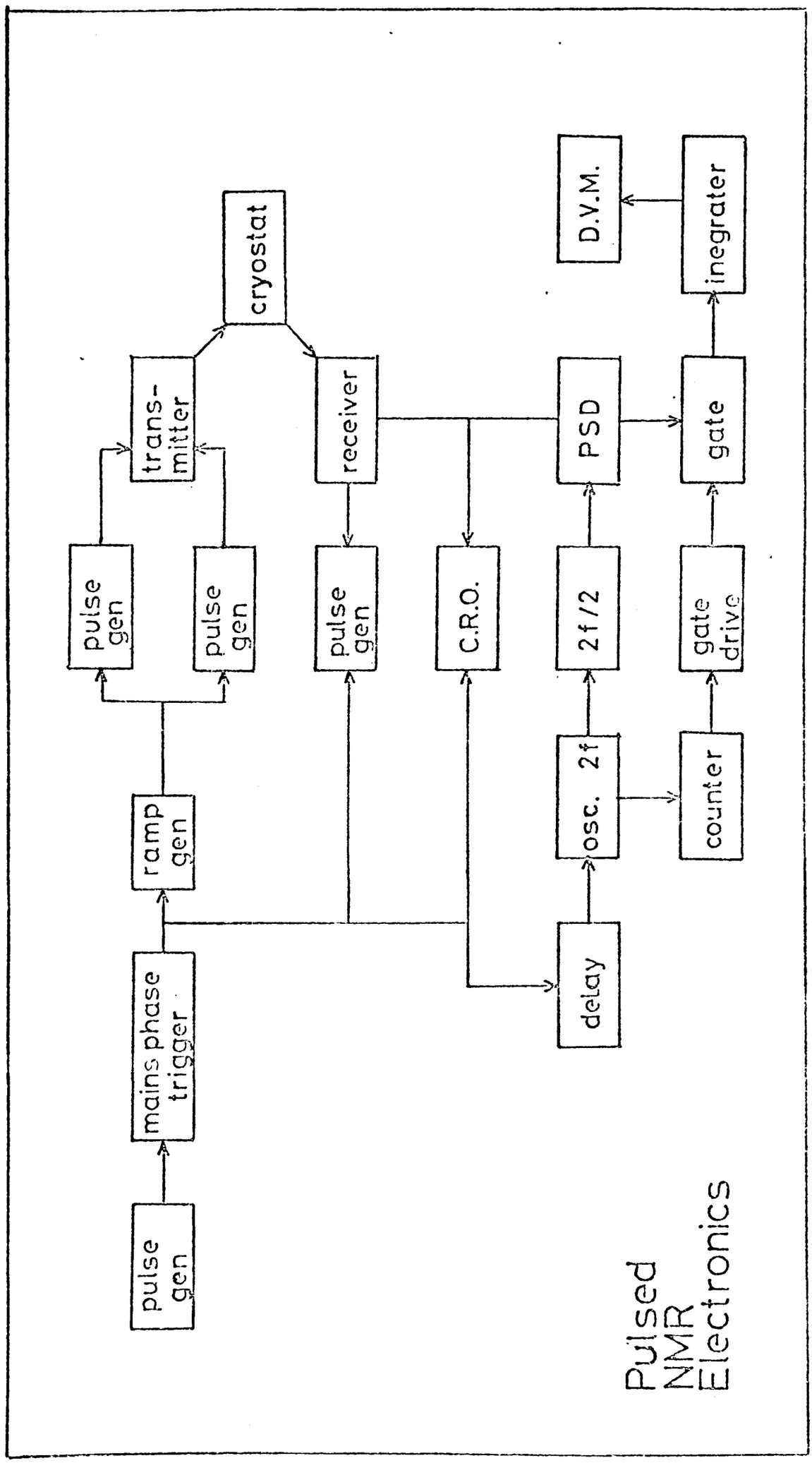

Pulsed NMR Electronics
pulse gen
mains phase trigger
ramp gen
pulse gen
pulse gen
trans-mitter
cryostat
pulse gen
receiver
C.R.O.
delay
osc. 2f
2f/2
PSD
D.V.M.
counter
gate drive
gate
inegrater

Fig. 3.8

The system is controlled by a master pulse generator, which can be operated manually or automatically at pre-set intervals and predetermined phase of the ac mains. This master pulse generator initiates several actions. It triggers the transmitter, the storage oscilloscope, the damping pulse for the receiver and the integrator. The reference oscillator is also triggered with a predetermined phase.

There are two transmitters. One operates at 100 kHz and the other at 10 kHz. Figure 3.7 shows the circuit diagram of the 10 kHz transmitter. They can produce either whole or half cycle pulses. The transmitters consist of a pair of capacitors that can be discharged through the transmitter coil. The capacitors are charged by a variable voltage supply (HT). The discharge of each capacitor is controlled by a thyristor. The output of each transmitter can be monitored by looking at the voltage across a small series resistance ($\sim 0.1\Omega$). The outputs are 1.4 A/V for the 100 kHz transmitter and 1.2 A/V for the 10 kHz one.

March (11) has shown that a perfectly conducting cylinder surrounding a transmitter coil attenuates the transmitter pulses by a factor

$$A = (1-a^2/b^2)^{-1} \qquad (3.1)$$

where a is the radius of the transmitter coil and b is the radius of the jacket. In this apparatus the attenuation factor is 1.48. The smallest voltage at which the transmitter can reliably work is 3 volts. This results in a minimum tipping angle of about $7^o$ for a one cycle pulse from the 100 kHz transmitter and about $35^o$ for a half cycle pulse from the 10 kHz transmitter. If smaller

pulses were desired, this could be arranged by charging the two capacitors in the transmitter to different voltages and simultaneously triggering both thyristors.

The recievers have gated inputs and are designed for fast recovery. The gating reduces the effect of the large transients caused by the transmitter. The gate is controlled by a pulse that is triggered at the same time as the transmitter. The recovery of the receivers was found to be dependent on the amplitude and polarity of the transmitter pulse. This is a result of the gate not being perfect. Both the gate signal and the transmitter pulses induce signals in the receiver. The recovery is fastest when these partially cancel each other. The length of the damping pulse and the polarity of the transmitter were always set to give the fastest recovery. The receiver for the 100 kHz has a band width of 70 to 350 kHz. It was designed for one of the leads to the receiver coil to be earthed. The recovery time of this amplifier is typically 25 $\mu$s. The other amplifier has sufficient band width to be used between 3 and 10 kHz. The design of this receiver requires that neither of the leads be earthed. Its recovery time is about 40 $\mu$s. To minimize electrical noise, both amplifiers are battery operated.

The integrator has a gated input. The output of the integrator is proportional to the time integral of the input during the time the gate is open. The integrator is controlled by a triggered oscillator operating at 200 kHz. The oscillator is triggered by a delayed pulse from the master trigger. The phase of the oscillator with respect to the master trigger pulse can be

set by varying the delay time. This oscillator acts as a clock for the integrator. The start and stop times of the integrator can be set in increments of one cycle (5 μs) of the oscillator. The integrated signal is stored and is displayed on a voltmeter. The number of cycles of the signal that can be integrated depends on the spin temperature and resonance frequency. At $10^{-6}$ K (the spin temperature after a demagnetization) the signal should be so large that it can be observed for a time equal to several $\tau_2$ (spin-spin relaxation time). For 10 kHz this will be about 6-7 x $\tau_2$ or 5 cycles. As the temperature rises, the number of observable cycles decreases until they disappear at about 10 mK. This last feature will make the 10 kHz system difficult to calibrate. Despite this, the 10 kHz system can be used to make relative measurements for demagnetizations from different H/T. With only a few cycles to integrate, the best signal to noise ratio can be achieved by rectifying the signal before it is integrated. The 100 kHz signal is larger and lasts for a larger number of cycles. This system can be calibrated at 10-30 mK where the signal lasts for about 5 cycles. With more cycles to integrate, a phase sensitive detector (PSD) can improve the signal to noise ratio. The 100 kHz signal is sent to a PSD before it is integrated. The reference signal for the PSD is derived from the triggered oscillator by a frequency divider. This reference signal can also be fed into the 100 kHz receiver. This is useful in setting up the integrator and it can be used as a gain check on the system. Using this feature, the overall reproducibility of the system was found to be ± 0.5%.

The following is the setting up proceedure for the 100 kHz NMR.

1. If a whole cycle transmitter pulse is desired, adjust the time delay on the two trigger pulses for the transmitter until the output is one complete cycle. For a half cycle pulse, turn off one of the trigger pulses.

2. Adjust the polarity of the transmitter pulse and the width of the damping pulse to achieve the minimum recovery time.

3. Send the reference signal to the receiver. Adjust the phase of this signal to maximize the output of the integrator.

4. Turn on the $H_o$ field and adjust it to give the desired resonance frequency.

5. Adjust the time delay on the triggered oscillator to maximize the integrator output. This can be done by adjusting the time delay until the phase of the NMR signal is the same as the phase of the gain check signal.

Except for omitting step 3, the 10 kHz system is set up the same way.

VIII. <u>The Nuclear Cooling Assembly, (The Salt Pill and Nuclear Cooling Sample)</u>.

Two types of nuclear samples have been used. They are both bundles of polyurethane insulated copper wires. One contains 25000 0.04 mm diameter (48 swg) wires and the other contains 9500 0.06 mm diameter (46 swg) wires. The purpose of using thin wires is to reduce the eddy current heating that occurs during the magnetization and demagnetization. The lower 400 mm of the bundle is formed into a 10 mm diameter cylinder and set in an

epoxy resin (four parts Araldite 103, one part hardner 956). A thin walled, German silver tube was used as a mould. After the epoxy set, the tube is peeled off. The wires at the upper end of the bundle are left loose to be immersed in the salt pill.

The salt pill is contained in a brass cylinder (80 mm diameter, 100 mm long) with one open end. A 10 mm diameter German silver tube runs coaxially turough the container. The upper end of the epoxied part of the bundle is held in this tube with wooden wedges cut from matchsticks. The loose wires are bent down and spread out in the annular space between the central German silver tube and the brass tube. The container is suspended from the bottom of the mixing chamber by three stainless steel tubes (2 mm diameter, 0.2 mm wall, 160 mm 16 cm long), which are attached to the bottom of the salt pill container so as to reduce their heat conductance.

Thermal contact between the salt pill and the mixing chamber is through a superconducting heat switch. The design of a heat switch is a compromise between several parameters. The ideal heat switch would have an infinite conductivity when closed and no conductivity when opened. For maximum efficiency ( i.e. the removal of the heat of magnetization in the shortest time possible), the heat switch should be closed at the beginning of the magnetization and opened at the beginning of the demagnetization. As these conditions can not be met, the following criteria were used in the design. The heat switch should remove the heat of magnetization of the paramagnetic salt at 200 mK ($6 \times 10^6$ ergs) in a time governed by the cooling power of the refrigerator (fig. 3.4). The ratio of the thermal conductivity in the normal state (switch closed ) to

that in the superconducting state (switch open) called the switching ratio, should be as large as possible. The switch is closed by applying a magnetic field exceeding the superconducting critical field. This switching field could be either the fringe field of the magnetizating solenoid of the salt pill or the field of a separate solenoid. The former method was used because it is the simpler. The drawback of this method is that the switch changes state at the same field on magnetization as it does on demagnetization. With this restriction, maximum efficiency for demagnetization is achieved by the switch changing state at as high a field as possible. This however, results in the magnetization being irreversible and therefore inefficient.

The material chosen was 99.999% pure lead. The high purity is important for achieving a good switching ratio. March and Symko (38) found that the thermal conductivity of this material at a temperature T, is 310 T W/ m/$^{o}$C in the normal state and 4.4 $T^3$ W/ m/$^{o}$C in the superconducting state. Other materials, such as tin and indium, have similar switching ratios, but lead was chosen because it has a higher critical field, 800 Gauss below 1 K. The switch is made of six 25 mm long 1 mm diameter lead wire. At one end, these wires are soldered with indium to a strip of copper. This strip is greased and bolted to the bottom of the mixing chamber. This allows the pill and nuclear stage to be removed and stored in a nitrogen dewar with out damaging the heat switch. At the other end, the lead wires are soldered with indium to a bundle of 9500 0.06 mm diameter (46 swg) copper wires. Before

being soldered, one end of this bundle is formed into a 10 mm diameter cylinder and set in epoxy resin. The end is then cut into a cone and "tinned" with indium. This procedure is to ensure that each of the closely packed wires is in contact with the heat switch. The other end of the copper wires are left loose to be immersed in the salt pill. Since, as said above, it is desirable to have the heat switch change states at as high a field as possible, the heat switch is placed far from the salt pill (i.e. as close to the mixing chamber as possible). In this configuration the heat switch changes state when the field at the centerof the pill is $\simeq$ 2.5 kGauss (i.e. about $\frac{1}{2}$ of the maximum field).

The two paramagnetic salts used in the experiments were chrome potassium alum (CPA) and cerium magnesium nitrate (CMN). The properties of these are given in the following table.

Table 3.2

Properties of Paramagnetic Salts

| | CPA | CMN |
|---|---|---|
| gram-ion weight (g) | 499 | 765 |
| density ($g/cm^3$) | 1.83 | 2.09 |
| spin | 3/2 | 1/2 |
| g-factor | 1.97 | $\parallel$ < 0.02 a) |
| | | $\perp$ 1.84 |
| ordering temperature (mK) | 10 | 1 |
| H/T to remove (kG/K) | | |
| 50% of entropy b) | 11 | 16 |
| 80% of entropy b) | 20 | 28 |

a) CMN is a flat hexangular crystal, c-axis (and $g_{\parallel}$)are normal to the plane.
b) There is very little to be gained by going to higher H/T.

The CPA was purchased from British Drug Houses ( BDH). The CMN was grown from a stoichiometric mixture of cerium nitrate and magnesium nitrate dissolved in distilled water. These were purchased from BDH.

The method of making the salt pills is similar to the method first used by Kurti, Simon, Spohr and Robinson (8). First the salt is finely ground. It is then made into a slurry by mixing it with a mixture of 50% glycerol and 50% saturated solution of the salt. The slurry has a consistancy of jam. The copper wires from the heat switch ( $\approx$ 200 mm long) and from the nuclear stage ( $\approx$ 400 mm long) are mixed with the slurry. Every attempt was made to distribute the wires uniformly. The mixture is then stuffed into the pill container. As soon as a pill is made it is put into liquid nitrogen where it is kept until the apparatus is assembled. This precaution is necessary to prevent the glycerol from absorbing the water of crystallization. If some of the water of crystallization is lost, the magnetic properties of the salt will change (see for instance ref. 39).

# Chapter Four

## Preliminary Experiments

### I. Early Chrome Potassium Alum (CPA) Experiments:

The experiments described in this section took place between July 1973 and January 1974. These are the first experiments to be done after the dilution refrigerator began to work reliably. They were done with CPA salt pills and nuclear samples containing 9500, 0.06 mm diameter copper wires.

The first pill contained 300 g of CPA and the copper bundle was cut off just below the pill container. A $^{60}$CoCo thermometer was attached to the bottom of the copper bundle. There was also a carbon resistor thermometer (CRT) imbedded in the pill. This was a 220 Ω Speers resistor. One end of about fifty, 100 mm long, 0.06 mm diameter wires were wrapped around the resistor and stuck down with G. E. varnish. The other ends of the wires were distributed through the pill. This CRT was to monitor the temperature of the pill during the magnetization.

The purpose of using this pill was to see if the heat switch was capable of extracting the heat of magnetization in a reasonable time and to try a pill demagnetization for the first time in this apparatus. This pill was run on two occasions, 25 July and 31 July. On both occasions, the pill was magnetized to only 3.72 kG, since it was not known at that time whether the leads could withstand higher currents. On 25 July, $1\frac{3}{4}$ hours was allowed to elapse between the magnetization and the demagnetization.

During this time the temperature of the pill went from 1 K to 240 mK as measured by the CRT. This gave an initial H/T of 15.5 kG/K. After the demagnetization a temperature of 13.4 mK was measured on the Co thermometer. The CRT indicated a temperature of 54 mK at this time. The discrepancy in these temperatures is thought to be due to the poor thermal conductance of the thick insulting layer surrounding the carbon in the resistor. On 31 July, 2 hours elapsed between the magnetization and the demagnetization. This time the demagnetization started at 200 mK (H/T of 18.7 kG/K). The final temperature was 12.3 mK on the Co and 43 mK on the CRT. These experiments showed that the heat switch had a satisfactory conductivity and that the temperature as measured on the Co was sufficient.

It was then decided to try the 100 kHz NMR system. For this, a full length (400 mm) nuclear sample was made with a 300 g CPA pill. This time the $^{60}$CoCo thermometer was not attached. The first experiment in which an NMR signal was observed was on 10 October. The temperature reached on this occasion was not known because the only thermometer was the CRT which the earlier experiments had shown to be inaccurate. Because the main solenoid was not in the apparatus, a nuclear demagnetization and thus a $\tau_1$ measurement (by the method to be described later) could not be made.

Now that an NMR signal had been seen, it was decided to try a nuclear demagnetization. As the magnet designed for this experiment was not yet ready, a 4.5 Tesla solenoid was borrowed. A new 300 g CPA pill was made and a $^{60}$CoCo thermometer

was soldered to the bottom of the nuclear sample. To improve the thermal contact between the CRT and the pill, the insulation on the resistor was ground off, leaving the carbon exposed. It was then varnished and attached to a small bundle of copper wire. After a few tests of the solenoid, a run was made on the 26 Nov. On this run the leads to the CRT broke, so it was not possible to monitor the temperature of the pill during its magnetization. By comparing the temperature of the mixing chamber for this run with those for the previous runs, an estimate of the temperature of the magnetized pill could be made. After the pill was demagnetized from an estimated 200 mK (H/T ~15 kG/K), the Co only showed a small effect, indicating a temperature greater than 20 mK. This run was used to learn more about the NMR system. The effect of varying the timing of the various pulses was studied by observing the NMR signal on an oscilloscope. On 11 December, this pill was demagnetized from 3.72 kG and 150 mK (H/T of 24.8 kG/K). Both the CRT and the Co indicated temperatures of 25 mK. This temperature is considerably higher than the temperatures measured with the Co for the first pill. On none of the succeeding experiments did the Co thermometer work. This is thought to be a result of the epoxy resin between the copper wires preventing a good solder joint. On the first pill the bundle had been cut off near the top of the epoxied region. Perhaps there was less epoxy in this region, which allowed a good solder joint to be made on that occasion. On 11 December, a nuclear demagnetization was done from 45 kG at a rate of 67 G/s. On the oscilloscope, the NMR amplitude was observed to increase by a factor of about 10. This run and a smiliar run on 17 January

1974 were useful in setting up the integrating part of the thermometer.

This set of experiments with CPA had served a useful purpose. They had shown that the heat switch between the salt pill and the mixing chamber was appropriate, that the demagnetization of the salt pill results in temperatures between 12 and 20 mK and that signals could be observed with the 100 kHz NMR system.

II. The Early Cerium Magnesium Nitrate (CMN) Experiments:

These experiments were performed between February and April 1974. They were all done with nuclear samples made of 9500 0.06 mm diameter copper wires. The pills were made of 1 kg of CMN. A CRT was in the pill. This was the same CRT that was used in the CPA experiments just described. A $^{60}$CoCo thermometer was attached to the bottom of the copper bundle, but as has been explained, it did not work. Most of the CMN demagnetizations were not done to a zero applied field because CMN has a very small heat capacity in zero field. In a non zero final field, the heat capacity is proportional to $H^2 + (40)^2$ and the final temperature is proportional to $(H^2 + (40)^2)^{\frac{1}{2}}$. Thus, a non zero final field results in an increase in the heat capacity at the expense of a small increase in the final temperature. The final fields varied between 100 and 250 G.

The purpose of this set of experiments was to reach lower salt pill temepratures by using CMN and to do a nuclear demagnetization from the large field available from the new magnet. Unfortunately, most of these runs were spent trying to sort out some difficulties with the magnet. As was mentioned in the previous

chapter , a combination of unstable power supplies and water condensation prevented the magnet from reaching high fields. However, some informative experiments were done.

Using the CRT to measure temperature, a group of salt pill demagnetizations were done. On 6 March, the first successful CMN demagnetization was done. When demagnetized from 3.72 kG and 175 mK (H/T of 21.2 kG/K), a temperature of 31 mK was reached in 250 G, instead of an expected 12 mK, and 26 mK in zero applied field. This was not very promising. On 13 March, the experiment was repeated. This time the demagnetization was stopped at various fields while the temperature was measured. These measurements are shown in figure 4.1 and summarized in the following table along with the result of three more runs.

Table 4.1

CMN Demagnetizations

| Date | H(Gauss) | T(mK) | H/T(kG/K) | heat leak in applied field (erg/s) | (Gauss) |
|---|---|---|---|---|---|
| 13/3 | 3720 | 170 | 21.9 | | |
| | 750 | 40 | 18.8 | | |
| | 375 | 29 | 12.9 | | |
| | 250 | 26 | 9.6 | | |
| | 100 | 22 | 4.9 | 40 | 100 |
| 22/3 | 3770 | 180 | 20.9 | | |
| | 100 | 23 | 4.6 | 20 | 0 |
| 28/3 | 3770 | 180 | 20.9 | | |
| | 100 | 24 | 4.5 | 20 | 0 |
| 28/3 | 3770 | 320 | 11.8 | | |
| | 100 | 24 | 4.5 | 40 | 100 |

Two important things were noticed. One was that the final temperature on the last two runs was the same despite the quite different initial H/T. This might have been symptomatic of poor thermal contact between

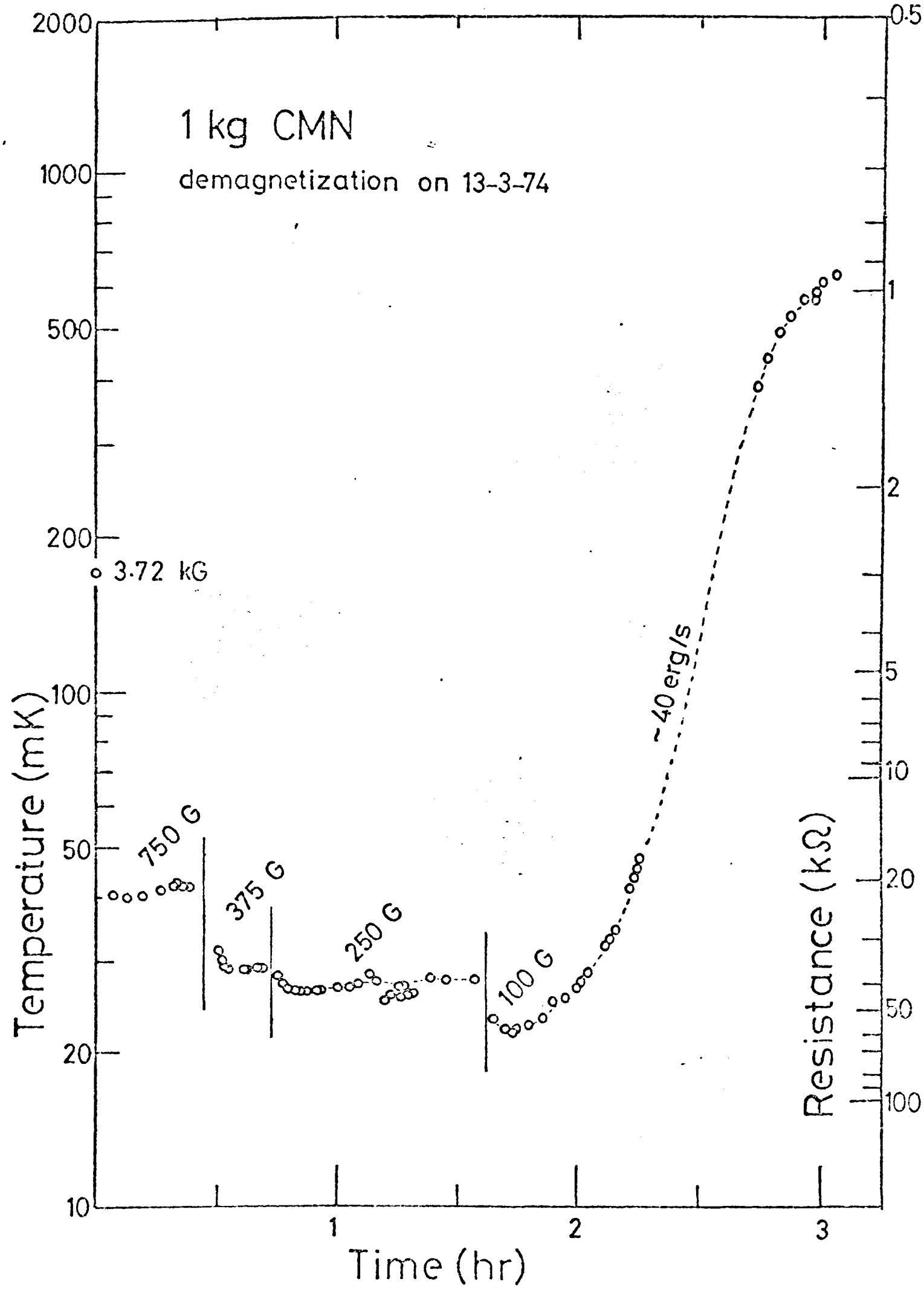

1 kg CMN
demagnetization on 13-3-74
3.72 kG
750 G
375 G
250 G
100 G
~40 erg/s
Temperature (mK)
Resistance (kΩ)
Time (hr)
2000
1000
500
200
100
50
20
10
0.5
1
2
5
10
20
50
100
1
2
3

Fig. 4.1

the pill and the CRT. The other and more important observation was the heat leak of 20-40 erg/s. This heat leak was calculated from the warm up of the pill at 100 mK. With a heat leak this large, the salt pill would rise by 15-20 mK during a nuclear magnetization. Between these runs the apparatus was disassembled, but nothing was obviously wrong. Since the nuclear sample, the salt pill and the IJ all have a large surface area, this heat leak could easily be the result of the continuous desorbtion of gas from the IJ. Since the desorbtion rate is highly temperature dependent, the heat leak to the nuclear sample can be greatly reduced by placing a surface colder than the IJ between the IJ and the nuclear sample. Originally no precaution had been taken against this form of heat leak, because some apparatus manage without.

To combat this heat leak a heat shield was attached to the mixing chamber. This shield completely encloses the salt pill and the nuclear stage. To prevent a touch between this heat shield and the IJ, several spacers are attached to the heat shield. These are short lengths of PTFE cut from thin walled sleeving and tied on with nylon thread. In designing the heat shield, the following factors have been considered. A high thermal conductivity is desired in the vertical direction. Eddy current heating should be small, to minimise the warming of the mixing chamber and the shield during the magnetization and demagnetization of the nuclear stage, which could result in the evolution of gas, contrary to the purpose of the shield.

Both of these requirements are met by making the heat shield out of "coil foil". This is made of 0.06 mm diameter enamelled copper wire which is first wound into a large diameter (the circumference must be $\geq$ the finished length of the shield) single layered coil, and then glued together with epoxy. When the epoxy is set, the coil is cut perpendicular to the wires. The resulting foil can then be shaped so the wires run in a vertical direction. More epoxy is used to ensure that the shield will keep its final shape.

This heat shield was used in the last two runs of this series, which showed that the heat shield vastly reduced the heat leak. The pills stayed cold for several hours and even absorbed the heat of two nuclear magnetizations ($\sim 10^5$ ergs each) without warming. No quantitative measurements were made of the heat leak because the runs ended when the magnet quenched. The results of both runs are summarized table 4.2, which shows that the final temperatures are, again, higher than the expected final temperatures,

$$T_f^{id} = T_i \left(H_f^2 + (40)^2\right)^{\frac{1}{2}} / H_i \text{ for CMN.}$$

The following method was used to measure the temperature with the NMR. In the early stages of the demagnetization, the NMR steady field is turned on. Since this field is horizontal and the main field is vertical, the nuclear magnetization starts in the vertical direction and rotates to the horizontal direction near the end of the demagnetization. To ensure that the final field is horizontal, it is important that the main solenoid is demagnetized to zero field. Immediately following a demagnetization,

the NMR system is pulsed at regular intervals. The integrated signals, $\zeta$ , are recorded. These signals decay with a time constant $\tau_1$ to an equilibrium value $\zeta_o$ corresponding to the temperature of the conduction electrons. Figure 4.2 shows a typical set of such readings. In this figure, the log of $\zeta$ has been plotted against time. Since the decay is exponential, $d \ln (\zeta - \zeta_o)/d t = -1/\tau_1$. As discussed in chapter 2, this can be converted into the temperature of the conduction electrons (the lattice) by using the Korringa relation, $\tau_1 T_L = K$. The temperature of the lattice is assumed to be the same as the temperature of the pill. The spin temperature, $T_S$, at a time, t, during the decay can be found from the relation $T_S = T_L(\zeta_o - \zeta_i)/(\zeta(t) - \zeta_i)$, where $\zeta_i$ is the background amplitude caused by the interference between the transmitter and the receiver and can be measured by pulsing the transmitter when the steady field is zero.

Table 4.2

CMN Demagnetizations

| date | $H_i$(kG) | $T_i$(mK) | $H_i/T_i$(kG/K) | $H_f$(G) | $T_f^{CRT}$(mK) | $T_f^{NMR}$ | $T_f^{id}$ |
|---|---|---|---|---|---|---|---|
| 4/4 | 3.77 | 270 | 13.9 | 100 | 24 | 17.5<br>20 | 7.7 |
| 9/4 | 3.77 | 235 | 16.0 | 100 | 21<br>19 | 17<br>15 | 6.7<br>2.5 |

The disagreement between the temperature measured with the CRT and the NMR is thought to illustrate the unreliability of the CRT at temperatures below 50 mK and not an error in the calibration. This view was confirmed on runs at a later date when it was found

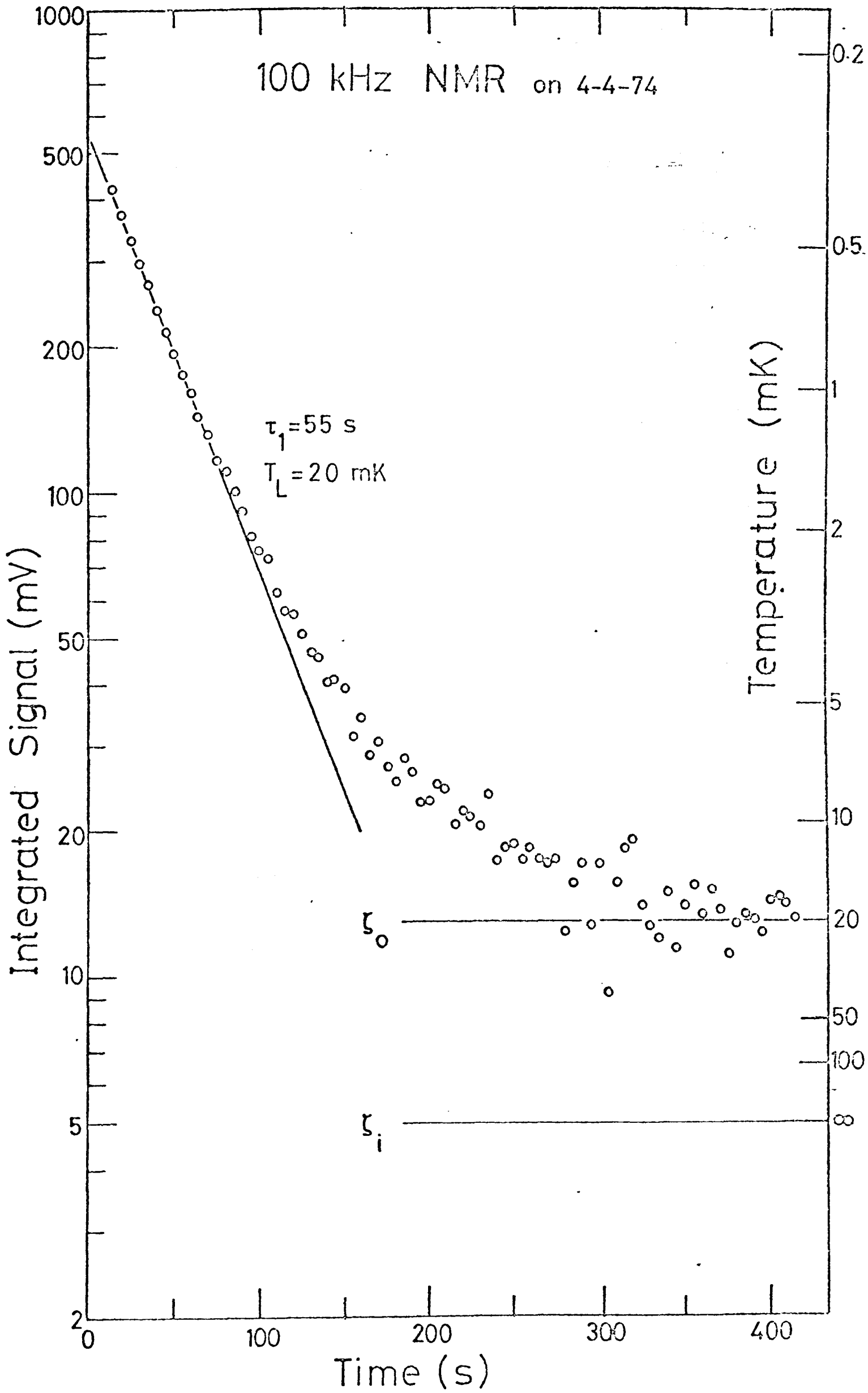

100 kHz NMR on 4-4-74
$\tau_1$=55 s
$T_L$=20 mK
$\tau_o$
$\tau_i$
Integrated Signal (mV)
Temperature (mK)
Time (s)
1000
500
200
100
50
20
10
5
2
0
100
200
300
400
0.2
0.5
1
2
5
10
20
50
100
∞

Fig. 4.2

that the amount of disagreement between the CRT and NMR varied from day to day. This is probably a result of the thermal contact changing slightly each time the pill is subjected to temperature cycling.

The results of the nuclear demagnetizations (shown in table 4.3) were disappointing. These demagnetizations were done at a rate of 83 G/s, i.e. about 600 s for the whole demagnetization which is many times longer than $\tau_1$. This was the fastest rate the power supply would allow. This rate is limited by the diodes in the output of the power supply which limit the inductive voltage during a demagnetization. The temperatures in the table are those found by the NMR. For reasons discovered later, the NMR signals did not begin until about 10 s after the end of the demagnetization (fig. 4.2). The spin temperature at the end of the demagnetization, $T_f$, is that corresponding to the first NMR signal seen. The high final temperatures of these experiments are probably a result of the slow demagnetization rate. Kurti (40) has shown that to achieve final temperatures within a few percent of the final temperature expected for a perfectly adiabatic demagnetization ($T_f^{id} = T_i(H_f^2 + (3)^2)^{\frac{1}{2}}/H_i$), the demagnetization must be done in a time $\lesssim \tau_1$ (i.e. $\gtrsim$ 1 kG/s) or else the spins absorb too much heat from the lattice during the demagnetization.

Table 4.3

Nuclear Demagnetizations to 89 G

| date | $H_i$(kG) | $T_i$(mK) | H/T(kG/K) | $T_f$(mK) | $T_f^{id}$(mK) |
|---|---|---|---|---|---|
| 4/4 | 49 | 17.5 | 2800 | 0.4 | 0.03 |
| | 49 | 20 | 2450 | 0.3 | 0.04 |
| 9/4 | 59 | 17 | 3460 | 0.12 | 0.03 |
| | 59 | 15 | 3930 | 0.11 | 0.02 |

One other experiment was tried on these runs. This was to measure $\tau_1$ by observing the relaxation after the NMR steady field, $H_o$, was suddenly changed from 0 to 89 Gauss. In this case the signal is expected to increase in time. This experiment was unsuccessful because the signal was lost in noise during most of the relaxation.

This set of CMN experiments had been partially successful. The 100 kHz NMR was now fully working. The disturbing heat leak had been identified and cured with the addition of a heat shield. However, three new difficulties were found. These are the slow demagnetization rate, the time gap between the end of the demagnetization and the first appearance of the NMR signals, and the apparent inability of the CMN to reach temperatures below about 20 mK. These problems are investigated in the next set of CMN experiments.

III. Further CMN Experiments:

These experiments were carried out during May and June 1974. In these experiments the nuclear sample contained 25000 0.04 mm diameter copper wires. There should be two effects from using smaller diameter wires. Per unit cross-section area, the area of contact between the CMN and the wires should be increased by a factor of 2 and the eddy current heating decreased by a factor of 4. The purpose of using smaller wires was to see if any of the difficulties associated with the previous experiments could be attributed to the size of the wires. It is difficult to judge whether the change in wire diameter had any effect since

most of these experiments were spent trying to achieve a rapid nuclear demagnetization.

A new pill containing 1 kg of CMN was run without much success on three occasions. On all of these occasions, no $\tau_1$ measurements were made with the NMR. On 9 May a lead to the transmitter coil broke. This run was spent by demagnetizing the pill to various fields and monitoring the temperature with the CRT. The results of these measurements are shown in figure 4.3. They show that H/T is fairly constant down to $\approx$ 35 mK and $\approx$ 450 G. This experiment was repeated on 5 June using the NMR as a thermometer. These results are also shown in figure 4.3. This time the deviation from constant H/T started at $\approx$ 40 mK and $\approx$ 450 G. It is unlikely that this behaviour is caused by the presence of a magnetic impurity in the CMN (specified as being greater than 99% pure), but it could be caused by poor thermal contact.

After this run, the power supply developed an instability that the laboratory's electronics workshop has not been able to fix. By 29 May, a stable power supply had been found and modified to withstand up to about 6 V during a demagnetization, which corresponds to a demagnetization rate of 400 G/s. Even though the demagnetization rate was faster, the results of the nuclear demagnetization done with this power supply were worse than those done with the other (sec. II). Several nuclear demagnetizations were tried from fields of 2, 5 and 60 kG and temperatures between 25 and 30 mK. After these demagnetizations there was a 20-30 s delay before an NMR signal could be seen, which was longer than the previous delay of about 10 s. When the signal was seen, it

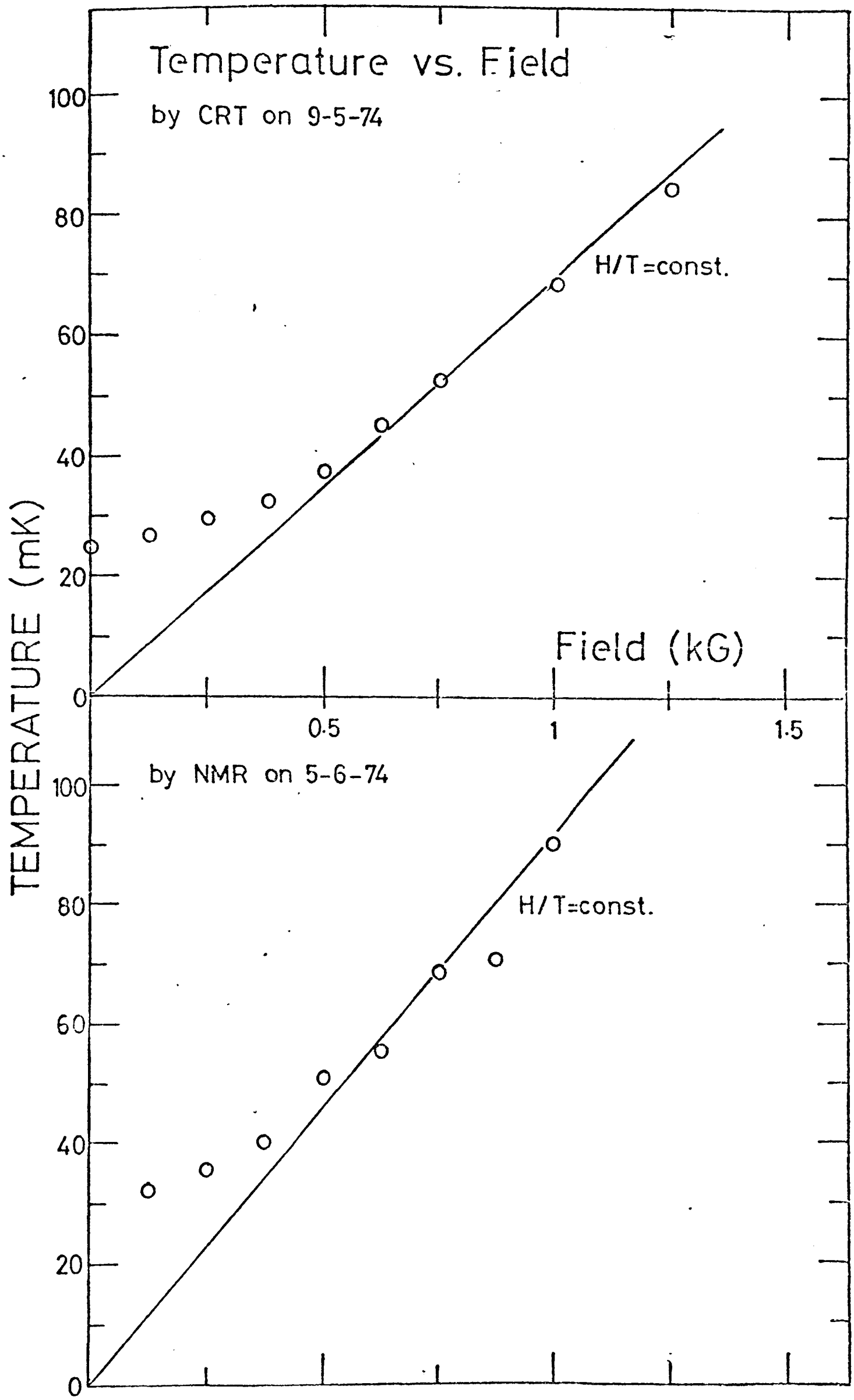

Temperature vs. Field
by CRT on 9-5-74
H/T=const.
Field (kG)
TEMPERATURE (mK)
0
20
40
60
80
100
0.5
1
1.5
by NMR on 5-6-74
H/T=const.

Fig. 4.3

was very small. On all of these runs, except for one from 5 kG and one from 2 kG, the maximum signal was only about twice the value corresponding to equilibrium with the conduction electrons. This change in amplitude was insufficient for measuring $\tau_1$. The results (table 4.4) of the two demagnetizations for which $\tau_1$ measurements were made show that the initial temperatures measured with the CRT and the NMR are not markedly different and that the ratio of the final temperatures to the expected temperatures are about the same as those in table 4.3.

Table 4.4

Nuclear Demagnetizations to 89 G

| $H_i$(kG) | $T_i$(mK) CRT | NMR | H/T (kG/K) | $T_f$(mK) | $T_f^{id}$(mK) |
|---|---|---|---|---|---|
| 5 | 22 | 22 | 230 | 4 | 0.4 |
| 2 | 29 | 32 | 63 | 8 | 1.4 |

At the end of the run, a cause of this behaviour was found. There was a leakage current from the power supply which decayed in time. This current came from the hot transistors and decayed as the transistors cooled. This caused the last part of the demagnetization to be very slow when it should be fast to reduce the amount of heat absorbed by the spins when they have the least heat capacity. This resulted in a high temperature at the end of the demagnetization and thus a small NMR signal. It also meant that the demagnetization did not stop at the time it was thought to have. This accounts for the 20-30 s wait for the NMR signals. The leakage current had been less for the other

power supply because the transistors were cooler after the slower demagnetization.

To stop the leakage current, a knife switch was installed between the power supply and the magnet. By opening it near the end of the demagnetization the current through the magnet is allowed to decay through a set of wire wound resistors in parallel with the magnet. The resistance is 7.8 Ω at 77 K and is not expected to change between there and 4.2 K. Since the inductance of the magnet is 15 H, the time constant is expected to be 2 s. In all of the following experiments, the knife switch was opened when 1 A was flowing through it, at which moment the current in the magnet will be greater than 1 A because the inductive voltage causes part of the current to flow in the resistors. The difference between the measured current and the actual current depends on the rate of current reduction. At the maximum demagnetization rate (400 G/s), the difference should be about 1 A, i.e. when the knife switch is opened at 1 A there is 2 kG(2 A) in the magnet.

On 5 June, the knife switch was used for the first time. Two nuclear demagnetizations were done, one from 1 kG and one from 59 kG. In both of these, there was a delay of approximately 20 seconds between the opening of the knife switch and the first NMR signal. This time was longer than expected and the results were only slightly better. The demagnetization from 1 kG and 32 mK resulted in a temperature of 5 mK instead of an expected 3 mK. After the demagnetization from 59 kG only an amplitude change of 2.5 times was observed.

Using a Hall probe external to the dewar, a remanant field of ~8 G was measured just below the solenoid and on the axis of the field. This remanant field is intrinsic property of the superconducting material. It was thought that the presence of the remanant field might be responsible for the longer than expected decay time. This field would certainly prevent the 10 kHz NMR from working.

To reduce the effect of this field, a magnetic shield was put between the solenoid and the OJ. This shield consists of 3 m of 15 cm wide 0.05 mm thick Telshield (a material similar to mumetal) wrapped about a 5 cm diameter brass tube. This shield was tested at room temperature in a water cooled solenoid and using a Hall probe to measure the field. The results of the test are shown in figure 4.4. No magnetic hysteresis effects were seen after an 11 kG field had been applied. The field at the ends of the shield is greater than the applied field ( $\approx$ 70 G in a 45 G field). Once inside the apparatus, this shield is outside of the NMR steady field which became enhanced. The 100 kHz resonance is now at 4.8 A instead of the previous 7.8 A.

On 26 June an experiment was run with the magnetic shield. At the same time it was decided to investigate whether the poor results of the CMN demagnetizations could be contributed to the inhomogeneity of the magnetic field. The homogeneity for the previous pills had been about 18%. A new pill containing only 600 g of salt was made. This pill is in the same pill container but the bottom 1 cm is filled with expanded polyurethane and the container is not as full as before. The homogeneity for this pill is about 10%.

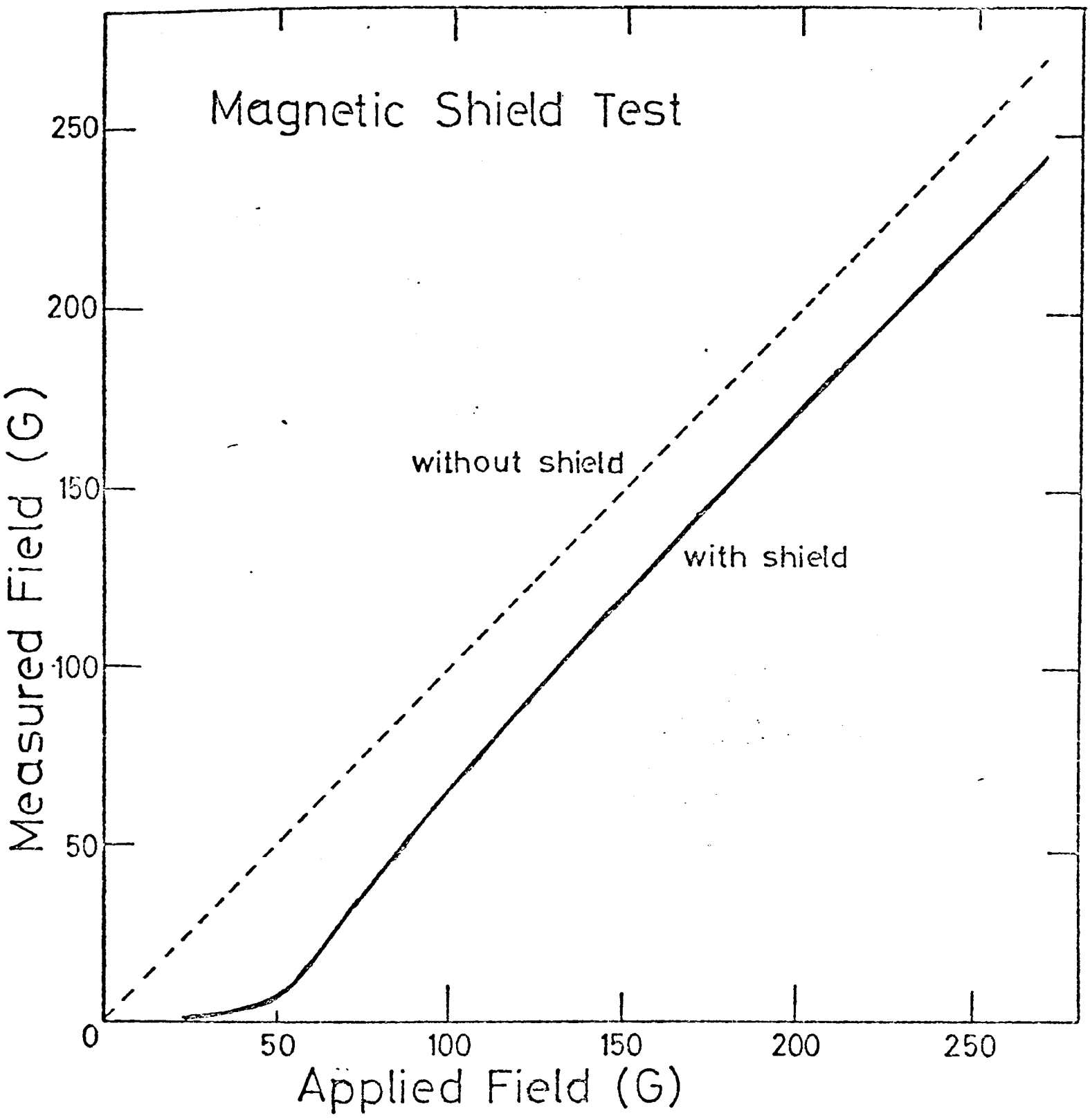

Magnetic Shield Test
Measured Field (G)
250
200
150
100
50
0
without shield
with shield
0
50
100
150
200
250
Applied Field (G)

Fig. 4.4

The smaller pill did not reach lower temperatures than the previous ones. The results of the demagnetizations of all the CMN pills used in this set of experiments are shown in table 4.5. This table shows that the smaller pill gave higher final temperatures than the bigger pill. This suggests that the inhomogeneity is not the cause of the poor results. A possible explanation is that since both pills contain the same amount of copper wire, it was harder to distribute them in the smaller pill. It is likely that many of the wires are not in good thermal contact with the salt. Since it is the average temperature of the wires that the NMR measures, this might be the cause of the difficult. Another possible cause of the problem is the anisotropy of the g-factor. Each small piece of CMN is the pill has a different orientation. Because the g-factor is anisotropic, each piece loses a different fraction of its entropy during the magnetization. Thus each piece cools to a different temperature on demagnetization. The equilibrium temperature of the pill will be greater than the temperature which could be achieved from a single crystal. This is contrary to the usual assumption that polycrystalline CMN behaves as an isotropic material with a g-factor equal to the g-factor of a single crystal averaged over all directions, which would be true if the demagnetization were carried out so slowly that there was always near complete equilibrium between the salt particles.

Table 4.5

CMN Demagnetizations

| date | $H_i$(kG) | $T_i$(mK) | $H_i/T_i$(kG/K) | $H_f$(g) | $T_f^{CRT}$(mK) | $T_f^{NMR}$(mK) |
|---|---|---|---|---|---|---|
| | | | 1 kg CMN | | | |
| 9/5 | 3.77 | 235 | 16.0 | 120 | 25 | |
| | 3.77 | 240 | 15.7 | 0 | 25 | |
| 16/5 | 3.77 | 245 | 15.4 | 120 | 27 | |
| 23/5 | 5.95 | 400 | 14.9 | 120 | 23 | |
| | 5.83 | 330 | 17.7 | 120 | 20 | |
| 29/5 | 5.83 | 330 | 17.7 | 120 | 24 | |
| | 5.70 | 330 | 17.0 | 120 | 22 | 22 |
| 5/6 | 5.95 | 300 | 19.8 | 120 | 22 | 32 |
| | | | 600 g CMN | | | |
| 26/6 | 5.95 | 310 | 19.1 | 60 | 29 | 33 |
| | 5.95 | 310 | 19.1 | 120 | 30 | 35 |
| | 5.95 | 310 | 19.1 | 120 | 29 | 35 |

The results of the nuclear demagnetizations using the new pill and the magnetic shield are shown in table 4.6. The results are slightly better than those done without the shield, as a bigger change in the NMR signal was observed, but there was still a 20 s delay between the opening of the knife switch and the beginning of the signals. These results are still not as good as the slow demagnetizations done earlier (sec II), however, $T_i$ is considerably higher on this occassion so $\tau_1$ is shorter and thus more relaxation can be expected to have occurred before the first signal is observed.

Table 4.6

Nuclear Demagnetizations to 89 G on 26/6

| $H_i$(kG) | $T_i$(mK) | H/T(kG/K) | $T_f$ | $T_f^{id}$ |
|---|---|---|---|---|
| 1 | 25 | 40 | 4 | 2.2 |
| 1 | 28 | 36 | 4 | 2.5 |
| 39 | 50 | 780 | 1.4 | 0.1 |
| 10 | 43 | 230 | 1.6 | 0.4 |
| 1 | 36 | 33 | 5 | 2.7 |
| 39 | 45 | 870 | 1.3 | 0.1 |
| 1 | 36 | 28 | 5 | 3.2 |

Whatever the cause of the high minimum temperatures in CMN, it was decided to ignore this problem until the difficulties with the nuclear demagnetizations could be sorted out. So, further CMN experiments were abandoned. Nevertheless, these experiments had been useful. They showed that there were two problems associated with the end of the nuclear demagnetizations. These were the leakage current from the power supply and the remanant field from the superconducting wire.

IV. Further CPA Experiments:

These experiments were carried out in July 1974. Since the previous experiments had shown that a lower temperature could be reached with CPA than with CMN, a pill with 400 g of CPA was made. The nuclear sample again contained 25000 0.04 mm diameter copper wires.

This pill was demagnetized twice on 10 July. Both demagnetizations were from 5.95 kG and 310 mK (H/T of 19.8 kG/K). Both were done to zero applied field and both times the CRT went off scale, i.e. the temperature was less than 16 mK. A $\tau_1$ measurement, after a demagnetization from 1 kG to 89 G, gave a temperature of 23 mK. The discrepancy suggests that the CRT is in better thermal contact with the salt than is the nuclear sample. Three more nuclear demagnetization were done, one from 10 kG and two from 20 kG. The results of these are given in table 4.7. An effect that had not been noticed before, was seen in the demagnetizations from 20 kG but not for those from 10 kG or 1 kG. As an example of each type, the NMR data for the demagnetization from 1 kG and one of those from 20 kG are shown in figure 4.5. On the 20 kG demagnetizations the first few data points, after the usual 20 s delay,

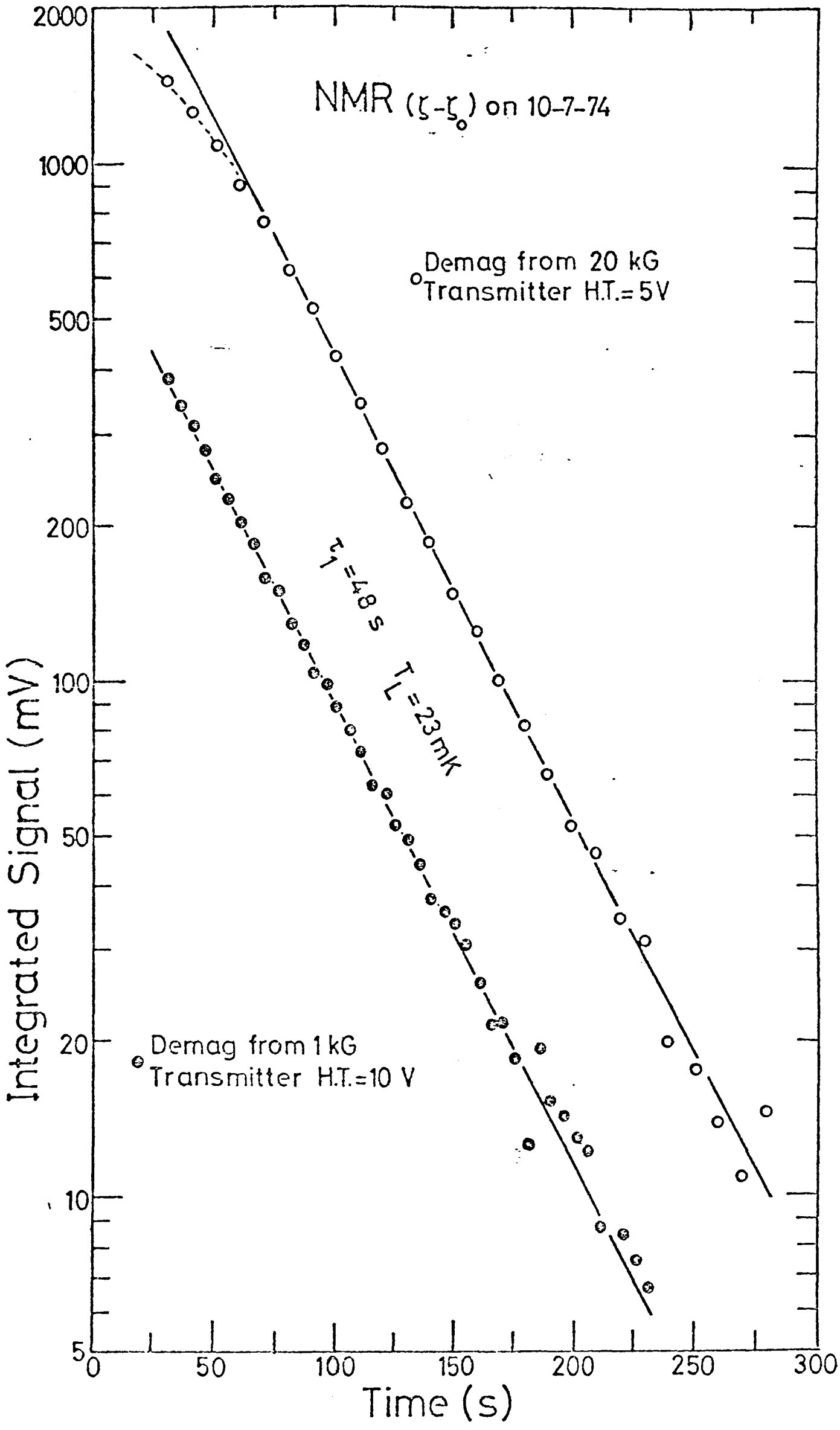

NMR (ζ-ζ₀) on 10-7-74
Demag from 20 kG
Transmitter H.T.= 5V
Demag from 1 kG
Transmitter H.T.=10 V
τ1 =48 s
TL =23mK
Integrated Signal (mV)
Time (s)
2000
1000
500
200
100
50
20
10
5
0
50
100
150
200
250
300

Fig. 4.5

lie below the line that fits the rest of the data. Since phase sensitive detection methods are used, this effect might be caused by a slight change in the phase of the signal caused by a slowly decaying field. But it is not known why this effect was only seen on these 20 kG demagnetizations.

Table 4.7

Nuclear Demagnetizations to 89 G on 18/7

| $H_i$(kG) | $T_i$(mK) | H/T(kG/K) | $T_f$(mK) | $T_f^{id}$(mK) |
|---|---|---|---|---|
| 1 | 23 | 43 | 3.1 | 2 |
| 20 | 23 | 870 | 0.3 | 0.1 |
| 20 | 24 | 820 | 0.3 | 0.1 |
| 10 | 25 | 390 | 0.6 | 0.2 |

The second pill demagnetization was used to test the 10 kHz NMR. For this test the integrator was not used. The signals were observed on the oscilloscope. No signal was found at the pill temperature, so several nuclear demagnetizations from 10 kG to various final fields were done. Resonance was expected at 9 G, but because of the enhancement of the field by the magnetic shield it was not known what current would produce this field. The enhancement factor was assumed to be roughly the same at 9 G as it was at 90 G. So the demagnetizations were done to 0, 0.2, 0.4 and 0.8 A in the $H_o$ magnet. No resonance was seen on the demagnetization to 0 A. A Resonance of about one cycle was seen on the other demagnetizations. Again there was a long delay (20-30s) before the signals appeared. When they did appear, they decayed in a time of the order of the expected $\tau_1$. The period of the resonance was 60-70 $\mu$s for all of the three final fields. These results showed that a resonance had been seen, but the amplitude and the

duration of the signals had been too small to make quantitative measurements.

It was decided to investigate the rate at which the magnetic field decays at the end of a demagnetization to see if this was responsible for the small NMR signals and for the delay that occurs before the signals start. To measure the field, the voltage induced in the receiver coil by the changing magnetic field was integrated by a Hewlett-Packard 2401C integrating digital voltmeter. It was found that with the knife switch closed the field decayed with a time constant of about 16 s. With the knife switch open the time constant was reduced to 5 s, but not to the expected value of 2 s. Also, during a rapid demagnetization the difference between the measured current and the actual current was found to be about 1.5 A instead of the expected 1A, i.e. the field was 0.5 kG higher than expected. Both of these discrepancies could be accounted for if some of the windings were shorting to each other through the copper that clads the superconductor.

Whatever the cause of the long decay time, it was decided to build a power supply that would demagnetize the main magnet at a constant rate to zero field. A block diagram of the power supply is shown in figure 4.6. This power supply is activated when the knife switch opens to cut out the main power supply. The new power supply is part of a negative feedback loop. A Hall probe, mounted in the annular space between the solenoid and the magnetic shield, measures the magnetic field. The output voltage of the probe is amplified by the power supply and applied to magnet terminals with a polarity to oppose the current flowing in the solenoid.

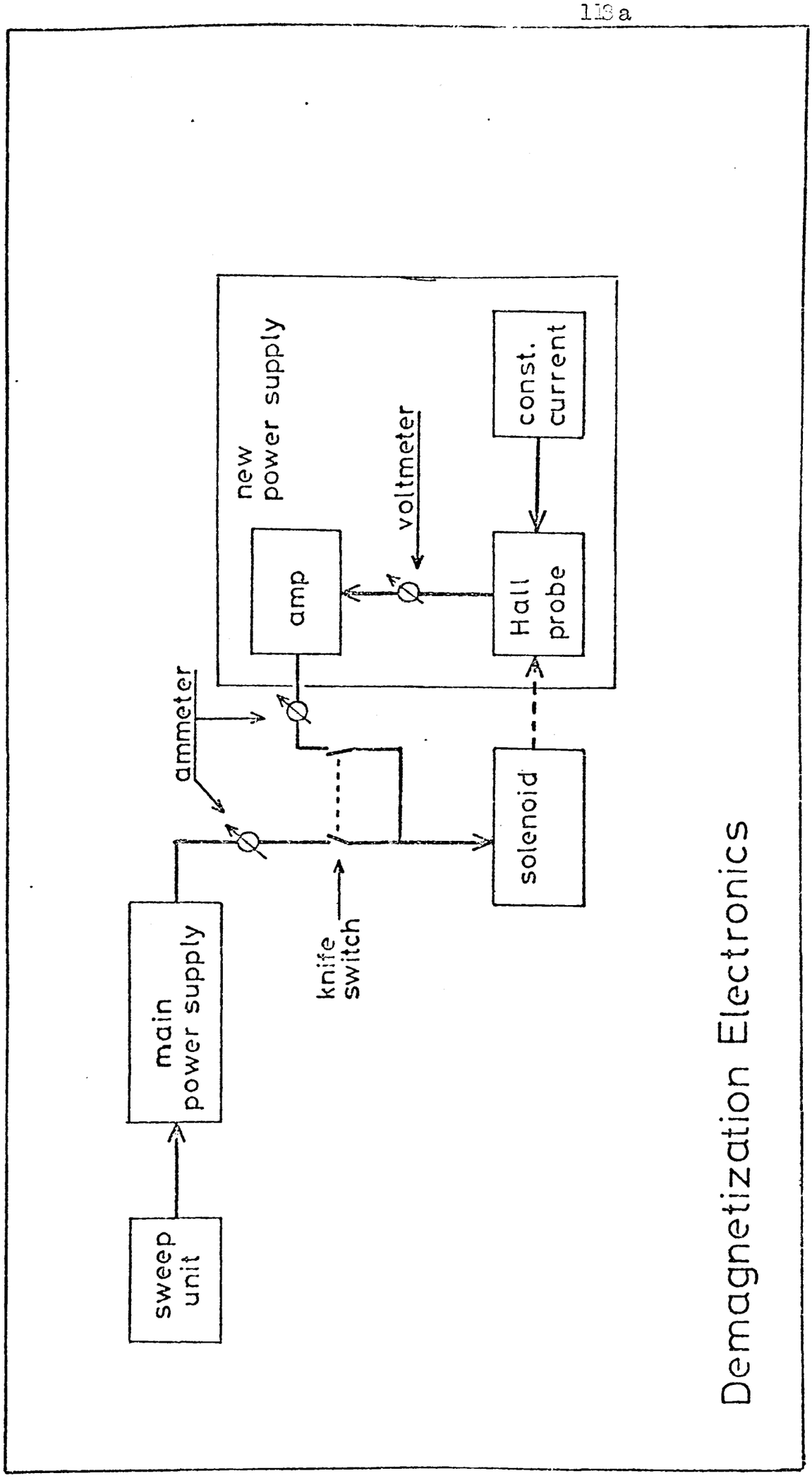

Demagnetization Electronics
sweep unit
main power supply
knife switch
ammeter
new power supply
amp
voltmeter
Hall probe
const. current
solenoid

Fig. 4.6

The gain of the system is adjusted so that the amplifier operates in an overload condition (constant output voltage of about 8 V) for all fields greater than about 2 G. The constant voltage decreases the current at a constant rate.

This system was tested on 18 July. Unfortunately a leak developed in the dilution refrigerator which prevented a complete experiment from being done. The new power supply was tested at 4.2 K by using the magnet in the usual way with the main power supply until it was at 1 A (about 2.5 kG). At this moment the knife switch was opened, activating the new power supply which reduced the field in 5 s to less than 2 G as measured by the Hall probe outside of the magnetic shield. This corresponds to a field less than 0.1 G at the nuclear sample. This was a demagnetization rate of 500 G/s.

Unfortunately a nuclear demagnetization could not be done after the above improvement was incorporated, because by the time the dilution refrigerator was repaired the laboratory had shut down for a six week holiday and maintanence period. I now believe that a rapid demagnetization can be done and that this would allow the 10 kHz NMR system to be used. The only remaining difficulty appears to be the high salt pill temperatures. A comparison of the results for the two types of nuclear samples shows that lower temperatures were reached with those containing the larger diameter wires (9500 0.06 mm diameter wires as opposed to 25000 0.04 mm diameter wires). So, inspite of the smaller diameter wires having a larger surface area per unit cross-section,

the thermal contact appears to be better for the larger diameter wires. This could be the result of the difficulty in uniformly distributing the smaller wires in the pill.

If I had more time, I would use the larger wires (9500 0.06 mm diameter) and a CPA salt pill. With these, I should be able to do a rapid nuclear demagnetization from about 60 kG and 12 mK (H/T of 5000 kG/K), first to 89 G and later to 9 G. Such a demagnetization should be sufficient to show that the 10 kHz integrating NMR system works and it might even be sufficient to observe some ordering effects.

## References for Part 2


1) P. D. Debye, Ann Phys 81 (1926) 1154

2) W. F. Giaugue, J. Am. Chem. Soc. 49 (1927) 1864, 1870

3) W. F. Giaugue and D. P. Mac Dougall, Phys. Rev. 43 (1933) 768

4) W. J. de Hass, E. C. Wiersma and H. A. Kramers, Physica 1 (1933/34) 1

5) N. Kurti and F. E. Simon, Nature 133 (1934) 907

6) N. Kurti and F. E. Simon, Proc. Roy. Soc. A149 (1935) 152

7) C. J. Gorter, Phys Z 35 (1934) 923

8) N. Kurti, F. E. Simon, A. Spohr and F.N.H. Robinson Nature 178(1956) 450

9) S. A. Al'tshuler, JETP Letters 3(1966) 112

10) K. Andres and E. Bucher, J. App. Phys. 42 (1971) 1522

11) R. H. March, Thesis (Oxford, 1965)

12) O.G. Symko, Thesis (Oxford, 1967) and J. Low Temp. Phys 1(1969)415

13) R. G. Gylling, Acta Polytechnica Scand 81(1971)

14) P. Hensel, Thesis (Oxford, 1973) and J. Low Temp. Phys 13 (1973)371

15) E. B. Osgood and J. M. Goodkind, Cryogenics 6 (1966) 54

16) J. M. Dundon, D. L. Stopha and J. M. Goodkind, Phys Rev Lett 30 (1973) 843

17) D. de Klerk, Handbuch der Physik, 15 (Springer-Verlag, 1956) 38

18) R. P. Hudson, Principles and Applications of Magnetic Cooling (North-Holland, 1972)

19) A. Abragam and N. G. Proctor, Phys. Rev. 109 (1958) 1441

20) M. Goldman, Spin Temperature and Nuclear Magnetic Resonance in Solids (Clarendon Press, Oxford, 1970)

21) L. C. Hebel Jr., Solid State Phys. (Ed. F. Seitz and D. Turnbull) 15 (Academic Press, 1963) 409

22) J. H. Van Vleck, J. Chem. Phys. 5 (1937) 320

23) J. H. Van Vleck, Phys. Rev. 74 (1948) 1168

24) M. V. Hobden and N. Kurti, Phil Mag 4 (1959) 1092, and M. V. Hobden, Thesis (Oxford, 1960)

25) R. E. Walstedt. E. L. Hahn, C. Froidevaux, and E. Geissler, Proc. Roy. Soc. A284 (1965) 499

26) P. Hensel and D. T. Smith, Cryogenics 14 (1974) 121 also see ref 14.

27) M. Aalto, P. Berglund, H. Collan, G. Ehnholm, R. Gylling, M. Krusius, and G. Pickett, Cryogenics 12 (1972) 184

28) C. P. Slichter, Principles of Magnetic Resonance, (Harper and Row, 1963)

29) A. Abragam, The Principles of Nuclear Magnetism (Oxford University Press, 1961)

30) F. Bloch, Phys Rev. 70 (1946) 460

31) J. Korringa, Physica 16 (1950) 601

32) A. G. Redfield, IBM J. Research Develop. 1 (1957) 19

33) L. C. Hebel and C. P. Slichter, Phys. Rev. 107(1957)901 and Phys. Rev. 113 (1959) 1504

34) A. G. Anderson and A. G. Redfield, Phys. Rev. 116 (1959) 583

35) E. Mendoza in Experimental Cryophysics, (Ed: F. E. Hoare, L. C. Jackson and N. Kurti) (Butterworths, 1961) 191

36) J. C. Wheatly, O. E. Vilches and W. R. Abel, Physics 4(1968)1

37) T. O. Niinikoski, Rev. Sci Inst. 43 (1972) 430

38) R. H. March and O. G. Symko, Proc. Grenoble Conf., I.I.R. Bulletin, Annexe 1965-2, see also ref 12).

39) G. J. Butterworth, C. B. P. Finn and K. Kiymac, J. Low. Temp. Phys. 15(1974) 537

40) N. Kurti, Cryogenics 1 (1960) 2

41) C. Froidevaux and J. R. Keyston, Proc VII Conf. Low Temp. Physics (Toronto, 1960) 93; also see M. V. Hobden and N. Kurti, Phil Mag 4 (1959) 1092

42) G. K. White, Experimental Techniques in Low-Temperature Physics (Oxford University Press, 1968)